Formation and Aggregation of Palladium(II)–Pyridylazo Complex at Liquid-Liquid Interfaces

by

Akira Ohashi

Department of Chemistry
Graduate School of Science
Osaka University

February, 2002

Contents

Part III

Molecular Recognizing Interfacial Aggregation of Palladium(II)–Pyridylazo Complex

Chapter 1

General Introduction

The liquid-liquid interface has received a great deal of attention in various fields of separation chemistry, biochemistry and electrochemistry,[1-3] because the liquid-liquid interface has specific characteristics, such as amphiphilic and two-dimensional media, extremely low saturated interfacial concentration of adsorbates, the orientational confinement for the adsorbates and so on. Therefore, there has been a growing demand for the elucidation of the kinetics and mechanisms proceeding at the liquid-liquid interface. Compared with the studies of chemical reactions in the bulk phase, ones at the liquid-liquid interface, however, have not been carried out extensively, since it is difficult to measure the interfacial concentration and reaction rate at the interface simultaneously.

Recently, several indirect and direct methods to observe the species at the liquid-liquid interface have been developed.[4] The centrifugal liquid membrane (CLM) method which has been developed in our laboratory is the most versatile technique for the research of the interfacial reaction. In this method, the ultra-thin two-phase liquid membranes were produced in a rotating optical cell. The CLM method was applied to the studies of the reaction kinetics of the demetallation of metal porphyrins and the fluorescence quenching reaction of ZnTPP with methylviologen at the liquid-liquid interface.[5,6] In order to apply CLM to the measurements of various reactions at the liquid-liquid interface, the improvement of the optical cell of CLM and the combination with other spectroscopic method are required.

Raman microprobe spectrometry has some potential for such a high sensitivity and a high spatial resolution. However, due to the inherent low sensitivity of Raman effect, the application of Raman spectroscopy to the study of a monolayer system is very difficult. When the excitation wavelength of the laser is close to the absorption band of the investigated species, Raman scattering is enhanced drastically (up to 10^6) as a result of the resonance Raman effect.[7] Therefore, resonance Raman spectroscopy can be used to study an adsorbate in a monolayer system at the liquid-liquid interface. To my knowledge, the study of the liquid-liquid interface with a resonance Raman spectroscopy has never been carried out except for only Takenaka et al[8-10] and Edwards et al,[11] though the resonance Raman spectroscopy gives much structural information for a sample. The development of a new

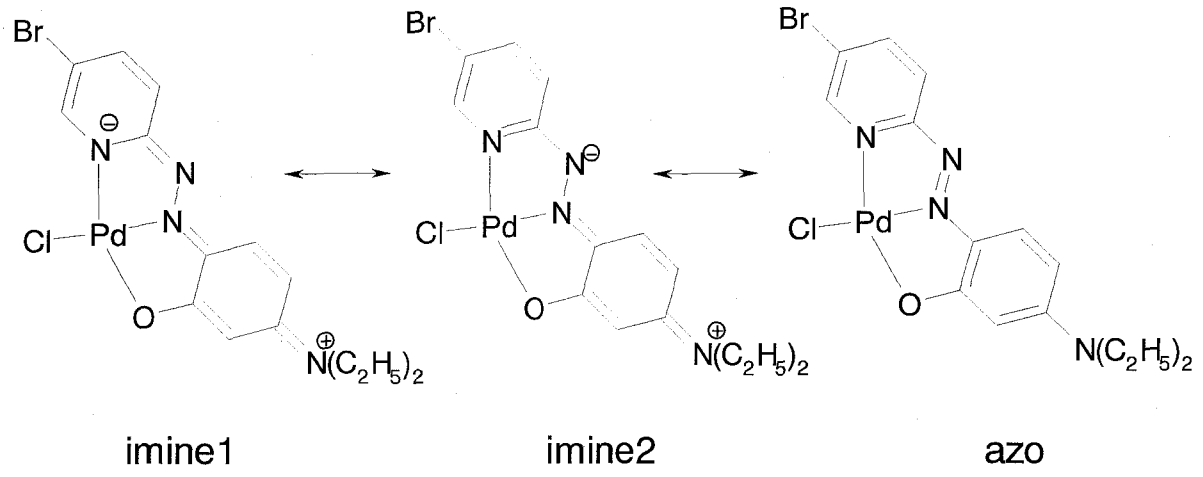

Figure 1.1 Proposed resonance structures of Pd(II)–5-Br-PADAP complex

method to measure the liquid-liquid interface with the resonance Raman spectroscopy will contribute the advance of the study on the liquid-liquid interface.

2-(Pyridylazo)-5-diethylaminophenol (PADAP) and its derivatives are one of the most important and useful reagents in analytical chemistry. They have a pyridylazo group as the same as 4-(pyridylazo)resorcinol (PAR) and 1-(2-pyridylazo)-2-naphthol (PAN), but the PADAP complexes are twice as sensitive as the PAR and the PAN complexes, having higher molar absorptivities of ca. 10^5 M^{-1} cm^{-1}.[12] 2-(5-Bromo-2-pyridylazo)-5-diethylaminophenol (5-Br-PADAP) was introduced by Gusev and Shchurova[13] and was used as a sensitive reagent in the determination of trace metal ions[14,15] and nucleic acids.[16] 5-Br-PADAP forms stable and colored complexes with various metal ions as a trident ligand and its complexes exist as a mixture of three tautomeric forms as shown in Figure 1.1.[17] The compounds that have electron donor and acceptor substituents on 5-position of both rings of azobenzene group tend to have a charged quinone structure. It is postulated that the charged quinone structure results in the high molar absorptivity.[12,14]

Palladium(II) ion can form a 1:1 complex with 5-Br-PADAP leaving one site for the coordination of another ligand. Pd(II)–5-Br-PADAP (PdL) complex has specific characteristics, such as extremely high molar absorptivity, interfacial adsorptivity and soft Lewis acid. Thus PdL is expected to be used as the interfacial molecular recognition reagent. Moreover, the complexation and the aggregation at the liquid-liquid interface may produce new specific species that are not formed in bulk phases.

This thesis comprises the results of the investigation of the reaction mechanism and

molecular recognition ability of Pd(II)–5-Br-PADAP complex at the liquid-liquid interface studied by various techniques including a new *in situ* method. In Chapter 2, a direct spectroscopic study of acid-catalyzed complexation of Pd(II) with 5-Br-PADAP at the heptane/water interface are described by the CLM method designed for the rapid sample injection. In this system, the complexation rate of Pd(II)–5-Br-PADAP was accelerated by H^+, because the 5-Br-PADAP concentrations in the aqueous phase and at the interface increased with the protonation to N_β at azo-group. The N_β at azo-group did not directly coordinate to Pd(II) ion, so that the reactivity of 5-Br-PADAP with Pd(II) was not affected by the protonation. This new-type acid-catalyzed effect has never been reported and is specific phenomenon at the liquid-liquid interface. Recently, the role of the liquid-liquid interface in solvent extraction has been clarified by a high-speed stirring method,[13] which can measure the interfacial adsorptivity of reagent dissolved in an organic phase.

In Chapters 3-4, a new Raman spectroscopic method, the centrifugal liquid membrane-resonance Raman microprobe spectroscopy (CLM-RRMS), was proposed for the detection of the interfacial complex formed between Pd(II) and 5-Br-PADAP in the heptane/water and toluene/water systems; the Raman microscopy was combined with the centrifugal liquid membrane (CLM) method. CLM-RRMS allowed us to obtaine the resonance Raman spectra of PdLCl, which was adsorbed in a monolayer system at the liquid-liquid interface, and to measure individually the resonance Raman spectra at the interface and in the bulk phase. The resonance Raman spectra of PdLCl adsorbed at the liquid-liquid interfaces were different from that in the solvents of the low dielectric constants and close to that in the solvents of the high dielectric constants. It was thought that the change of the resonance Raman spectra of PdLCl with the change of the solution was caused with the change of the ratio of the azo and imine resonance structures. Resonance Raman spectra obtained by CLM-RRMS suggested that PdLCl complex existed with the strong influence of hydration at the liquid-liquid interface and adsorbed at the interface of the aqueous phase side. This study showed that CLM-RRMS could be used to discuss about the microenvironment around the species adsorbed at the liquid-liquid interface.

In Chapters 5-6, the formation of the aggregate of PdLCl at the heptane/water interface and the comparison of crystal and aggregate of PdLCl are described. The aggregation of adsorbed molecules is one of the specific phenomena at the liquid-liquid interface. But, the aggregation mechanism at the interface has never been studied in detail very much. In Chapter 5, the aggregation proceeding at the heptane/water interface was

measured by CLM and CLM-RRMS. The charged quinone structure in the resonance of PdLCl was kept in its aggregate. Moreover, the first attempt to measure the interfacial reaction kinetics by resonance Raman spectroscopy was carried out by CLM-RRMS. The absorption and Raman spectra of the aggregate were different from ones of the interfacial complex and suggested the formation of H-aggregate with azo form. In Chapter 6, from the microscopic images, absorption spectra and resonance Raman spectra of the aggregate and the crystal of PdLCl, it was suggested that the structure of the aggregate was close to that of the crystal but was not the same. This showed the possibility that the liquid-liquid interface could be used as the specific synthetic field of the aggregate of metal-complexes that differs from those prepared in the bulk solutions.

In Chapters 7-8, the recognitions of diazine isomers by the complexation and the aggregation with Pd(II)–5-Br-PADAP complex at the toluene/water interface are described. As noted above, PdL complex is used as the molecular recognition reagent at the liquid-liquid interface. There are only few reports that metal-chelate complexes have been applied to the molecular recognition at the liquid-liquid interface.[18] The present investigation demonstrated the feasibility of the liquid-liquid interface as a new reaction medium for the molecular recognition and aggregation synthesis. In Chapter 7, the recognition of diazine (Dz) isomers by the complexation with Pd(II)–5-Br-PADAP complex is carried out by the high-speed stirring method. The interfacial formation constants (β_i) of 1:1 PdL-diazine isomer complexes were different between diazine isomers. The value of β_i for 1,2-Dz was larger than ones for 1,3-Dz and 1,4-Dz. It was revealed that the interfacial formation constants of 1:1 PdL-diazine complexes were mainly influenced to the basicity of Dz. In Chapter 8, the molecular recognizing aggregation of Pd(II)–5-Br-PADAP with diazine isomers at the toluene/water interface is studied by the CLM method. The absorptivities of the interfacial aggregates of PdL-diazine complexes were drastically reduced. This suggested that the formation of the charged quinone structure in the aggregates of PdL-Dz complexes was prevented by the interaction with ClO_4^-. The differences of the structure and the composition ratio of the interfacial aggregate of PdL-Dz were observed between Dz isomers; that of 1,2-Dz was as a blue domain and the composition ratio 1,2-Dz/PdL 1:1, whereas that of 1,4-Dz was as a membrane and 1,4-Dz/PdL 1:2. In spite of the lowest ability for 1:1 complexation between PdL and 1,4-Dz at the toluene-water interface, the ability for the formation of the interfacial aggregate became the highest among the Dz isomers. This result revealed that the formation of the interfacial aggregate of PdL-Dz isomer was greatly

influenced by the structure of Dz, not the basicity of Dz. The molecular recognizing interfacial aggregation of Pd(II)–5-Br-PADAP could be applied to the base systems. The interfacial reaction developed in these study will be applied to the recognition, separation and detection of the various species in the aqueous phase.

References

1. *Liquid-Liquid Interfaces. Theory and Methods*; Volkov, A. G.; Deamer, D. W., Eds.; CRC Press: Boca Raton, FL, 1996.
2. *Liquid Interfaces in Chemical, Biological, and Pharmaceutical Applications*; Volkov, A. G., Ed.; Marcel Dekker, New York, 2001.
3. *Liquid Interfaces in Chemistry and Biology*; Volkov, A. G.; Deamer, D. W.; Tanelian, D. L.; Markin, V. S., Eds.; John Wiley & Sons CRC Press, Chicester, 1998.
4. Watarai, H. In *Liquid Interfaces in Chemical, Biological, and Pharmaceutical Applications*; Volkov, A. G., Ed.; Marcel Dekker, New York, 2001; Chapter 14.
5. Nagatani, H.; Watarai, H. *Anal. Chem.* **1998**, *70*, 2860.
6. Nagatani, H.; Watarai, H. *Anal. Chem.* **1999**, 701.
7. *Raman Bunkouhou*; Hamaguchi, H.; Hirakawa, A., Eds.; Gakkai Syuppan Center, Tokyo, 1998; p54.
8. Takenaka, T.; Nakanaga, T. *J. Phys. Chem.* **1976**, *80*, 475.
9. Takahashi, H.; Umemura, J.; Takenaka, T. *J. Phys. Chem.* **1982**, *86*, 4660.
10. Takahashi, H.; Umemura, J.; Takenaka, T. *J. Phys. Chem.* **1983**, *87*, 739.
11. Edwards, H. G. M.; Hughes, M. A. Smith, D. N. *Vib. Spectrosc.* **1996**, *10*, 281.
12. Ueno, K.; Imamura T.; Cheng, K. L. *Handbook of Organic Analytical Reagents* 2nd ed.; CRC Press: Boca Raton, 1992, pp237-243.
13. Gusev, S. I.; Shchurova, L. M. *Zh. Anal. Khim.* **1966**, *21*, 1042.
14. Shibata, S.; Furukawa, M. *Bunseki Kagaku* **1974**, *23*, 1412.
15. Miura, J. *Analyst* **1989**, *114*, 1323.
16. Hao, Y. M.; Guo, Z. X.; Wang, X. X.; Shen, X. H. *Anal. Chim. Acta* **1999**, *402*, 21.
17. Johnson, D. A.; Florence, T. M. *Talanta* **1975**, *22*, 253.
18. Feng, P.; Shu, W. Q.; Huang, C. Z.; Li, Y. F. *Anal. Chem.* **2001**, *73*, 4307.

Part I

Interfacial Complexation of Palladium(II)–Pyridylazo Complex

Chapter 2

Direct Spectrophotometric Measurements of Acid-catalyzed Complexation of Palladium(II) with 2-(5-Bromo-2-pyridylazo)-5-diethylaminophenol at the Heptane/Water Interface by a Centrifugal Liquid Membrane Method

Introduction

Chemical reactions at the interfaces between two immiscible liquids have became a more interesting subject in various fields, including solvent extraction chemistry, biological chemistry and electrochemistry.[1,2] Although the interfacial complexation has been studied in some solvent extraction systems, catalytic reactions at the interface have not been reported enough compared with those in the aqueous phase. We have previously clarified the various reaction mechanisms proceeding at the liquid-liquid interface in solvent extraction systems by a high-speed stirring method[3-7] that can simultaneously measure the extraction rate of a metal complex and the interfacial concentration of a ligand or the complex from the change of the absorbance in the organic phase. However, this method has one drawback: it cannot directly measure the interfacial species. When the complex was not extracted into the organic phase and exists only at the interface, the complexation rate was indirectly determined from the consumption rate of the ligand in the organic phase in the high-speed stirring method.[6] Recently, in our laboratory we developed a new *in situ* spectrophotometric method, the centrifugal liquid membrane (CLM) method, to measure the species adsorbed at the liquid-liquid interface.[8,9] This method utilizes an ultra-thin two-phase liquid membrane in a rotating optical cell by a centrifugal force and can directly measure the interfacial species by transmission spectrophotometry or other spectrometries. But the previous rotating cell did not permit us to inject the sample solution rapidly while the cell was rotating. Therefore, there were some problems: fast reactions were difficult to measure and it was impossible to change the solution conditions in the course of the measurement. To solve these problems, in the present study we made a modified rotating cell that had a hole in the bottom.

2-(5-Bromo-2-pyridylazo)-5-diethylaminophenol, 5-Br-PADAP or HL, has been known as a highly sensitive colorimetric reagent that forms colored complexes with various metal ions and has been used to detect trace amounts of various metal elements.[10-12] It was

reported that 5-Br-PADAP formed a complex with Pd(II) with the mole ratio of 1:1.[13]

In the present study, we directly measured the formation kinetics of Pd(II)–5-Br-PADAP complex, which was not extracted into the heptane phase and existed only at the interface, from the spectral change in the heptane/water system. We clarified the kinetic mechanism of the catalytic effect of acid on the complexation reaction. Also, the advantage of the modified centrifugal liquid membrane cell in the kinetic study was demonstrated.

Experimental

Reagents

5-Br-PADAP (Dojindo Lab.) was used as purchased and was dissolved in purified heptane. For the purification, heptane (G.R., Katayama Chemical) was stirred with concentrated sulfuric acid for one day (repeated three times), washed successively with distilled water and 5% sodium hydroxide aqueous solution, dehydrated by calcium chloride dehydrate overnight, and fractionally distilled. Water was distilled and deionized with a Milli-Q system (Milli-Q SP.TOC., Millipore).

A stock solution of 1.0×10^{-2} M (1 M = 1 mol dm^{-3}) palladium(II) was prepared by dissolving $PdCl_2$ (99.99%, Wako Pure Chemicals) in 0.1 M hydrochloric acid.

Measurement of distribution ratio of 5-Br-PADAP

The distribution ratio of 5-Br-PADAP between heptane and water was measured by a batch method. The heptane phase (5 cm^3) and aqueous phase (5-40 cm^3) were shaken for 1 h in a thermostated room at 298±2 K, and then the absorption spectra of the heptane phase were measured in the range of 350-800 nm. The pH was changed in the range of 1.0-5.8, and the ionic strength was fixed to 0.1 M with (H^+, Na^+)Cl^-. 2-Morpholinoethanesulfonic acid monohydrate (MES, Dojindo Laboratories) was used as a buffer reagent. The absorption spectra were measured with a spectrophotometer (V-550, Jasco) at 298±2 K.

Interfacial adsorption measurements

The interfacial adsorptivity of 5-Br-PADAP was measured with a high-speed stirring apparatus as reported previously.[5,6] Pure heptane and aqueous phases in the stirring-cell were thermostated at 298±0.2 K. The organic phase was continuously separated with a

PTFE phase separator, passed through a flow-cell with 1 cm optical path length in a photodiode array spectrophotometric detector (SPD-M6A, Shimadzu) and returned to the stirring-cell at a flow rate of 15 cm^3 min^{-1} with a pump (Lab pump Jr. model RHSY, Fluid Metering Inc). After two phases were agitated in the stirring-cell at a stirring speed of 5000 rpm, HL heptane solution was added. Then the organic phase concentration of 5-Br-PADAP was measured from the absorbance at 452 nm. The final volumes of the heptane phase and the aqueous phase were both 0.050 dm^3. The HL concentration and pH were changed in the range of 1.5×10^{-6}-2.8×10^{-5} M and 1.07-5.93, respectively. The ionic strength and the chloride ion concentration were kept at 0.1 M with (H^+, Na^+)Cl^-. Pd(II) existed mainly as $PdCl_3^-$ and $PdCl_4^{2-}$ in 0.1 M chloride ion system.[14]

When the stirring speed was changed from 200 to 5000 rpm, the concentration of 5-Br-PADAP in the organic phase decreased due to the interfacial adsorption. The total concentrations of 5-Br-PADAP under the low- and high-speed stirring are respectively described as:

$$[HL]_T = [HL]_{a,200} + [HL]_{o,200} \tag{2.1}$$

$$[HL]_T = [HL]_{a,5000} + [HL]_{o,5000} + [HL]_{i,T}\frac{S_i}{V_o} \tag{2.2}$$

where the subscripts T, a, o, and i refer to total, aqueous phase, organic phase and interface, respectively, the subscripts 200 and 5000 refer to the conditions of 200 rpm and 5000 rpm stirring speed, respectively, and S_i (17000 cm^2)[15] and V_o (0.050 dm^3) are the interfacial area under the high-speed stirring conditions and the volume of the organic phase, respectively. $[HL]_a$ (M) and $[HL]_{i,T}$ (mol cm^{-2}) include neutral and protonated species in the aqueous phase and at the interface, respectively. From Eqs. (2.1) and (2.2), $[HL]_{i,T}S_i/V_o$ is described as:

$$[HL]_{i,T}\frac{S_i}{V_o} = ([HL]_{o,200} - [HL]_{o,5000})(1+D^{-1}) \tag{2.3}$$

where D is the distribution ratio of 5-Br-PADAP at a given pH. Equation (2.3) is rewritten by using the absorbances (A_{200} and A_{5000}) in the organic phase under the low-speed stirring (200 rpm) and high-speed stirring (5000 rpm) as:

$$[\mathrm{HL}]_{\mathrm{i,T}} = (A_{200} - A_{5000})(1 + D^{-1})\frac{V_o}{S_i \varepsilon_{452} b} \qquad (2.4)$$

where ε_{452} is the molar absorptivity of 5-Br-PADAP in the heptane phase (ε_{452} = 5.16×10^4 M^{-1} cm^{-1})[6] and b the optical length of the flow-cell (b = 1 cm)

Measurements of complexation rate

The modified centrifugal liquid membrane cell is shown in Figure 2.1. The inner diameter and inner height of the cylindrical cell were 19 mm and 30 mm, respectively. A hole of 2-mm in diameter as a sample inlet was drilled at the bottom of the cylindrical cell. The cylindrical cell was placed horizontally in the diode array spectrophotometer (Hewlett-Packard HP8452A) and rotated at about 10000 rpm by a high-speed motor (Nakanishi Inc., NK-260) with a speed controller (Nakanishi Inc., NE-22E).

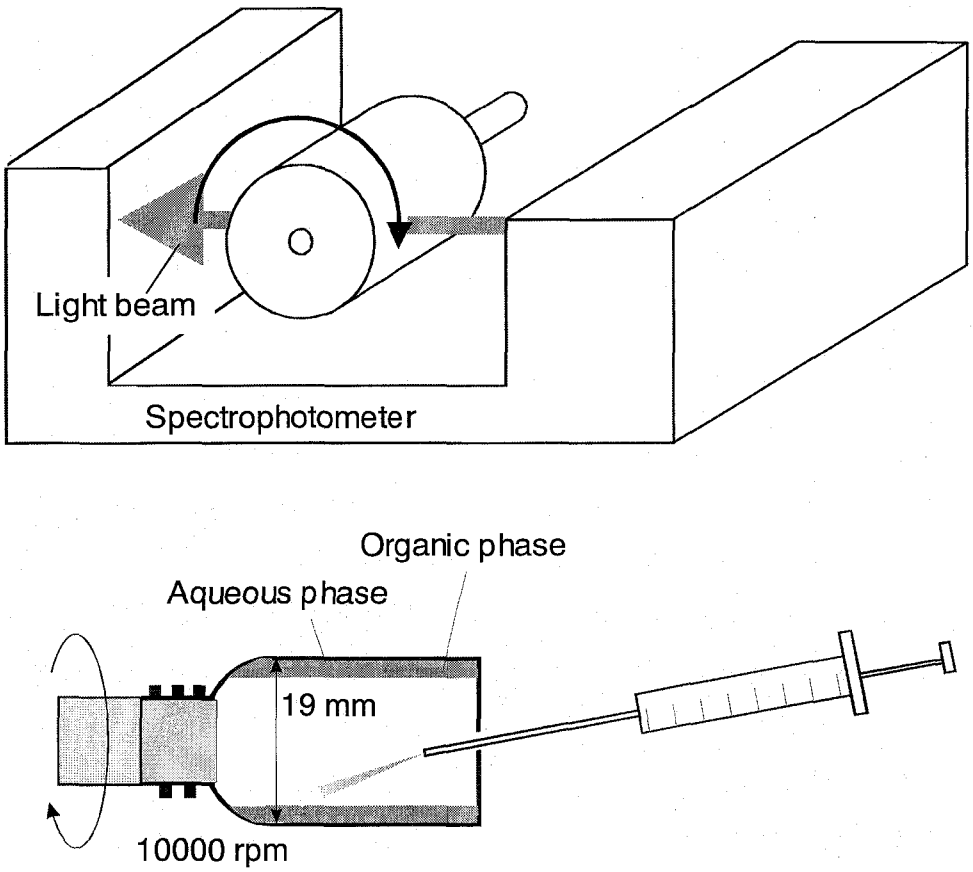

Figure 2.1. Schematic drawing of the centrifugal liquid membrane spectrophotometry with the modified cell having a sample injection hole at the bottom.

Because of the difference in densities between heptane and aqueous phases, the organic phase was spread out on the aqueous phase at the inner wall of the cylindrical cell under the high-speed rotation. When the volumes of the organic and aqueous phases were 0.150 cm^3 and 0.250 cm^3, respectively, the thicknesses of the organic and aqueous phases were 77-μm and 128-μm, respectively. The interfacial area between two phases was 19.4 cm^2.

After the cylindrical cell containing heptane (0.050 cm^3) and Pd(II) aqueous solution (0.250 cm^3) was rotated, HL heptane solution (0.100 cm^3) was injected rapidly by a microsyringe from the hole at the bottom (see Figure 2.1) to initiate the complexation of Pd(II) with 5-Br-PADAP. The light beam of the spectrophotometer passed through the liquid membranes perpendicular to the rotation axis. The sum of the absorption spectra of the interface, the bulk organic phase and the bulk aqueous phase was measured with the diode array spectrophotometer. The complexation rate was monitored as the absorbance increase of Pd(II)–5-Br-PADAP complex at 580 nm. The absorbance change was fitted to a second-order equation by the least-squares regression method and the observed initial complexation rate, r^0_{obs}, was calculated by differentiating the second-order equation at the injection time. The Pd(II) concentration, HL concentration and pH were changed in the range of 8.0×10^{-5}-5.6×10^{-4} M, 2.0×10^{-6}-1.6×10^{-5} M and 1.1-2.8, respectively. The ionic strength was controlled at 0.1 M with HCl and NaCl.

Spectral measurement of protonated 5-Br-PADAP

To identify the structure of the protonated 5-Br-PADAP, absorption and Raman spectra of 5-Br-PADAP in 40% EtOH solutions at pH 1.16 and 5.84, respectively. The absorption spectra were measured with a spectrophotometer (V-550, Jasco). The Raman spectra were measured with a Raman microscopy constructed by Photon Design (Japan) and this apparatus was described in Chapters 3 and 4 in detail. A 5-Br-PADAP solution in a 1-cm quartz cell was put under the object lens (45×, NA 0.55) lain on the stage. The laser beam of 514.5 nm wavelength of Ar^+-ion laser was focused into the sample through the objective lens. The scattering light was collected by the same objective lens. The laser power and exposure time were 40 mW and 50 s, respectively. The concentration of 5-Br-PADAP was 7.2×10^{-6} M in the absorption spectral measurement and 1.5×10^{-5} M in the Raman spectral measurement. The ionic strength was controlled at 0.1 M with HCl and NaCl.

Results and Discussion

Structure identification of protonated 5-Br-PADAP

Figure 2.2 and 2.3 show the absorption spectra and Raman spectra of 5-Br-PADAP in 40% EtOH solutions at pH 1.16 and 5.84, respectively. The value of pK_a for H_2L^+ in 50% EtOH was reported as 2.02 in the literature.[10] Therefore, almost 5-Br-PADAP is protonated at pH 1.16. The maximum absorption wavelength of 5-Br-PADAP was shifted from 444 nm to 468 nm due to the protonation, but the molecular absorptivity did not decrease. Raman spectra of H_2L^+ were greatly different in that of HL. In particular, Raman shift at 1380 cm^{-1} assigned to N=N bond disappeared in the spectrum of H_2L^+. We have ever thought that 5-Br-PADAP was protonated to diethylamino-group as shown in Figure 2.4a according to the literature by Johnson et al.[10] However, if 5-Br-PADAP was protonated to diethylamino-group, Raman shift at 1380 cm^{-1} would not disappear, and the molecular absorptivity would decrease in the protonation due to the prevention of the formation of the charged quinone structure which resulted in the high molar absorptivity.[16,17] Absorption and Raman spectra of H_2L^+ implied that 5-Br-PADAP was not protonated to diethylamino-group. Instead of the protonation to diethylamino-group, we thought that 5-Br-PADAP was protonated to N_β at azo-group as shown in Figure 2.4b according to the literature by Kawai et al.[18] This structure seems to be agreement with the results of absorption and Raman spectra.

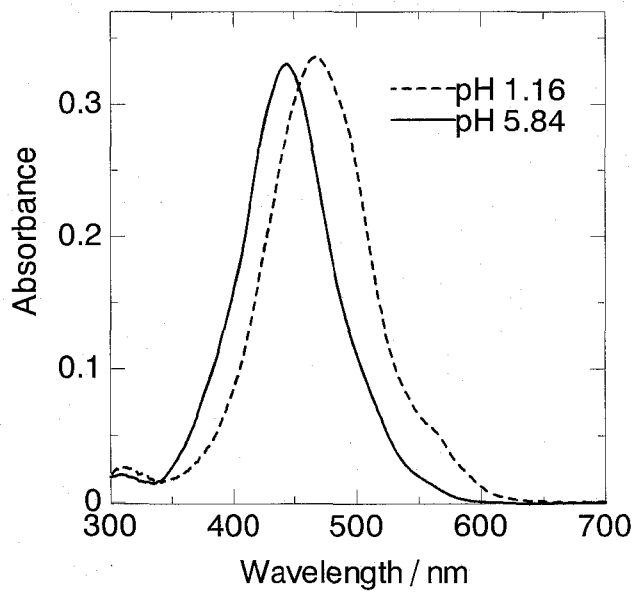

Figure 2.2. Absorption spectra of neutral and protonated 5-Br-PADAP in 40% EtOH solution. $[HL]_T = 7.2\times10^{-6}$ M, $[Cl^-] = 0.1$ M.

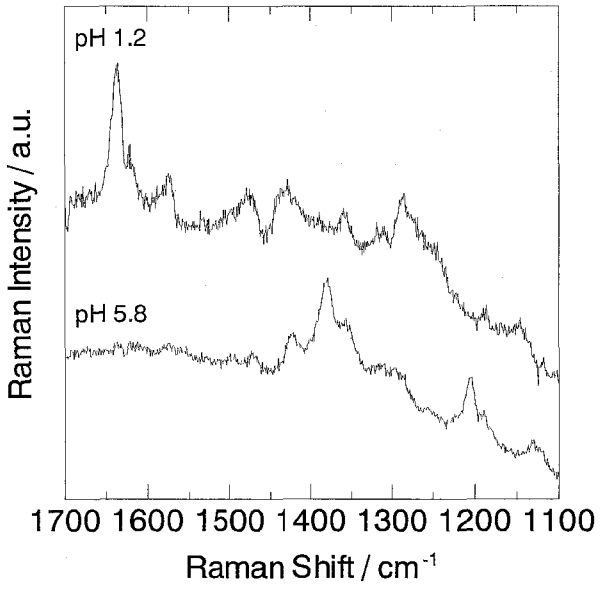

Figure 2.3. Resonance Raman spectra of protonated and neutral 5-Br-PADAP in 40% EtOH solution. $[HL]_T = 1.5\times10^{-6}$ M, $[Cl^-] = 0.1$ M, $\lambda_{ex} = 514.5$ nm.

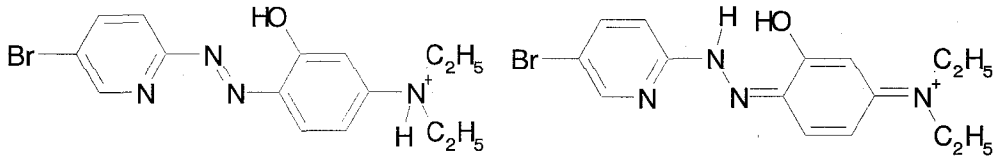

Figure 2.4. Proposed structures of protonated 5-Br-PADAP

Distribution equilibrium of 5-Br-PADAP

The distribution ratio, D, of 5-Br-PADAP was obtained from the following equations:

$$D = \frac{[HL]_o}{[HL]+[H_2L^+]} = \frac{A_{o,f}}{A_{o,init}-A_{o,f}} \cdot \frac{V_a}{V_o} \qquad (2.5)$$

where the subscripts init and f refer to the initial and the final absorbances, respectively. HL and H_2L^+ correspond to the neutral and the protonated 5-Br-PADAP, respectively. The logarithm of D was represented as:

$$\log D = \log K_D - \log(1 + \frac{[H^+]}{K_a}) \qquad (2.6)$$

where K_D is the distribution constant of neutral 5-Br-PADAP, defined as $K_D = [HL]_o/[HL]$, and K_a is the acidic dissociation constant of H_2L^+. From the analysis of the observed distribution ratios according to Eq. (2.6), log K_D and pK_a values were obtained as 2.71±0.04 and 2.95±0.07, respectively.

Interfacial adsorption of 5-Br-PADAP

Figure 2.5 shows the interfacial adsorption of 5-Br-PADAP in the high-speed stirring condition at various pH values. The absorbance change of 5-Br-PADAP due to the stirring increased with the decrease of pH. This is ascribable to the adsorption of a protonated 5-Br-PADAP (H_2L^+) under the low pH condition, because the adsorptivity of HL is expected to be independent of pH.[6] By assuming the concentration of vacant site at the interface s (mol cm^{-2}), one can defined the saturated interfacial concentration a_{sat} (mol cm^{-2}) as:

$$a_{sat} = [HL]_i + [H_2L^+]_i + s \qquad (2.7)$$

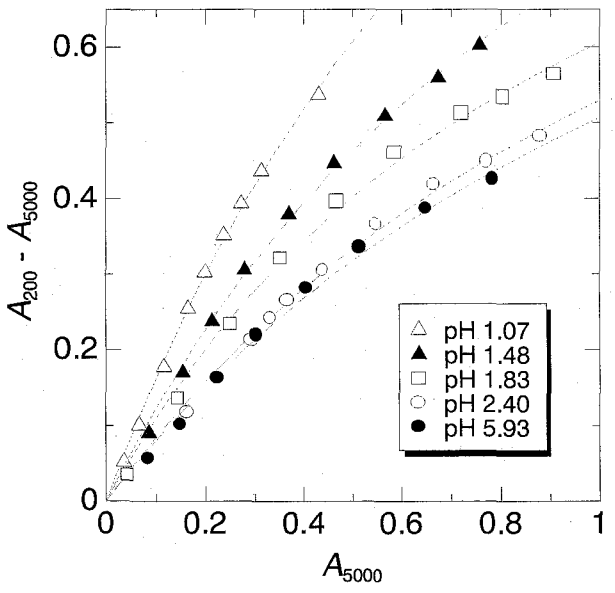

Figure 2.5. The interfacial adsorption isotherms of 5-Br-PADAP at 298 K under the various pH values. The solid lines are ones fitted by Eq. (2.12).

Furthermore, the adsorption constant K of HL and the acidic dissociation constant K_a of H_2L^+ at the interface are defined as:[19]

$$K = \frac{[HL]_i}{[HL]_o s} \tag{2.8}$$

$$K_{a,i} = \frac{[HL]_i [H^+]}{[H_2L^+]_i} \tag{2.9}$$

From Eqs. (2.7) – (2.9), $[HL]_i$ is represented by

$$[HL]_i = \frac{a_{sat} K'[HL]_o}{a_{sat} + (1 + \frac{[H^+]}{K_{a,i}})K'[HL]_o} \tag{2.10}$$

where K ' is equal to $a_{sat}K$. Consequently, assuming that the values of a_{sat} of HL and H_2L^+ are almost same, we can represent the total interfacial concentration by

$$[HL]_{i,T} = [HL]_i + [H_2L^+]_i = \frac{a_{sat}(1 + \frac{[H^+]}{K_{a,i}})K'[HL]_o}{a_{sat} + (1 + \frac{[H^+]}{K_{a,i}})K'[HL]_o} \tag{2.11}$$

From Eqs. (2.4) and (2.11), $A_{200} - A_{5000}$ is represented by

$$A_{200} - A_{5000} = \frac{\varepsilon_{452} b a_{sat} K'_{app} A_{5000}}{\varepsilon_{452} b a_{sat} + K'_{app} A_{5000}} \frac{S_i}{(1 + D^{-1})V_o} \tag{2.12}$$

where K'_{app} is the apparent adsorption constant,

$$K'_{app} = K'(1 + \frac{[H^+]}{K_{a,i}}) \tag{2.13}$$

Table 2.1. The saturated interfacial concentrations, the apparent adsorption constants of 5-Br-PADAP and the interfacial dissociation constants in the heptane/water system under various pH values.

pH	a_{sat} / mol cm^{-2}	K'_{app} / cm	p$K_{a,i}$
1.07	1.3×10^{-10}	6.1×10^{-3}	1.2
1.48	9.3×10^{-11}	4.2×10^{-3}	1.3
1.83	7.2×10^{-11}	3.6×10^{-3}	1.5
2.40	7.4×10^{-11}	2.6×10^{-3}	1.0
5.93	7.1×10^{-11}	2.5×10^{-3}	—
Average	$(8.8\pm2.5)\times10^{-11}$	—	1.3 ± 0.2

The value of total interfacial area (S_i) was 17000 cm^2.[15]
The values of p$K_{a,i}$ were calculated from Eq. (2.13).

The plots in Figure 2.5were analyzed by Eq. (2.12) and the values of a_{sat} and K'_{app} at each pH were obtained as listed in Table 2.1. The value of D in Eq. (2.12) at each pH was calculated by Eq (2.6). The averaged value of a_{sat} was obtained as $(8.8\pm2.5)\times10^{-11}$ mol cm^{-2}. This value is close to a typical value of a_{sat}, which is at the order of 10^{-10} mol cm^{-2}.[20] The value of a_{sat} at pH 1.07 seemed to be slightly larger than those at the other pH values. This was ascribed to a poor curvature in the plot at pH 1.07 in Figure 2.5, which was not enough to obtain an accurate value of a_{sat}. The value of K' was obtained as 2.5×10^{-3} cm, assuming no protonation of HL at pH 5.93. Substituting the value of K' in Eq. (2.13) yields the value of $K_{a,i}$ at each pH and 1.3±0.2 was obtained as the average value of $K_{a,i}$. The value of p$K_{a,i}$ at the heptane/water interface was smaller than 2.95, pK_a in the aqueous phase. The dielectric constant of heptane (ε_r = 1.924 at 293 K) is lower than that of water (ε_r = 80.10 at 293 K). Moreover it was reported that the value of pK_a in the 1:1 EtOH/water solution was 2.02;[10] this was smaller than that of pK_a in water. Therefore, it is expected that the equilibrium between H_2L^+ and HL at the interface will favor the neutral form, in comparison with the case in bulk aqueous phase.[21,22]

Interfacial complexation mechanism

Figure 2.6 shows the absorption spectra of 5-Br-PADAP and Pd(II)–5-Br-PADAP complex measured by the CLM method. From the result of batch experiments, we confirmed that Pd(II)–5-Br-PADAP complex was not extracted into the heptane phase. Moreover, the spectrum with the maximum at 580 nm obtained by the CLM method was

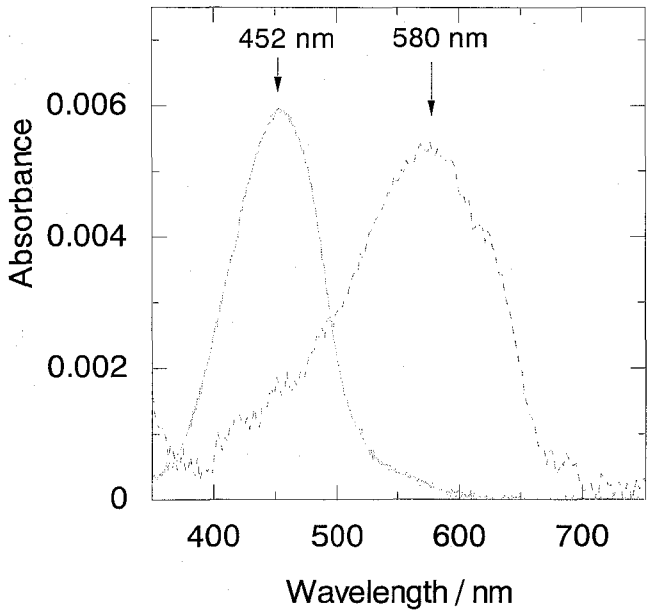

Figure 2.6. The absorption spectra of 5-Br-PADAP and Pd(II)–5-Br-PADAP complex in the centrifugal liquid membrane cell: (——) in the absence of Pd(II); $[HL]_T$ = 7.8×10^{-6} M, [Cl$^-$] = 0.1 M, pH 1.07: (-----) in the presence of Pd(II); $[Pd(II)]_T$ = 4.0×10^{-4} M in addition to the above condition.

different from the one in the aqueous phase that had two maximal absorption wavelengths at 575 nm and 620 nm.[23] Thus, we concluded that the spectrum obtained by the CLM method was ascribable to the interfacial complex and the concentration of Pd(II)–5-Br-PADAP complex in the aqueous phase in CLM system is negligibly smaller than that at the interface.[21] The absorbance at 580 nm was proportional to the interfacial concentration of Pd(II)–5-Br-PADAP complex. The observed absorbance in CLM method was correlated with the molar absorptivity at 580 nm of Pd(II)–5-Br-PADAP interfacial complex, ε_{580},

$$A = 2[\mathrm{PdL}]_i \varepsilon_{580} 10^3 = 2[\mathrm{PdL}]_i \frac{S_i}{V_a} \varepsilon_{580} b_a \qquad (2.14)$$

where V_a and b_a are the aqueous volume and the thickness of the aqueous phase in the CLM system, respectively. The plots of the absorbance at 580 nm vs. $[\mathrm{PdL}]_i S_i/V_a$ in the range of 1.7×10^{-6}-7.0×10^{-6} M gave the value of ε_{580} = 4.22×10^4 M^{-1} cm^{-1}.

Figure 2.7 shows a typical result of the complexation rate profile obtained by CLM method at the absorption maximum wavelengths of HL in the heptane phase (452 nm) and

Pd(II)–5-Br-PADAP complex at the interface (580 nm). As shown in this figure, the observed initial complexation rate (r^0_{obs}) was obtained from the initial slope of the absorbance increase at 580 nm.

Figure 2.8 shows that r^0_{obs} was proportional to the concentration of palladium(II) in the aqueous phase at pH 1.07. If the complexation reaction of Pd(II) with 5-Br-PADAP occurs only in the aqueous phase, the observed initial complexation rate is given by the following equation:

$$Pd(II) + HL \xrightarrow{k_{a,HL}} PdL^+ + H^+, \quad (2.15)$$

$$Pd(II) + H_2L^+ \xrightarrow{k_{a,H2L+}} PdL^+ + 2H^+, \quad (2.16)$$

$$r^0_{obs} = [Pd(II)]_T(k_{a,HL}[HL] + k_{a,H2L+} [H_2L^+])2\varepsilon_{580}b_a \quad (2.17)$$

where $k_{a,HL}$ and $k_{a,H2L+}$ are the rate constants for the reaction of Pd(II) with HL and H_2L^+ in the aqueous phase, respectively. The previous report revealed that the value of $k_{a,HL}$ and $k_{a,H2L+}$ were almost the same.[7] This seems to result in the protonation to N_β at azo-group, which did not directly coordinate to the metal ion. Thus, Eq. (2.17) is rewritten as

$$r^0_{obs} = k_a[Pd(II)]_T([HL] + [H_2L^+])2\varepsilon_{580}b_a \quad (2.18)$$

where $k_a = k_{a,HL} = k_{a,H2L+}$. The value of k_a was reported as 5.7×10^2 M^{-1} s^{-1}.[6] In the two-phase liquid membrane system, the total 5-Br-PADAP concentration is represented as

$$[HL]_T = [HL]_o + ([HL]+[H_2L^+])\frac{V_a}{V_o} + ([HL]_i + [H_2L^+]_i)\frac{S_i}{V_o} \quad (2.19)$$

The volumes of the aqueous phase and the organic phase are 0.250 cm^3 and 0.150 cm^3, respectively. When the total 5-Br-PADAP concentration is 7.8×10^{-6} M, [HL] and $[H_2L^+]$ can be calculated from Eq. (2.19) as 1.5×10^{-8} M and 1.1×10^{-6} M, respectively. The solid line in Figure 2.5 was calculated from Eq. (2.18) with these values. The slope of the solid line was about two times smaller than the experimentally observed one. This result suggests that the rate-determining step of the formation reaction of Pd(II)–5-Br-PADAP is not only the reaction in the aqueous phase; the interfacial reaction also has to be considered.

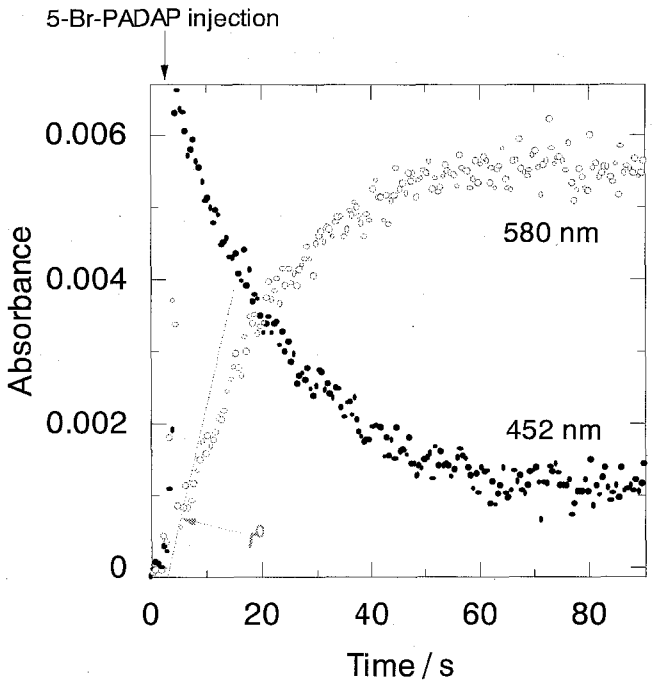

Figure 2.7. Typical kinetic profile observed by the centrifugal liquid membrane method for the complexation of Pd(II)–5-Br-PADAP complex: $[Pd(II)]_T = 4.0\times10^{-4}$ M, $[HL]_T = 7.8\times10^{-6}$ M, $[Cl^-] = 0.1$ M, pH 1.07.

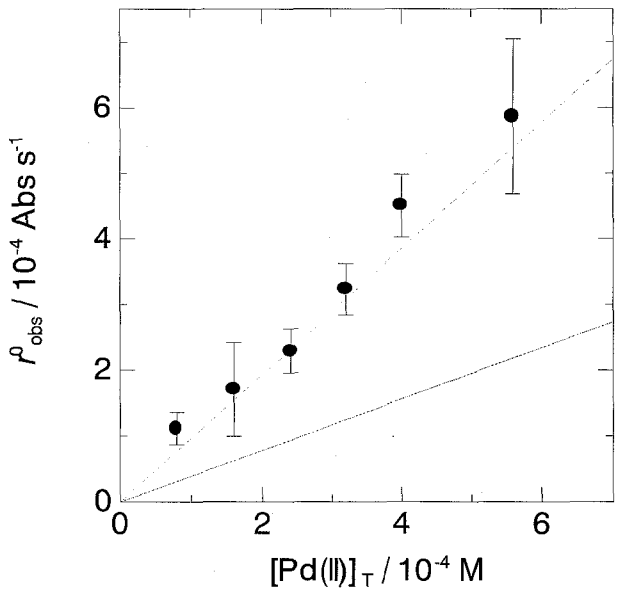

Figure 2.8. The dependency of the observed initial complexation rate (r^0_{obs}) on the concentration of Pd(II): $[HL]_T = 7.8\times10^{-6}$ M, $[Cl^-] = 0.1$ M, pH 1.07. The solid line is the hypothetical r^0_{obs}, provided that there is no interfacial reaction between Pd(II) and the interfacially adsorbed 5-Br-PADAP. The dashed line is the one calculated from Eq. (2.22) using the values of the estimated rate constants.

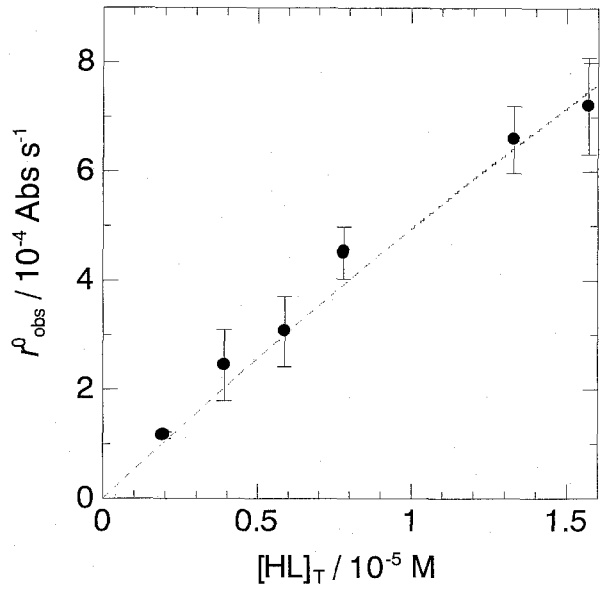

Figure 2.9. The dependency of the observed initial complexation rate (r^0_{obs}) on the total concentration of 5-Br-PADAP: $[Pd(II)]_T = 4.0\times10^{-4}$ M, $[Cl^-] = 0.1$ M, pH 1.07. The dashed line is the one calculated from Eq. (2.22) using the values of estimated rate constants.

Figure 2.9 shows the dependency of r^0_{obs} on the total 5-Br-PADAP concentration. As expected, the r^0_{obs} increased with the total 5-Br-PADAP concentration.

Figure 2.10 shows r^0_{obs} as a function of pH. The log r^0_{obs} values increased with the decrease in pH, because the concentration of 5-Br-PADAP in the aqueous phase and at the interface increased due to the protonation.

The experimental results suggest the complexation mechanism of Pd(II)–5-Br-PADAP in heptane/water system which is shown in Figure 2.11. The interfacial Pd(II)–5-Br-PADAP complex is formed through the following two pathways:

$$Pd(II) + HL_i \xrightarrow{k_{i,HL}} PdL_i + H^+ \qquad (2.20)$$

$$Pd(II) + H_2L^+_i \xrightarrow{k_{i,H2L+}} PdL_i + 2H^+ \qquad (2.21)$$

where $k_{i,HL}$ and $k_{i,H2L+}$ are the reaction rate constants for HL and H_2L^+ with Pd(II) at the interface, respectively. Thus, r^0_{obs} can be described as follows:

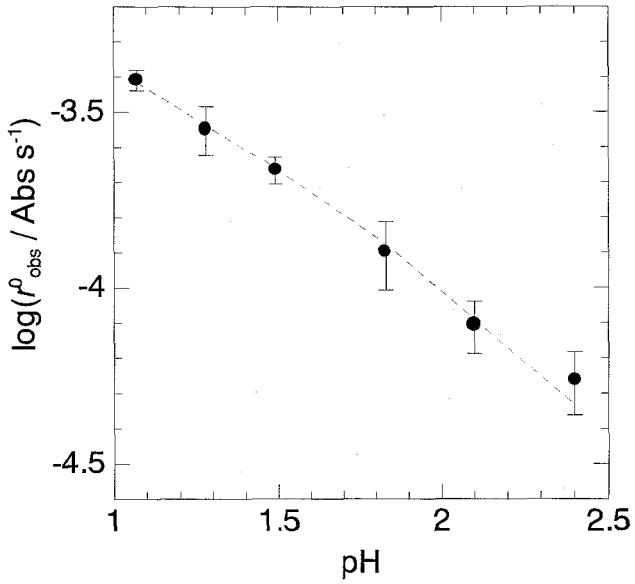

Figure 2.10. The observed initial complexation rate (r^0_{obs}) as a function of pH: $[Pd(II)]_T = 4.0\times10^{-4}$ M, $[HL]_T = 7.8\times10^{-6}$ M, $[Cl^-] = 0.1$ M. The dashed line is the one calculated from Eq. (2.22).

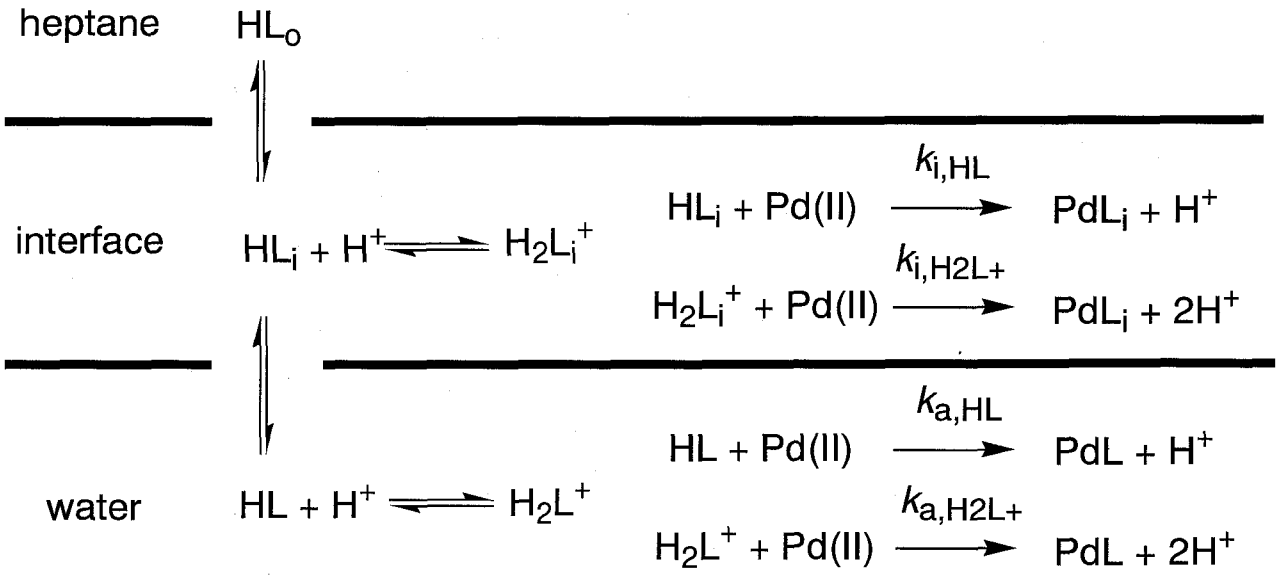

Figure 2.11. Kinetic scheme for the formation of the interfacial Pd(II)–5-Br-PADAP complex in the heptane/water system.

$$r^0_{obs} = [Pd(II)]_T\{k_a([HL]+[H_2L^+]) + (k_{i,HL}[HL]_i + k_{i,H2L+}[H_2L^+]_i)\frac{S_i}{V_a}\}2\varepsilon_{580}b_a \quad (2.22)$$

Because the value of k_a, $[Pd(II)]_T$ and the concentrations of 5-Br-PADAP in the various states are known, Eq. (2.22) can be rewritten as:

$$X = k_{i,HL}[HL]_i + k_{i,H2L+}[H_2L^+]_i \quad (2.23)$$

Here X is

$$X = \{\frac{r^0_{obs}}{[Pd(II)]_T 2\varepsilon_{580}b_a} - k_a([HL]-[H_2L^+])\}\frac{V_a}{S_i} \quad (2.24)$$

The value of X at each pH is obtained from the experimental results. Therefore, a matrix determinant can be introduced as:

$$\begin{pmatrix} X_{1.07} \\ X_{1.48} \\ X_{1.83} \\ X_{2.40} \end{pmatrix} = \begin{pmatrix} [HL]_{i,1.07} & [H_2L^+]_{i,1.07} \\ [HL]_{i,1.48} & [H_2L^+]_{i,1.48} \\ [HL]_{i,1.83} & [H_2L^+]_{i,1.83} \\ [HL]_{i,2.40} & [H_2L^+]_{i,2.40} \end{pmatrix} \begin{pmatrix} k_{i,HL} \\ k_{i,H2L+} \end{pmatrix} \quad (2.25)$$

where the subscript of the number is the value of each corresponding pH. The values of $k_{i,HL}$ and $k_{i,H2L+}$ were obtained from the solution of the matrix (2.25) as 5.3×10 M^{-1} s^{-1} and 5.1×10^2 M^{-1} s^{-1}, respectively. The values of $k_{i,H2L+}$ was somewhat larger than that of $k_{i,HL}$. It can be expected that the reaction of HL with Pd(II) at the interface is slower than that in the aqueous phase because of the solvation of HL by heptane molecules, while the reactivity of H_2L^+ will be similar to that in the aqueous phaase due to the lowering of such kind of solvation; H_2L^+ is probably adsorbed at the aqueous phase side of the interface. A similar tendency was obtained also in the reactions at the toluene/water interface[7] (Table 2.2). The dashed lines shown in Figures. 2.8, 2.9, and 2.10 are the ones calculated from Eq. (2.22) using the values

Table 2.2. The rate constants for the reaction of Pd(II) with the neutral and the protonated 5-Br-PADAP in the aqueous phase, at the heptane/water interface and at the toluene/water interface

	Nuertral 5-Br-PADAP (HL)	Protonated 5-Br-PADAP (H_2L^+)
Aqueous phase[7]	$k_{a,HL} = 5.7\times10^2\ M^{-1}\ s^{-1}$	$k_{a,H2L+} = 5.7\times10^2\ M^{-1}\ s^{-1}$
Heptane/water interface	$k_{i,HL} = 5.3\times10\ M^{-1}\ s^{-1}$	$k_{i,H2L+} = 5.1\times10^2\ M^{-1}\ s^{-1}$
Toluene/water interface[7]	$k_{i,HL} = 6.6\times10\ M^{-1}\ s^{-1}$	$k_{i,H2L+} = 3.3\times10^2\ M^{-1}\ s^{-1}$

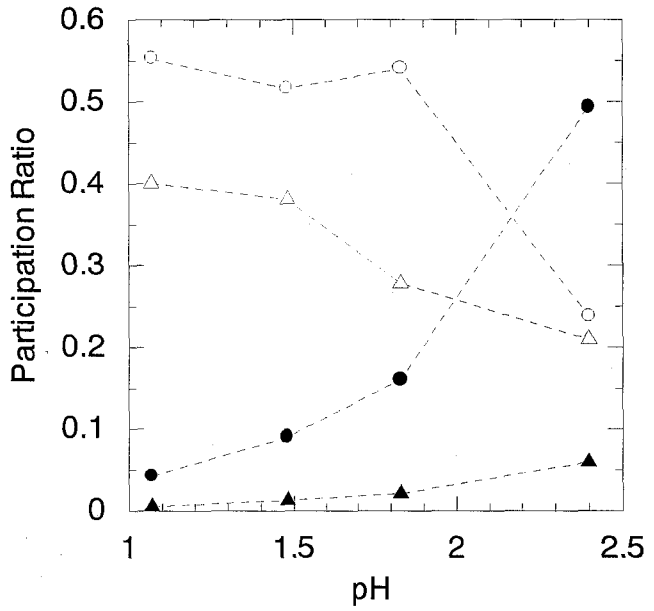

Figure 2.12. The participation ratio of calculated initial rate for each reaction to the r^0_{obs} as a function of pH; (△) the reactions of Pd(II) with H_2L^+ in the aqueous phase, (▲) with HL in the aqueous phase, (○) with H_2L^+ at the interface, and (●) with HL at the interface.

of the rate constants. The calculated curves were in fairly good agreement with the experimentally observed plots.

Figure 2.12 shows the participation ratio of the initial rate of each reaction of Eqs. (2.15), (2.16), (2.20), and (2.21) in the values of r^0_{obs} in Figure 2.10. The predominant reaction pathways at pH 1.07 were Eqs. (2.16) and (2.21), which were the reactions of palladium(II) with H_2L^+ in the aqueous phase and at the interface, respectively. This figure indicates that the reaction of palladium(II) with H_2L^+ in the aqueous phase cannot be ignored

in the heptane/water system, though it could be neglected in the toluene/water system, because of the high distribution constant of HL (log K_D = 4.78)[7]. However, the formation rates of Pd(II)–5-Br-PADAP complex were accelerated by the protonation of 5-Br-PADAP in both systems.

Conclusion

The acid-catalysis in the complexation of Pd(II) with 5-Br-PADAP in the heptane/water system was elucidated in this study. In this system, the complexation rate of Pd(II)–5-Br-PADAP was accelerated by H^+, because the 5-Br-PADAP concentrations in the aqueous phase and at the interface increased with the protonation to N_β at azo-group. The N_β at azo-group did not directly coordinate to Pd(II) ion, so that the reactivity of 5-Br-PADAP with Pd(II) was not affected by the protonation. Moreover, the rate constant for the reaction of protonated 5-Br-PADAP with Pd(II) at the interface was close to that in the aqueous phase. This suggested that the reactivity of H_2L^+ increased by the lowering of the solvation of H_2L^+ by heptane molecules at the interface. This suggestion seems to be supported by the result that the equilibrium between H_2L^+ and HL at the interface will favor the neutral form in comparison with the case in bulk aqueous phase; pK_a 2.95, p$K_{a,i}$ 1.3.

The centrifugal liquid membrane method using the modified cell was applied to the kinetic study of the formation of interfacial Pd(II)–5-Br-PADAP complex in the heptane/water system. It was demonstrated that this cell was very useful for the measurement of relatively fast interfacial reactions. The formation rate of Pd(II)–5-Br-PADAP complex that existed only at the liquid-liquid interface could be measured directly by the centrifugal liquid membrane method and the interfacial formation rate constants were determined.

References

1. *Liquid-Liquid Interfaces. Theory and Methods*; eds by Volkov, A. G.; Deamer, D. W., Eds.; CRC Press: Boca Raton, FL, 1996.
2. Watarai, H. *Tre. Anal. Chem.* **1993**, *12*, 313.
3. Watarai, H.; Cunningham, L.; Freiser, H. *Anal. Chem.* **1982**, *54*, 2390.
4. Watarai, H.; Sasaki, K.; Takahashi, K.; Murakami, J. *Talanta* **1995**, *42*, 1691.
5. Onoe, Y.; Tsukahara, S.; Watarai, H. *Bull. Chem. Soc. Jpn.* **1998**, *71*, 603.
6. Watarai, H.; Gotoh, M.; Gotoh, N. *Bull. Chem. Soc. Jpn.* **1997**, *70*, 957.
7. Ohashi, A.; Tsukahara, S.; Watarai, H. *Anal. Chim. Acta* **1998**, *364*, 53.
8. Nagatani, H.; Watarai, H. *Anal. Chem.* **1998**, *70*, 2860.
9. Nagatani, H.; Watarai, H. *Chem. Lett.* **1999**, 701.
10. Johnson D. A.; Florence, T. M. *Talanta* **1975**, *22*, 253.
11. Wang, H.; Miao, Y.; Zhang, H.; Cheng, J. *Talanta* **1994**, *41*, 685.
12. Oxspring, D. A.; Maxwell, T. J.; Smyth, W. F. *Anal. Proc.* **1995**, *32*, 489.
13. Busev, S. I.; Vin'kova, V. A. *Zh. Anal. Khim.* **1967**, *22*, 552.
14. Elding, L. I. *Inorg. Chim. Acta* **1972**, *6*, 647.
15. The value of total interfacial area (S_i) in the toluene/water system was substituted for the one in the present system.
16. Ueno, K.; Imamura T.; Cheng, K. L. *Handbook of Organic Analytical Reagents* 2nd ed.; CRC Press: Boca Raton, 1992, pp237-243.
17. Shibata, S.; Furukawa, M. *Bunseki Kagaku* **1974**, *23*, 1412.
18. K. Kawai, H. Masago, K. Kanamori, I. Kanesaka, I. Kasahara, and K. Goto, *J. Raman Spectrosc.*, **18**, 205 (1987).
19. Tsukahara, S.; Yamada, Y.; Watarai, H. *Langmuir* **2000**, *16*, 6787.
20. Watarai, H.; Satoh, K. *Langmuir* **1994**, *10*, 3913.
21. Perera, J. M.; Stevens, G. W.; Grieser, F. *Colloids Surf. A* **1995**, *95*, 185.
22. Bessho, K.; Uchida, T.; Yamauchi, A.; Shioya, T.; Teramae, N. *Chem. Phys. Lett.* **1997**, *264*, 381.
23. Po, C. Y.; Nan, Z. *Talanta* **1986**, *33*, 939.
24. Ohashi, A.; Watarai, H. *Chem. Lett.* **2001**, 1238.

Chapter 3

Resonance Raman Spectroscopic Detection of Pyridylazo Complex Formed at Liquid-Liquid Interface in Centrifugal Liquid Membrane System

Introduction

Liquid-liquid interface is expected to be an effective reaction or synthetic field, because the concentration of adsorbate at the interface is used to become higher than those in bulk phases.[1-2] Recently, several spectroscopic methods to measure interfacial species directly have been reported.[3-5] But, there are few reports[6-8] in which vibrational spectroscopy such as Raman spectroscopy has been applied to the measurement of the liquid-liquid interface, though the vibrational spectroscopy is highly informative for the discussion of structural properties of a sample.

In the present study, a new Raman spectroscopic method was proposed for the detection of the interfacial complex formed between Pd(II) and 5-Br-PADAP[9] in the heptane/water system; the Raman microscopy was combined with the centrifugal liquid membrane (CLM) method,[10] that could make a stable and thin two-phase liquid membrane and could reduce the undesirable Raman scattering from bulk phases.

Experimental

Reagents

5-Br-PADAP, 2-(5-bromo-2-pyridylazo)-5-(N-propyl-N-sulfopropylamino)phenol (5-Br-PAPS) disodium salt (Dojindo Laboratories), malachite green (MG) oxalate (G.R., Wako Pure Chemicals) and palladium(II) chloride (99.99%, Wako Pure Chemicals) were used as purchased. Stock solutions of $PdCl_2$ and 5-Br-PADAP were prepared by dissolving them in 0.1 mol dm^{-3} hydrochloric acid and heptane, respectively, and those of 5-Br-PAPS and MG were prepared with pure water. MG and 5-Br-PAPS were used as the indicators to measure the positions of an inner surface of the cylindrical cell and the bulk aqueous phase, respectively. Heptane (G.R., Katayama Chemical) was purified with same means in Chapter 2.[11] Water was purified by a Millipore Milli-Q SP.TOC.

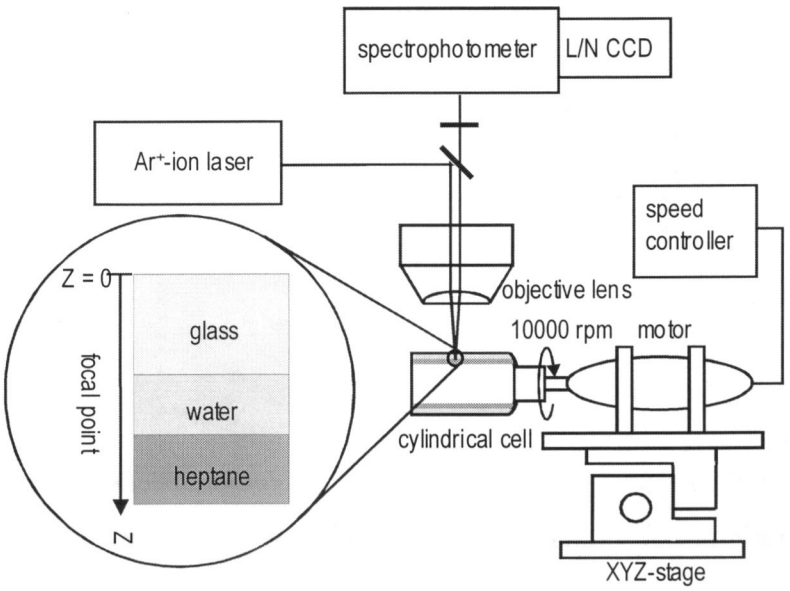

Figure 3.1. Schematic drawing of the apparatus for CLM-Raman microprobe spectroscopy.

Resonance Raman spectra measurements

Figure 3.1 shows the apparatus of Raman microscopy combined with CLM cell. The heptane solution and the aqueous solution were put into the cylindrical cell, whose height and outer diameter were 3.3 and 2.1 cm, respectively. The cylindrical cell was placed horizontally under the objective lens (Mitutoyo, 45×, NA 0.55) and rotated at about 10000 rpm by the high-speed motor (Nakanishi Inc., NK-260) fixed on a XYZ-stage. The heptane phase was spread as an inner liquid membrane and the aqueous phase as an outer liquid membrane by a centrifugal force under the rotating condition. The apparatus of Raman microscopy that contained an Ar^+-ion laser (Spectra-Physics, Stabilite 2017), a liquid-nitrogen-cooled/CCD detector (Roper Scientific, LN/CCD-1100-PB/UVAR/1) and a spectrophotometer (Jobin Yvon, HR-320) was constructed by Photon Design (Japan). The laser beam of 514.5 nm wavelength was focused into the sample through the objective lens. The scattering light was collected by the same objective lens. The focal point was moved along the Z-axis, which was perpendicular to the interface, in the range from 530 and 925 μm by controlling the height of XYZ-stage. The position of $Z = 0$ was defined at an outer surface of the cylindrical cell. The laser power was kept at 40 mW. To improve the S/N ratio and to reduce the photo-breaching of reagents, the exposure time was chosen as short as 15 s. The concentrations of 5-Br-PADAP, $PdCl_2$ and 5-Br-PAPS were 1.7×10^{-5}, 3.3×10^{-4} and

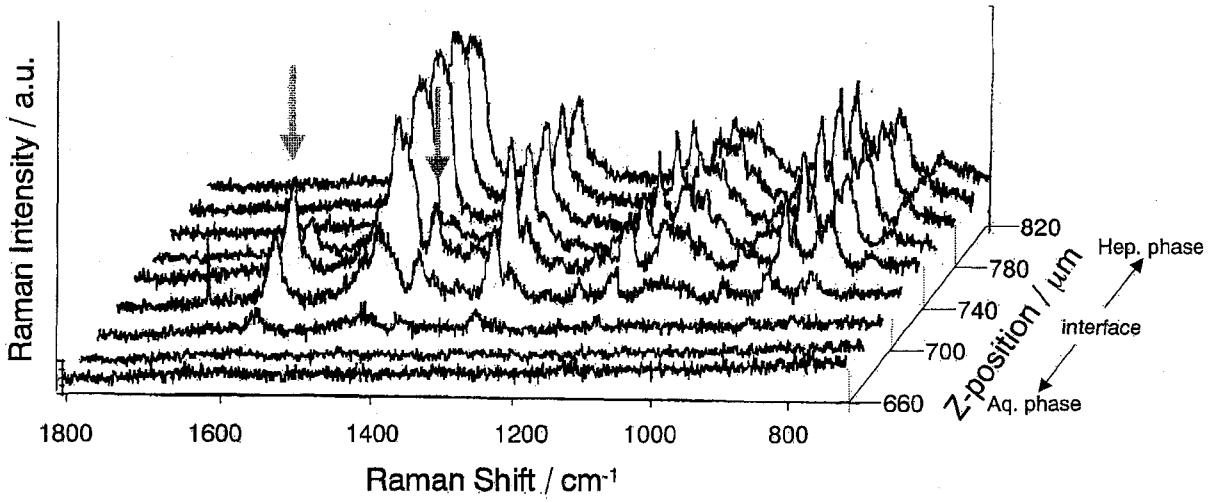

Figure 3.2. Raman spectra at various focal points obtained by CLM-Raman microprobe spectroscopy. [Pd(II)] = 3.3×10^{-4} M, [HL] = 3.8×10^{-5} M, [Cl$^-$] = 0.1 M, pH 1.0, $V_a = V_o = 0.300$ cm^3.

1.0×10^{-4} mol dm^{-3}, respectively. Ionic strength was adjusted at 0.1 mol dm^{-3} with HCl or $NaClO_4$. The volumes of the heptane phase and the aqueous phase were fixed at 0.300 cm^3. Moreover, the measurement was carried out with a cylindrical cell in which MG adsorbed at the inner surface in order to determine its position. The MG adsorbed cell was prepared in the following ways; the MG aqueous solution of 1.1×10^{-2} mol dm^{-3} was introduced into the cylindrical cell, and after a few minutes, it was taken out, and then the cell was dried in an oven. All measurements were carried out in the thermostated room at 298±2 K. Absorption spectrum of Pd(II)–5-Br-PADAP complex was also measured by CLM method with V-570 UV/VIS/NIR spectrophotometer (Jasco).

Results and Discussion

From the result of batch experiments, we confirmed that Pd(II)–5-Br-PADAP complex was not extracted into the heptane phase. Therefore, we thought that the spectrum obtained by CLM method was ascribable to the interfacial complex.[11] The absorption spectrum of Pd(II)–5-Br-PADAP complex has a broad peak at 580 nm and the absorbance at 514.5 nm was enough for the resonance Raman spectroscopy as shown in Figure 2.3. Figure

3.2 shows the depth profile of Raman spectrum in two-phase system observed using 0.300 cm^3 as the volumes of both phases. Strong peaks of Pd(II)-5-Br-PADAP complex formed at the interface were appeared around 1405 and 1597 cm^{-1}. Figures 3.3a, 3.3b and 3.3c show Raman spectra observed at the three different focal points of Z = 660, 740 and 820 μm, which corresponded to the bulk aqueous phase, the interface and in the bulk heptane phase, respectively. Raman spectrum from the heptane phase (Z = 820 μm) was mainly that of heptane itself. Figure 3.3d shows the interfacial Raman spectrum (Z = 740 μm) which was obtained by subtracting the spectrum in the absence of the complex from that in the presence of the complex. This spectrum was due to Pd(II)–5-Br-PADAP complex formed at the heptane/water interface. The bands at 1597, 1473, 1403 and 1303 cm^{-1} were assigned to the benzene and pyridine rings, pyridine rings, N=N, and CNNC stretchings, respectively.[12-15]

The relative Raman intensities of Pd(II)–5-Br-PADAP complex (1597 cm^{-1}) and heptane (902 cm^{-1}) were profiled along the Z-axis (Figure 3.4a). Moreover, the relative Raman intensities of MG (1617 cm^{-1}) that was adsorbed at the inner surface of the cylindrical cell and 5-Br-PAPS (1623 cm^{-1}) dissolved in the aqueous phase, which have the absorbance at 514.5 nm, were profiled for comparison (Figure 3.4b and 3.4c). The maximum in the Raman intensity of MG appeared at Z = 600 μm where was the position of the inner wall of the cell. On the other hand, the Raman intensity of 5-Br-PAPS, which existed in the aqueous phase, was distributed in the range of 600-740 μm with a broad maximum around 680 μm. The profile for Pd(II)–5-Br-PADAP complex was clearly different from both of MG and 5-Br-PAPS, having a maximum at Z = 740 μm (interface). The plots of the relative Raman intensities of MG and of Pd(II)–5-Br-PADAP complex in Figure 3.4 were fitted to Gaussian curve and the average values of Z-position were obtained as 605±30 and 743±26 μm, respectively. These values indicated the positions of the inner surface and the heptane/water interface. The relatively large deviations seemed to result from the vibration of the cylindrical cell under the high-speed rotation, because the depth resolution of Raman microscopy was obtained as 4 μm from the measurement of the dependency of the Raman intensity of silicon on the distance from the silicon surface to the focal point (data not shown). The average values gave the thickness of the aqueous phase under the CLM condition as 138 μm. This value was close to 154 μm, which value was calculated from the volume of the aqueous phase. These results confirmed that Pd(II)–5-Br-PADAP complex existed only at the heptane/water interface in the CLM system.

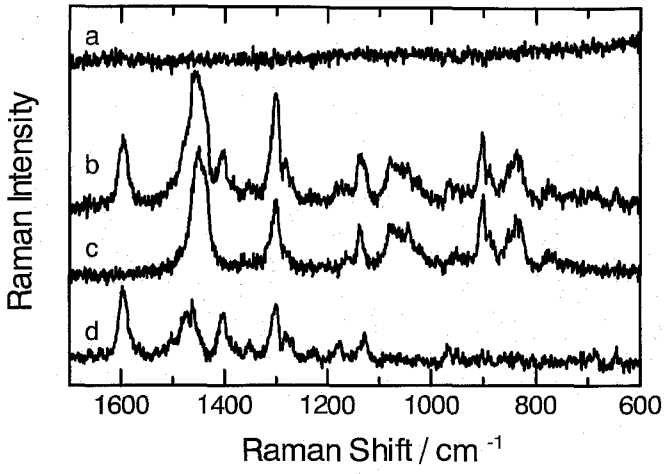

Figure 3.3. Raman spectra measured at the various focal points by CLM-Raman microprobe spectroscopy. aqueous phase: $PdCl_2$ 3.3×10^{-4} mol dm^{-3}, HCl 0.1 mol dm^{-3}, pH 1.0; heptane phase: 5-Br-PADAP 1.7×10^{-5} mol dm^{-3}. The volumes of both phases were 0.300 cm^3. Z-position of the focal point: (a) 660 μm (the aqueous phase), (b) 740 μm (the interface), (c) 820 μm (the heptane phase). (d) the difference spectrum between the spectra in the presence of Pd(II)–5-Br-PADAP complex and the absence of the complex at Z = 740 mm.

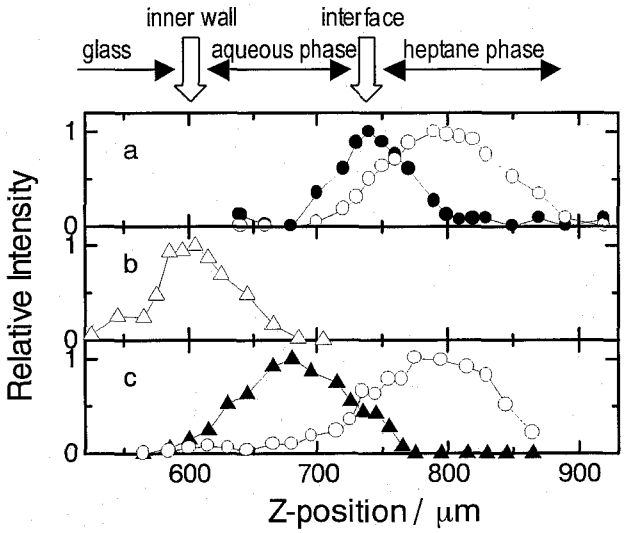

Figure 3.4. Depth profiles of the relative Raman intensities along the Z-axis under the various systems. ●: Pd(II)–5-Br-PADAP complex (1597 cm^{-1}), ○: heptane (902 cm^{-1}), △: MG (1617 cm^{-1}), ▲: 5-Br-PAPS (1623 cm^{-1}). (a) experimental conditions were same in Figure 3.2. (b) MG was adsorbed at the inner surface of the cylindrical cell, and no solution. (c) 5-Br-PAPS 1.0×10^{-4} mol dm^{-3}, $NaClO_4$ 0.1 mol dm^{-3}, pH 6.8, in the aqueous phase. Each volume of the aqueous phase and the heptane phase was 0.300 cm^3.

Conclusion

It was demonstrated in the present study that CLM-resonance Raman microprobe spectroscopy was very useful for the measurement of the interfacial species as well as the bulk species for the first time. This method allowed us to obtain the spatial distribution of the chemical species around the liquid-liquid interface. Moreover, in the present method, photo-breaching of the ligand and complex was reduced by the rotation of the cell; the decrease of resonance Raman intensity was less than 10% after the irradiation of 240 s. This method can be applied to the studies of various interfacial reaction systems such as complexation kinetics and redox reaction.

References

1. *Liquid Interfaces in Chemistry and Biology*; Volkov, A. G.; Deamer, D. W.; Tanelian D. L.; Markin, V. S., Eds.; John Wiley & Sons CRC Press, Chicester, 1998.
2. *Liquid-Liquid Interfaces. Theory and Methods*; Volkov, A. G.; Deamer, D. W., Eds.; CRC Press: Boca Raton, FL, 1996.
3. H. Watarai, In *Liquid Interfaces in Chemical, Biological, and Pharmaceutical Applications*; Volkov, A. G., Ed.; Marcel Dekker, New York, 2001.
4. Corn, R. M.; Higgins, D. A. *Chem. Rev.* **1994**, *94*, 107.
5. Zheng, X. Y.; Harata, A. *Anal. Sci.* **2001**, *17*, 131.
6. T. Takenaka and T. Nakanaga, *J. Phys. Chem.* **1976**, *80*, 475.
7. H.G.M. Edwards, M.A. Hughes, and D.N. Smith, *Vib. Spectrosc.*, **1996**, *10*, 281.
8. Conboy, J. C.; Messmer, M. C.; Richmond, G. L. *J. Phys. Chem.* **1996**, *100*, 7617.
9. D.A. Johnson and T.M. Florence, *Talanta* **1975**, *22*, 253.
10. H. Nagatani and H. Watarai, *Anal. Chem.* **1998**, *70*, 2860.
11. A. Ohashi and H. Watarai, *Anal. Sci.* **2001**, *17*, 1313.
12. Drozdzewski, P. M. *Spectrochim. Acta* **1985**, *41*, 1035.
13. Drozdzewski, P. M. *J. Raman Spectrosc.* **1988**, *19*, 111.
14. Dines, T. J.; Wu, H. *J. Chem. Soc. Faraday Trans.* **1995**, *91*, 463.
15. K. Kawai, H. Masago, K. Kanamori, I. Kanesaka, I. Kasahara, and K. Goto, *J. Raman Spectrosc.*, **18**, 205 (1987).

Chapter 4

Azo-Imine Resonance in Palladium(II)–Pyridylazo Complex Adsorbed at Liquid-Liquid Interface Studied by Centrifugal Liquid Membrane-Resonance Raman Microprobe Spectroscopy

Introduction

Adsorption and reaction at the liquid-liquid interface have become attractive subjects in relation to solvent extraction kinetics of metal ions, molecular recognition in the biological membrane system and the interfacial synthesis.[1,2] Information on the adsorbates at the liquid-liquid interface, such as the interfacial concentration, solvation or orientation, has been investigated by various indirect and direct measurement methods, e.g., an interfacial tension measurement,[3] a high-speed stirring method,[4-8] an attenuated total internal reflection (ATR) spectroscopy,[9] a total internal reflection fluorometry (TIRF),[10-12] a total internal reflected resonance light scattering (TIR-RLS),[13] an external reflection (ER) spectroscopy,[14] and a second harmonic generation (SHG) spectroscopy.[15] However, there are few studies that applied vibrational spectroscopy except for some uses of resonance Raman spectroscopy[16,17] and sum frequency generation (SFG),[18,19] though the vibratinoal spectroscopy is highly sensitive for the structural properties of an adsorbate.

Our laboratory has developed an *in situ* spectrophotometric method, a centrifugal liquid membrane (CLM) method,[20] to measure the interfacial species. This method utilizes an ultra-thin two-phase liquid membrane in a rotating optical cell by a centrifugal force and can directly measure the interfacial species by spectrophotometry[20-22] or fluorometry.[23] Recently, we have developed a new microscopic method, named as a centrifugal liquid membrane-resonance Raman microprobe spectroscopy (CLM-RRMS),[24] that was a combination of Raman spectromicroscopy having a high spatial resolution with CLM method. This method allowed us to obtain each information of the interface and the bulk phases in the CLM system.

2-(5-Bromo-2-pyridylazo)-5-diethylaminophenol (5-Br-PADAP or HL) has been known as a highly sensitive reagent for various metal ions, because it forms stable and colored complexes with metal ions as a trident ligand.[25,26] It was reported that 5-Br-PADAP formed a complex with Pd(II) with the mole ratio of 1:1[5,26] and this complex had a high

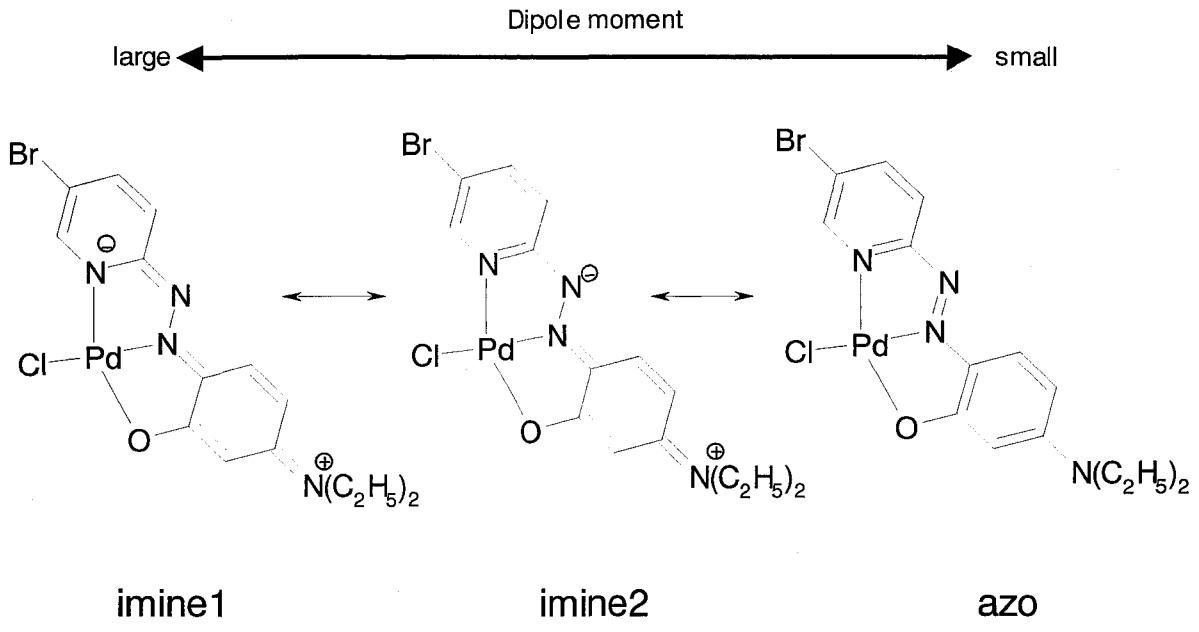

Figure 4.1. Proposed resonance structure of Pd(II)-5-Br-PADAP complex.

adsorptivity at toluene/water and heptane/water interfaces.[5,21] It has been thought that Pd(II)–5-Br-PADAP complex exists as a mixture of three resonance forms as shown in Figure 4.1 and the ratio of imine and azo forms depends on the dielectric constant of solvents.[25]

In the present study, we measured resonance Raman spectra of the complexes of Pd(II) with 5-Br-PADAP at toluene/water and heptane/water interfaces by CLM-RRMS and compared with those in various solvents to investigate the electronic state of Pd(II)–5-Br-PADAP complex at the interface.

Experimental

Chemicals

5-Br-PADAP (Dojindo Laboratory and Tokyo Kasei) was used as purchased and dissolved in toluene, heptane and ethanol. Toluene (G.R., Nacalai Tesque) and heptane (G.R., Katayama Chemical) were purified with same means in the literature.[5,21] Stock solution of palladium(II) was prepared by dissolving palladium(II) chloride (99.99%, Wako Pure Chemicals) in 0.1 M chloride acid. A PdLCl toluene solution was prepared by the extraction from 1.0×10^{-3} M palladium(II) chloride in the 0.1 M hydrochloric acid with

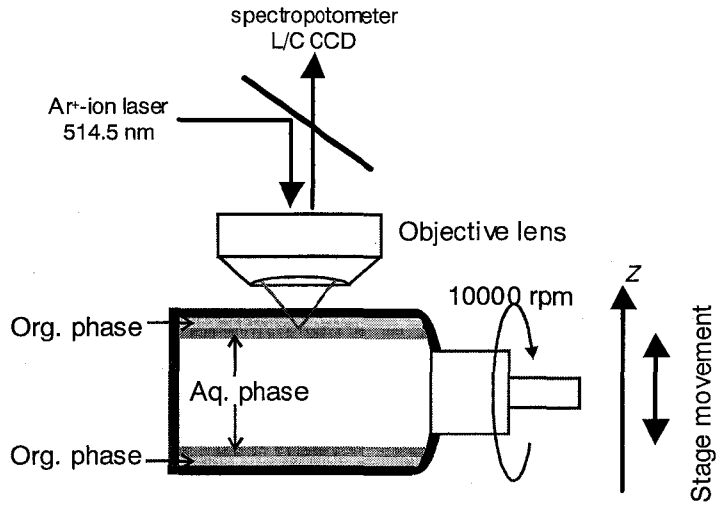

Figure 4.2. Schematic drawing of the centrifugal liquid membrane-resonance Raman microprobe spectroscopy (CLM-RRMS).

5.6×10^{-5} M 5-Br-PADAP in toluene. PdLCl solutions of ethanol, acetone, 1-butanol, 1-octanol and chloroform were prepared by dissolving a weighted PdLCl powder, which was obtained from the PdLCl toluene solution by the evaporation of solvent to dryness on a heated desiccator. Ethanol-water (50, 70, 90%) solutions of PdLCl were prepared by the addition of $PdCl_2$ aqueous solution into 5-Br-PADAP ethanol solution: the concentrations of palladium(II) ion, hydrochloric acid and 5-Br-PADAP were kept at 1.0×10^{-4} M, 1.0×10^{-2} M and 4.6×10^{-5} M, respectively. All HL reacted with Pd(II) and formed PdLCl complex. Ethanol (G.R., Katayama Chemical), acetone (E.R., Katayama Chemical), 1-butanol (G.R., Nacalai Tesque), 1-octanol (G.R., Tokyo Kasei) and chloroform (G.R., Aldrich) were used as purchased. Water was distilled and deionized with a Milli-Q system (Milli-Q SP.TOC., Millipore).

Resonance Raman measurement

Direct measurements of resonance Raman spectra of PdLCl adsorbed at the interfaces were carried out by CLM-RRMS, whose apparatus was the same as the one reported previously[24] and schematically shown in Figure 4.2. In the measurement of toluene/water system, 0.300 cm^3 of aqueous solution (0.01 M $HClO_4$ and 0.09 M $NaClO_4$) and 0.300 cm^3 of toluene solution (5.6×10^{-5} M PdLCl) were introduced into the cylindrical cell of 3.3 cm height and 2.1 cm outer diameter. In heptane/water system, 0.250 cm^3 of aqueous solution of 4.0×10^{-4} M $PdCl_2$ in 0.1 M hydrochloric acid and 0.150 cm^3 of heptane solution of

7.4×10^{-6} M HL were used. The cylindrical cell was placed horizontally under the objective lens (Mitutoyo, 45×, NA 0.55) and rotated at about 10000 rpm by the high-speed motor (Nakanishi Inc., NK-260) fixed on a XYZ-stage (Suruga Seiki, B72-60C). The laser beam of 514.5 nm wavelength from an Ar^+-ion laser (Spectra-Physics, Stabilite 2017) was focused into the two-phase liquid membrane system through the objective lens. The scattering light was collected by the same objective lens and was led to a spectrophotometer (Jobin Yvon, HR-320) with a liquid-nitrogen-cooled/CCD detector (Roper Scientific, LN/CCD-1100-PB/UVAR/1). The focal point was moved along the *Z*-axis, which was perpendicular to the interface, in the range from 600 to 900 μm by controlling the height of XYZ-stage, which was moved in a 10-μm interval. The outer surface of the cylindrical cell was defined as $Z = 0$. The value of *Z* of the liquid-liquid interface in the heptane/water system was determined by measuring the distribution of Raman scattering intensity of PdLCl, which existed only at the interface. When the volume of the aqueous phase was changed from 0.250 cm^3 to 0.300 cm^3 under the constant heptane phase of 300 cm^3, the *Z* value giving a maximum intensity of Raman scattering shifted from $Z = 720$ to 740 μm. The maximum position was assigned to the liquid-liquid interface. The resolution of Z-direction, which was obtained from the distribution of Raman scattering intensity of PdLCl, was about 28 μm. This relatively poor resolution seemed to result from the vibration of the cylindrical cell under the high-speed rotation, because the depth resolution of the present Raman microscopy was obtained as 4 μm from the measurement of the depth profile of the Raman intensity of a silicon surface.

Resonance Raman spectra of PdLCl in various solvents were measured by the same Raman microscopy that was described above, with a sample stage of microscopy instead of XYZ-stage. A PdLCl solution in a 1-cm quartz cell was put under the object lens lain on the stage. The PdLCl concentrations of various solutions were about in the range of $(3.0\text{-}4.5)\times10^{-5}$ M. The Raman spectrum of each solvent was also measured and it was subtracted from each spectrum in the presence of PdLCl to obtain the spectrum of PdLCl. The laser power was fixed at 40 mW. The exposure time was selected at 50 s. The observed frequencies were calibrated with respect to Raman peaks of toluene and were accurate to within ±2 cm^{-1}. All measurements were carried out in the thermostated room at 298±2 K.

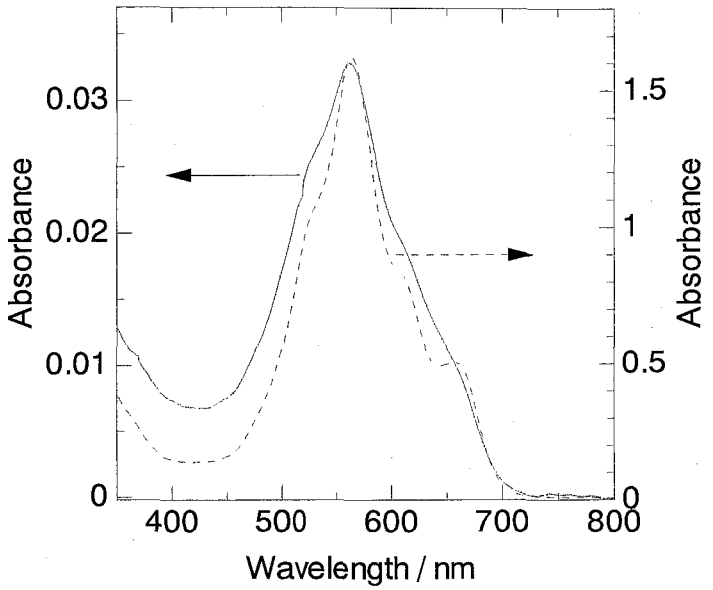

Figure 4.3. Absorption spectra of PdLCl in the toluene/water two-phase liquid membrane (——) and in toluene solution (---). toluene/water liquid membrane system: V_a = 0.250 cm^3, V_o = 0.150 cm^3, $[PdLCl]_T = 5.6\times10^{-5}$ M, $[ClO_4^-]$ = 0.1 M, pH 2.0; toluene solution: $[PdLCl]_T = 2.3\times10^{-5}$ M.

Absorption spectral measurement

Absorption spectra of PdLCl in various solvents and two-phase liquid membrane of toluene/water system produced by CLM were measured with an UV/VIS spectrophotometer (Jasco, V-570). Absorption spectral measurement by CLM was described in the literatures in detail.[21,22] The experimental conditions in CLM measurements were as follows: the volumes of the aqueous phase and the toluene phase were 0.250 and 0.150 cm^3, respectively, the concentrations of PdLCl and ClO_4^- were 5.6×10^{-5} M and 0.1 M, respectively, and pH was 2.0.

Results and Discussion

Resonance Raman spectra of PdLCl adsorbed at the liquid-liquid interface

The absorption spectrum of PdLCl in toluene/water system measured by the CLM method was slightly different from the one in toluene solution as shown in Figure 4.3. This implied that PdLCl adsorbed at the interface was in a different environment than in toluene. But it was difficult to take out only the spectrum of the interface, because the absorption spectrum measured by the CLM method was the sum of the interface and the bulk phases.

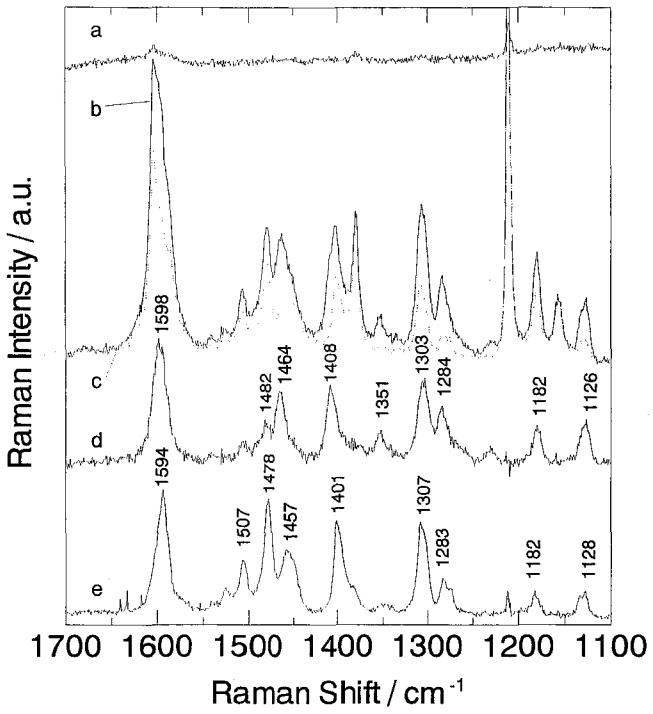

Figure 4.4. Raman spectra in the toluene/water system measured at the various focal points by CLM-RRMS. $V_a = V_o = 0.300$ cm^3, $[PdLCl]_T = 5.1\times10^{-5}$ M, $[ClO_4^-] = 0.1$ M, pH 2.0. Z-position: (a) 660 mm (the aqueous phase), (b) 740 mm (the interface), (c) 820 mm (the toluene phase). The spectra (b) and (c) were normalized at the Raman intensity of 1210.5 cm^{-1}. (d) the difference spectrum between the spectra (b) and (c) after the normalization. (e) resonance Raman spectrum of PdLCl in the toluene solution after subtracting the Raman spectrum of toluene.

Figures 4.4a-4.4c show Raman spectra observed in the toluene/water system at the three different focal points of Z = 660, 740 and 820 μm, which corresponded to the bulk aqueous phase, the interface and the bulk toluene phase, respectively. The Raman spectra obtained at Z = 740 μm and Z = 820 μm were normalized with the Raman intensity at 1210.5 cm^{-1}, the Raman shift of toluene. Raman spectra from the aqueous phase (Z = 660 μm) and the toluene phase (Z = 820 μm) contained the information of only the aqueous phase and the toluene phase, respectively. On the other hand, Raman spectrum from Z = 740 μm contained the information of the interface and both bulk phases. Raman intensity from the aqueous phase was almost negligible in the present condition. Subtracting Raman spectrum at Z = 820 μm from the one at Z = 740 μm after the normalization gave the spectrum of the toluene/water interface (Figure 4.4d). This spectrum was thought from PdLCl adsorbed at

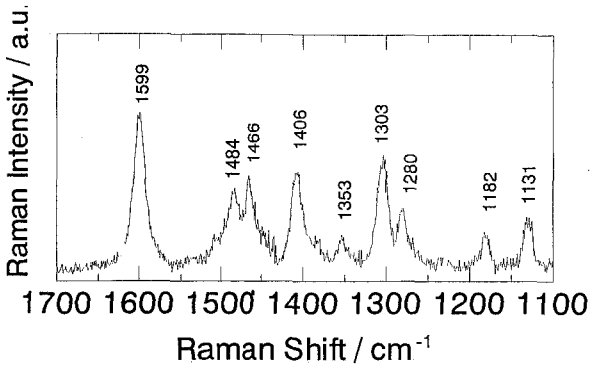

Figure 4.5. Resonance Raman spectrum of PdLCl formed at the heptane/water interface measured by CLM-RRMS. V_a = 0.250 cm^3 V_o = 0.150 cm^3, $[Pd(II)]_T$ = 4.0×10^{-4} M, $[HL]_T$ = 7.4×10^{-6} M, $[Cl^-]$ = 0.1 M, pH 1.0, Z = 720 mm.

Table 4.1. Observed Raman shifts (cm^{-1}) of PdLCl at the liquid-liquid interface and in toluene solution

Toluene	Toluene/water interface	Heptane/water interface
1594(100)[a]	1598(100)	1599(100)
1507(43)	1504(18)	
1478(93)	1482(37)	1484(52)
1457(54)	1464(58)	1466(60)
1401(77)	1408(64)	1406(63)
1349(13)	1351(28)	1353(22)
1307(82)	1303(69)	1303(73)
1283(29)	1284(47)	1280(40)
1182(24)	1182(29)	1182(24)
1128(22)	1126(36)	1131(34)

[a] Relative intensity

the toluene/water interface. Figure 4.4e is the resonance Raman spectrum of PdLCl in toluene solution after subtracting Raman spectrum of toluene. The Raman spectrum of PdLCl adsorbed at the toluene/water interface was basically similar to that of PdLCl in the toluene solution, but was largely different in the region from 1490 to 1420 cm^{-1}. Raman shift of each solution is listed in Table 4.1.

Figure 4.5 shows the resonance Raman spectrum of PdLCl complex formed at the heptane/water interface measured by CLM-RRMS (Z = 720 μm). As for this Raman spectrum, Raman spectrum of heptane was already subtracted. The Raman shifts are also

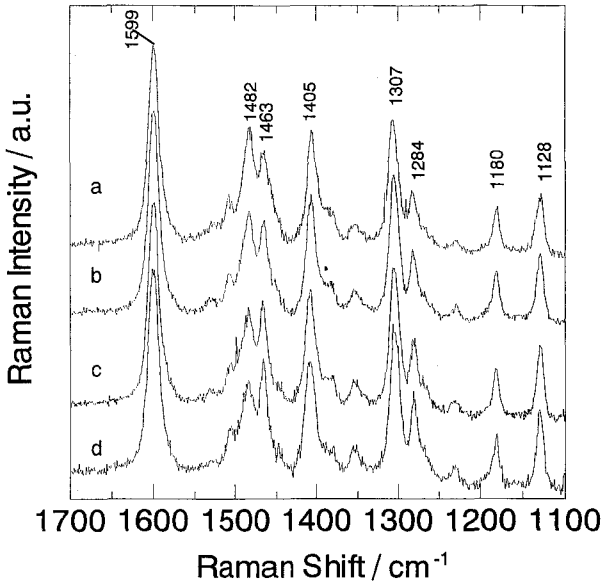

Figure 4.6. Resonance Raman spectrum of PdLCl in various EtOH-water mixture. (a) 100% EtOH [PdLCl] = 5.1×10^{-5} M, (b) 90% EtOH, (c) 70% EtOH (d) 50% EtOH, (b)-(d) [Pd(II)] = 1.0×10^{-3} M, [HL] = 4.6×10^{-5} M, [HCl] = 0.01 M.

listed in Table 4.1. The Raman shifts and relative Raman intensity of the resonance Raman spectrum of PdLCl at the heptane/water interface were similar to the ones at the toluene/water interface. This similarity suggests that electronic states of PdLCl at the toluene/water and heptane/water interface were similar to each other.

Electronic configuration of PdLCl at the liquid-liquid interface

In order to discuss the configuration of PdLCl at the toluene/water and heptane/water interface, resonance Raman spectra of PdLCl in various solvents were measured. Figures 4.6a-4.6d show the resonance Raman spectra of PdLCl in EtOH-water mixed solvent with various compositions. Dielectric constants and observed Raman shifts are listed in Table 4.2. As the percentage of water increased, in other words, a dielectric constant of solution increased, Raman intensity around 1482 cm^{-1} decreased and that around 1463 cm^{-1} increased. It was thought that this spectral change was caused by the change of the ratio of azo and imine resonance structures. In the resonance Raman spectrum in toluene solution, which has the lowest dielectric constant (ε_r = 2.379) in the present experiment, Raman intensity at 1478 cm^{-1} was stronger than that at 1457 cm^{-1}. This tendency agreed with that measured in EtOH-water system. Relative changes of Raman intensity of the two bands corresponded to

Table 4.2. Observed Raman shifts of PdLCl in various solvents

Wavenumber / cm^{-1}								Assignment
50%EtOH (48.9)[a]	70%EtOH (38.0)	90%EtOH (28.1)	EtOH (24.3)	Acetone (20.7)	1-BuOH (17.5)	1-OcOH (10.3)	Chloroform (4.81)	
1600(100)[b]	1598(100)	1598(100)	1599(100)	1598(100)	1598(100)	1599(100)	1599(100)	ν(CC) ; B,P-ring
		1507(21)	1508(27)		1507(24)	1508(27)	1508(27)	ν(CC) ; B,P-ring
1485(49)	1485(50)	1484(52)	1482(61)	1480(60)	1483(62)	1482(67)	1480(79)	ν(CC) ; P-ring
1466(59)	1466(54)	1464(49)	1463(49)	1465(54)	1464(48)	1463(52)	1462(52)	ν(CNNC)
1408(58)	1407(61)	1406(61)	1405(60)	1405(64)	1406(61)	1404(65)	1404(74)	ν(N=N)
1356(20)	1356(18)	1355(15)	1354(15)	1354(12)	1353(14)	1354(14)	1353(13)	
1307(78)	1307(72)	1306(71)	1307(66)	1304(60)	1306(65)	1306(74)	1307(74)	ν(CNNC)
1282(47)	1283(38)	1283(35)	1284(31)	1282(29)	1281(33)	1282(34)	1283(34)	ν(CNNC)
1181(27)	1183(25)	1181(25)	1180(25)	1181(22)	1182(21)	1182(21)	1180(21)	
1130(40)	1130(37)	1129(34)	1128(32)	1129(27)	1129(27)	1128(31)	1129(27)	ν(N-N)

[a] Dielectric constant

[b] Relative intensity

the change of the dielectric constant of the solvent. Therefore, resonance Raman spectra of PdLCl in various solvents, which have different dielectric constants, were measured. Figures 4.7a-4.7d show the resonance Raman spectra of PdLCl in acetone, 1-BuOH, 1-OcOH and chloroform, respectively, and each dielectric constant and band positions are listed in Table 4.2. Band assignments were deduced by comparison with those reported for pyridylazo complexes[27-30] and the Raman spectral change with the change of the dielectric constant of the solvent. Molecular orbital calculation by PM3/MOPAC[31] showed that the dipole moment of $ZnLCl(H_2O)_2$ complex increased with the increase of the dielectric constant of the medium; 5-Br-PADAP and Cl coordinated to Zn atom were arranged in co-plane to mimic the structure of PdLCl. The values of the dipole moment calculated are given in Table 4.3. This result suggests that the imine form is favored than the azo form in a higher dielectric constant solvent, because the imine form has a larger polarizability than the azo form. Figure 4.8 shows the dependency of the ratio of Raman intensities at two peak positions on the dielectric constant of the solvent. The ratios of Raman intensities at the peak positions around 1482 and 1463 cm^{-1} (I_{1482}/I_{1463}), and 1307 and 1284 cm^{-1} (I_{1307}/I_{1284}) increased with the decrease in the dielectric constant of the solution. The bands at 1482, 1463, 1307 and 1284 cm^{-1} were assigned to ν(C=C) of pyridine ring in azo form, ν(CNNC) in imine form, ν(CNNC) in azo form and ν(CNNC) in imine form, respectively. Dipolar structure of PdLCl is stabilized by the free energy evaluated by a Born equation as:

Table 4.3. The values of the dipole moment of $ZnLCl(H_2O)_2$ in the media of the various dielectric constants calculated by CAChe-MOPAC

Dielectric constant	Dipole moment
2.38 (toluene)	4.67
4.81 (chloroform)	5.68
10.3 (1-octanol)	6.03
24.3 (EtOH)	6.22
48.9 (50%EtOH)	6.30

$$\Delta G = -N_A Z^2 e^2 (1-\varepsilon_r^{-1})/(4\pi\varepsilon_0 2r) = -16.59 Z^2 (1-\varepsilon_r^{-1})/r \qquad (4.1)$$

where ΔG is the free energy for the transfer of an ion from a vacuum to a solution with the ε_r, and N_A, Ze, ε_0 and r are Avogadro constant, electric charge, the dielectric constant in vacuum and the radius of the ion, respectively. Equation (4.1) is combined with the ratio of Raman intensities as:

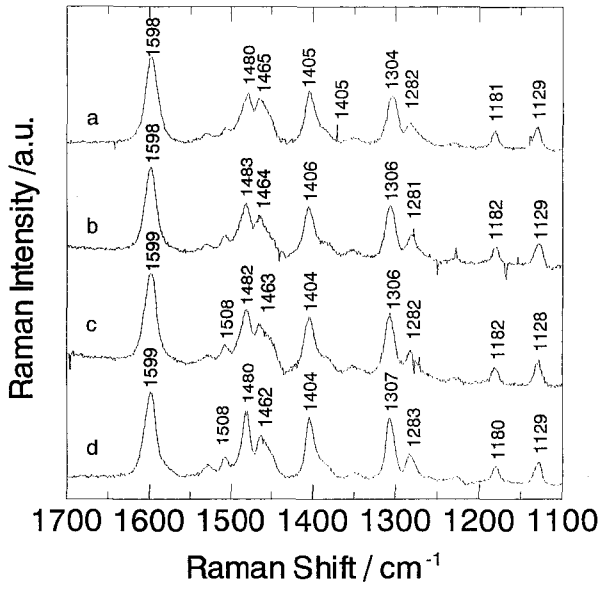

Figure 4.7. Resonance Raman spectrum of PdLCl in various solvents. (a) acetone, (b) 1-BuOH, (c) 1-OcOH, (d) chloroform. The concentration of PdLCl was about 3.0-4.5x10^{-5} M as estimated from the absorbance of the solution.

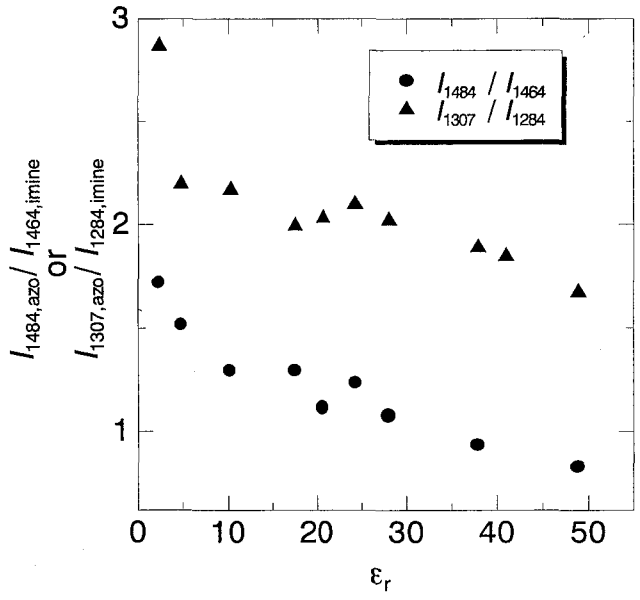

Figure 4.8. Change of the relative Raman intensity of azo and imine bands with the change of the dielectric constant of the solvents.

$$\ln(I_{azo}/I_{imi}) = a\varepsilon_r^{-1} + b \qquad (4.2)$$

where a and b are constants. Figure 4.9 shows the plots of $\ln(I_{azo}/I_{imi})$ against reciprocal number of the dielectric constant ($1/\varepsilon_r$). The values of $\ln(I_{1482}/I_{1463})$ and $\ln(I_{1307}/I_{1284})$ were proportional to $1/\varepsilon_r$ except for EtOH-water mixture systems. It was thought that the deviation of the values of $\ln(I_{azo}/I_{imi})$ obtained in EtOH-water system from the Born equation were caused by the dissociation of PdLCl to PdL^+ and Cl^- or the interaction of H_3O^+ or H_2O to the imine group. Therefore, it was thought that PdLCl tended to take the imine form in EtOH-water solution. The values of I_{1482}/I_{1463} and I_{1307}/I_{1284} in resonance Raman spectra of PdLCl adsorbed at the toluene/water interface were 0.63 and 1.47, respectively, and those of PdLCl complex formed at the heptane/water interface were 0.86 and 1.85, respectively. These values were close to the one obtained from the solution with a higher dielectric constant as plotted in Figure 4.9. Moreover, the peak positions and shapes of resonance Raman spectra of PdLCl adsorbed at the toluene/water and heptane/water interfaces were more similar to the ones measured in the high dielectric constant solvents than the ones in the low dielectric constant solvents. The dielectric constants at the toluene/water and

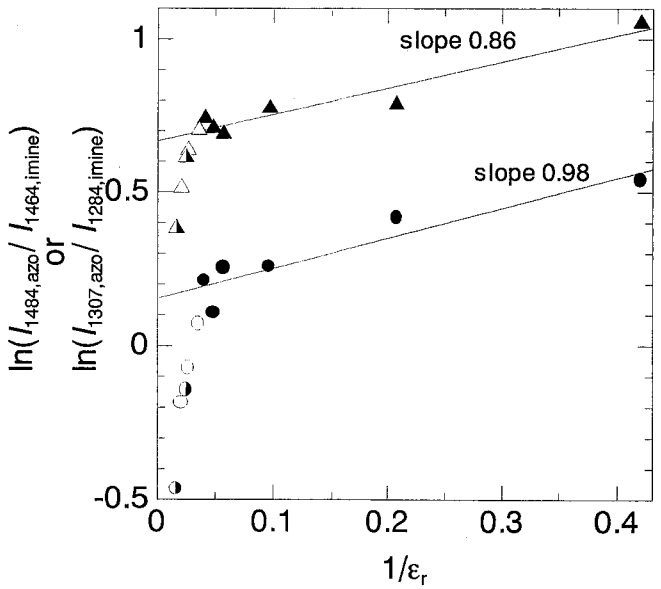

Figure 4.9. Dependency of the relative intensity azo and imine bands on the reciprocal number of the dielectric constant. Circle : I_{1484}/I_{1464}, Triangle : I_{1307}/I_{1284}. Opened circle and opened triangle are the plots obtained in EtOH-water mixture. Half closed circles and half closed triangles are the plots, when the dielectric constants at the heptane/water and toluene/water interfaces were used as 40 and 62, respectively. Solid lines are the results fitted by the equation (4.2).

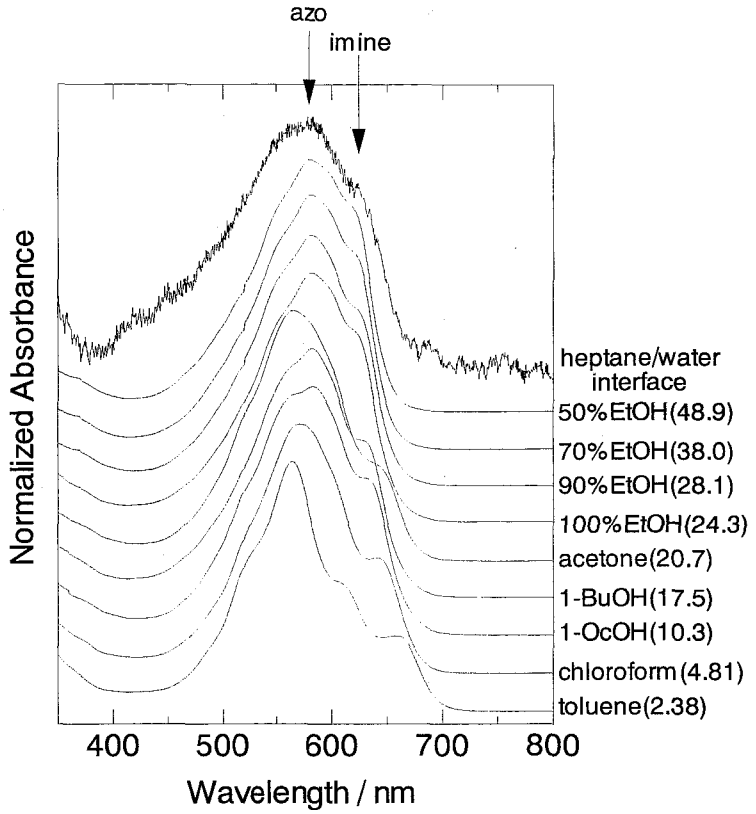

Figure 4.10. Normalized absorption spectra of PdLCl in various solvents and at the heptane/water interface. The value in parentheses is the dielectric constant of the solvent.

heptane/water interfaces were roughly estimated from Figure 4.9 as 62 and 40, respectively. These values suggested that the interfacial PdLCl was strongly influenced by the hydration from the aqueous phase in both toluene/water and heptane/water systems and PdLCl adsorbed at the interface of the aqueous phase side. Because toluene has higher dielectric constant and solubility of H_2O than heptane, PdLCl adsorbed at the toluene/water interface tends to be hydrated than that adsorbed at the heptane/water interface. Therefore, the value of the dielectric constant at the toluene/water interface seems to become higher than the one at the heptane/water interface.

In order to discuss the correlation between resonance Raman spectra and absorption spectra, absorption spectra of PdLCl in various solvents were measured. Figure 4.10 shows the absorption spectra of PdLCl in various solvents. As the dielectric constant of solvent increased, absorbance around 630 nm increased. It was also thought that this spectral change was caused by the change of the ratio of azo and imine resonance structure. Spectral

Table 4.4. Band positions of azo and imine in absorption spectra of PdLCl in various solvents

Solvent	Band position / nm	
	azo	imine
Toluene	564	662
Chloroform	571	644
1-OcOH	584	635
1-BuOH	583	632
Acetone	566	645
100% EtOH	582	624
90% EtOH	581	626
70% EtOH	582	624
50% EtOH	582	621
Heptane/water interface	580	622

change due to the change of the dielectric constant of the solvent have been found for metal-pyridylazo complexes.[25,29] Absorption band around 580 nm and 630 nm were attributed to the azo form and imine form, respectively, and these band positions in various solvents are listed in Table 4.4. The ratio (A_{azo}/A_{imine}) of absorbance at the band positions of azo and imine structures was plotted in Figures 4.11. The dependency of the value of A_{azo}/A_{imine} on the dielectric constant of the solvent was similar to the one of the value of I_{azo}/I_{imine} except for acetone; the large difference in the acetone system might be attributed to the presence of the enol form of acetone, which could interact with the complex with specific manner. This implied that the change of absorption spectra was closely related with the one of resonance Raman spectra. The absorption spectrum of PdLCl at the heptane/water interface was similar to the ones in EtOH-water system. This result also suggested that PdLCl adsorbed at the heptane/water interface was strongly influenced by the hydration from the aqueous phase.

Conclusion

In the present study, we demonstrated that CLM-RRMS was a useful method to measure the conformation of the observed species at the liquid-liquid interface.

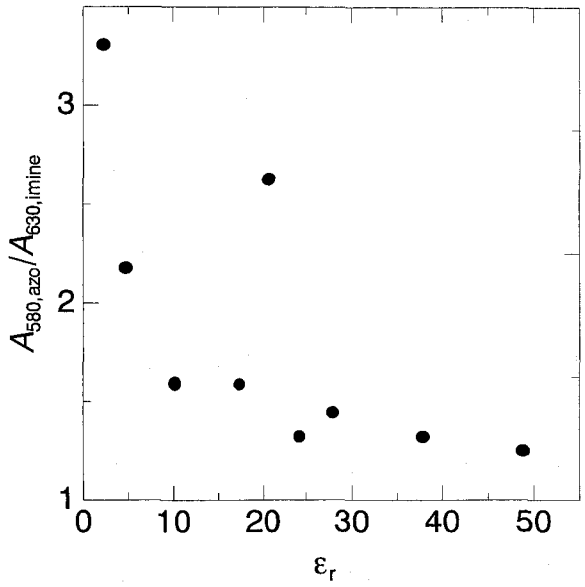

Figure 4.11. Change of the relative absrbance of azo and imine bands with the change of the dielectric constant of the solvents.

CLM-RRMS allowed us to measure the resonance Raman spectra of PdLCl, which was adsorbed at the liquid-liquid interface. CLM-RRMS could measure individually the resonance Raman spectra at the interface and in the bulk phase. It was suggested that PdLCl at the toluene/water and heptane/water interfaces existed under the similar condition with the dielectric conductivity as 62 and 40, respectively. Resonance Raman spectra obtained by CLM-RRMS suggested that PdLCl complex existed with the strong influence of hydration at the liquid-liquid interface and adsorbed at the interface of the aqueous phase side. It was thought that the change of the resonance Raman spectra of PdLCl with the change of the solution was caused with the change of the ratio of the azo and imine resonance structures.

CLM-RRMS is more superior with the following points than the Raman measurement by the total reflection method; (i) this method can be used in the system that the organic phase has high absorption at the excitation wavelength, (ii) an adsorption equilibrium is attained shortly, (iii) photo-breaching of adsorbate is reduced by the rotation of the cell, (iv) simultaneous measurements of Raman and absorption spectra are possible, (v) time-resolved Raman spectrum can be measured.[32] Therefore, we are applying now this method to measure the various interfacial reactions such as the complexation kinetics and redox reaction. Moreover, an examination of more detail structure of the interfacial adsorbate is possible by the comparison of Raman and absorption spectra.

References

1. *Liquid-Liquid Interfaces. Theory and Methods*; eds by Volkov, A. G.; Deamer, D. W., Eds.; CRC Press: Boca Raton, FL, 1996.
2. *Liquid Interfaces in Chemical, Biological, and Pharmaceutical Applications*; Volkov, A. G., Ed.; Marcel Dekker, New York, 2001.
3. Shioya, T.; Tsukahara, S.; Teramae, N. *Chem. Lett.* **1996**, 469.
4. Watarai, H.; Cunningham, L.; Freiser, H. *Anal. Chem.* **1982**, *54*, 2390.
5. Ohashi, A.; Tsukahara S.; Watarai, H. *Anal. Chim. Acta* **1998**, *364*, 53.
6. Ohashi, A.; Tsukahara S.; Watarai, H. *Anal. Chim. Acta* **1999**, *394*, 23.
7. Watarai, H.; Gotoh, M.; Gotoh, N. *Bull. Chem. Soc. Jpn.* **1997**, *70*, 957.
8. Yulizar, Y.; Ohashi, A.; Nagatani; H., Watarai, H. *Anal. Chim. Acta* **2000**, *419*, 107.
9. Perera, J. M.; Stevens, G. W.; Grieser, F. *Colloids Surf., A* **1995**, *95*, 185.
10. Fujiwara, M.; Tsukahara, S.; Watarai, H. *Phys. Chem. Chem. Phys.* **1999**, *1*, 2949.
11. Tsukahara, S.; Yamada, Y.; Watarai, H. *Langmuir* **2000**, *16*, 6787.
12. Bessho, K.; Uchida, T.; Yamauchi, A.; Shioya, T.; Teramae, N. *Chem. Phys. Lett.* **1997**, *264*, 381.
13. Feng, P.; Shu, W. Q.; Huang, C. Z.; Li, Y. F. *Anal. Chem.* **2001**, *73*, 4307.
14. Fujiwara, K.; Watarai, H. *Bull. Chem. Soc. Jpn.* **2001**, *74*, 1885.
15. Corn, R. M.; Higgins, D. A. *Chem. Rev.* **1994**, *94*, 107.
16. Takenaka, T.; Nakanaga, T. *J. Phys. Chem.* **1976**, *80*, 475.
17. Takahashi, H.; Umemura, J.; Takenaka, T. *J. Phys. Chem.* **1983**, *87*, 739.
18. Conboy, J. C.; Messmer, M. C.; Richmond, G. L. *J. Phys. Chem.* **1996**, *100*, 7617.
19. Brevet, P. F. In *Liquid Interfaces in Chemical, Biological, and Pharmaceutical Applications*; Volkov, A. G., Ed.; Marcel Dekker, New York, 2001.
20. Nagatani, H.; Watarai, H. *Anal. Chem.* **1998**, *70*, 2860.
21. Ohashi, A.; Watarai, H. *Anal. Sci.* **2001**, *17*, 1313.
22. Yulizar, Y.; Ohashi, A.; Watarai, H. *Anal. Chim. Acta* **2001**, *447*, 247.
23. Nagatani, H.; Watarai, H. *Chem. Lett.* **1999**, 701.
24. Ohashi, A.; Watarai, H. *Chem. Lett.* **2001**, 1238.
25. Johnson, D. A.; Florence, T. M. *Talanta* **1975**, *22*, 253.
26. Busev, S. I.; Vin'kova, V. A. *Zh. Anal. Khim.*, 1967, *22*, 552.
27. Drozdzewski, P. M. *Spectrochim. Acta* **1985**, *41*, 1035.
28. Dines, T. J.; Wu, H. *J. Chem. Soc. Faraday Trans.* **1995**, *91*, 463.

29. Drozdzewski, P. M. *J. Raman Spectrosc.* **1988**, *19*, 111.
30. Kawai, K.; Masago, H.; Kanamori, K.; Kanesaka, I.; Kasahara, I.; Goto, K. *J. Raman Spectrosc.*, **1987**, *18*, 205.
31. Molecular orbitals were calculated by PM3, MOPAC Version 94.10 in CAChe, Version 3.7, CAChe Scientific, 1994.
32. Ohashi, A.; Watarai, H. *in preparation*.

Part II

Interfacial Aggregation of Palladium(II)–Pyridylazo Complex

Chapter 5

Time-Resolved Resonance Raman Microprobe Spectroscopy of the Complexation and Aggregation of Palladium(II) with Pyridylazo Ligand at the Heptane/Water Interface

Introduction

The liquid-liquid interface has an important role in the reaction kinetics of the solvent extraction, the liquid membrane separation and the interfacial synthesis.[1,2] Therefore, a lot of studies on the measurement of the interfacial reaction have been developed, so far.[3] But, as far as we know, Raman spectroscopy has not been used to the kinetic study at the liquid-liquid interface at all. The application of Raman spectroscopy is expected to allow us to discuss in detail on the structure of the interfacial species, because the vibrational spectroscopy such as Raman spectroscopy has much information for the structure of the sample molecule. Recently, we developed a new *in situ* Raman spectroscopic method, centrifugal liquid membrane-resonance Raman microprobe spectroscopy (CLM-RRMS)[4] in which the Raman microscopy was combined with the centrifugal liquid membrane (CLM) method[5] to measure Raman spectrum of the interfacial species. Several studies of resonance Raman spectra of the adsorbates at the liquid-liquid interface were reported using the total reflection method.[6-8] But this method cannot be used to measure the reaction kinetics at the interface, when thick two phases require the chemical species long time diffusion to the interface. CLM-RRMS allows us to measure a time-resolved resonance Raman spectra of interfacial reactions in a time range of several seconds, because an ultra-thin two-phase layer was formed in an optical cell by a centrifugal force.

The aggregation of adsorbed molecules is one of the specific phenomena at the liquid-liquid interface. Because the concentration of the molecules adsorbed at the liquid-liquid interface is ready to be higher than that in the bulk phase, the molecules tends to aggregate at the liquid-liquid interface, even in the diluted concentration in the bulk phase. But, the aggregation mechanism at the interface has never been studied in detail very much.

In the present paper, we applied time-resolved resonance Raman microprobe spectroscopy to the study of the complexation of Pd(II) with 2-(5-bromo-2-pyridylazo)-5-diethylaminophenol[9] (5-Br-PADAP or HL) at the heptane/water

interface for the first time and revealed that this method was useful to study the interfacial reaction.

Experimental

Reagents

5-Br-PADAP (Tokyo Kasei) was used as purchased and dissolved in heptane. Heptane (G.R., Katayama Chemical) were purified with same means in the literature.[10] Stock solution of palladium(II) was prepared by dissolving palladium(II) chloride (99.99%, Wako Pure Chemicals) in 0.1 M chloride acid. Water was distilled and deionized with a Milli-Q system (Milli-Q SP.TOC., Millipore).

Resonance Raman spectroscopic measurements

The Raman intensity changes in the course of the formation of the complex and the aggregate of Pd(II)–5-Br-PADAP at the heptane/water interface were measured by CLM-RRMS. The structure of Pd(II)–5-Br-PADAP complex was shown in Figure 5.1. The chloride ion was probably coordinated to the reminder one of the site of palladium(II) in the present study. The apparatus of CLM-RRMS was the same as the one reported previously[4] and schematic drawing of the apparatus was shown in Figure 5.2. A cylindrical cell had a hole of 2-mm diameter as a sample inlet at the bottom.[10] The inner diameter and inner height of the cylindrical cell were 19 and 30 mm, respectively. After the cylindrical cell containing heptane (0.050-0.100 cm^3) and Pd(II) aqueous solution (0.250 cm^3) was placed horizontally under the objective lens (Mitutoyo, 45×, NA 0.55) and rotated at about 10000 rpm by the high-speed motor (Nakanishi Inc., NK-260) fixed on a XYZ-stage (Suruga Seiki, B72-60C), HL heptane solution (0.050-0.100 cm^3) was injected rapidly by a microsyringe from the hole at the bottom (see Figure 5.2) to initiate the complexation of Pd(II) with 5-Br-PADAP. Total volume of the heptane phase was 0.150 cm^3 at all

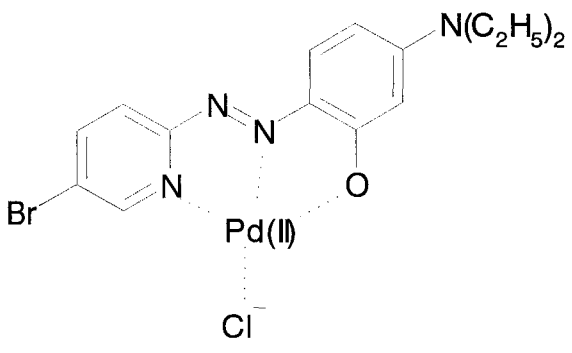

Figure 5.1. Structure of Pd(II)-5-Br-PADAP complex.

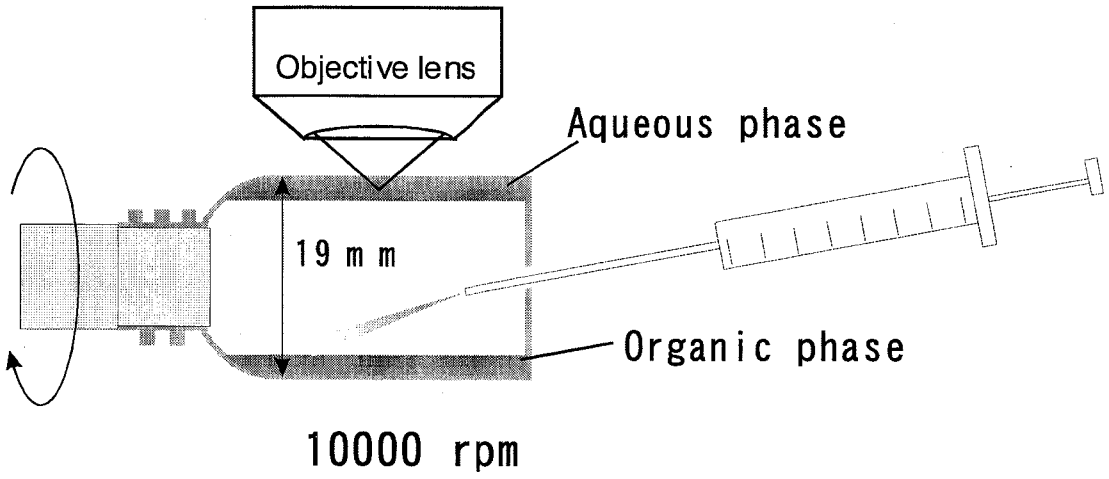

Figure 5.2. Schematic drawing of an observation part for CLM-RRMS.

time. The excitation beam (514.5 nm) by an Ar^+-ion laser (Spectra-Physics, Stabilite 2017) was focused into two-phase liquid membrane through the objective lens. The back scattering was collected by the same objective lens and was led to a spectrophotometer (Jobin Yvon, HR-320) with a liquid-nitrogen-cooled/CCD detector (Roper Scientific, LN/CCD-1100-PB/UVAR/1). The focal point was moved along with the Z-axis of XYZ-stage. An outer surface of the cylindrical cell was defined as $Z = 0$. The value of Z corresponding to a position of the liquid-liquid interface was determined as $Z = 720$ μm by measuring maximum Raman scattering intensity of PdLCl which existed only at the interface in the heptane/water system.[4] The laser power and the gate time to acquire Raman scattering were varied from 40 to 120 mW and from 2 to 5 s, respectively, in the time-resolved measurements. The time-resolved Raman spectra of PdLCl complex or aggregate at an equilibrium were measured with the laser power of 40 mW and the exposure time of 50 s. Raman spectra were measured in the range of 1800-800 cm^{-1}. The observed frequencies were calibrated with respect to the Raman peaks of toluene and were accurate to within ±2 cm^{-1}. All measurements were carried out in the thermostated room at 298±2 K. The Pd(II) concentration and HL concentration were changed in the range of 8.0×10^{-5}-1.0×10^{-3} M and 7.4×10^{-7}-2.5×10^{-4} M, respectively. The ionic strength and pH were fixed at 0.1 M and 1.0, respectively, with HCl.

Measurements by absorption spectra

The absorption spectra of Pd(II)–5-Br-PADAP complex and aggregate at the

heptane/water interface were measured by CLM. The apparatus of CLM was the same as the one reported previously.[10] The change of absorption spectra with the formation of Pd(II)–5-Br-PADAP complex or aggregate at the interface was measured with a diode array spectrophotometer (Hewlett-Packard HP8452A). Absorption spectra were measured in the range of 300-750 nm and obtained in a 4-6 s interval. The Pd(II) concentration and HL concentration were changed in the range of 3.0×10^{-4}-1.0×10^{-3} M and 7.4×10^{-6}-2.5×10^{-4} M, respectively. The ionic strength and pH were controlled at 0.1 M and 1.0, respectively, with HCl.

Results and Discussion

Absorption spectra

Before the measurements by resonance Raman spectroscopy were carried out, the formation of the aggregate of PdLCl was confirmed by the measurements of absorption spectra. When the concentration of HL was as low as 3.0×10^{-5} M, the complex of PdLCl existed stable at the interface. But the formation of the aggregate of PdLCl appeared, when the concentration of HL exceeded 4.4×10^{-5} M. In these systems, all HL in the heptane phase complexed with Pd(II) and existed at the heptane/water interface.[4,10] Therefore, the interfacial concentration of PdLCl was 3.4×10^{-10} mol cm^{-2}, when the concentration of HL was 4.4×10^{-5} M. The formation of the aggregate of PdLCl at the heptane/water interface

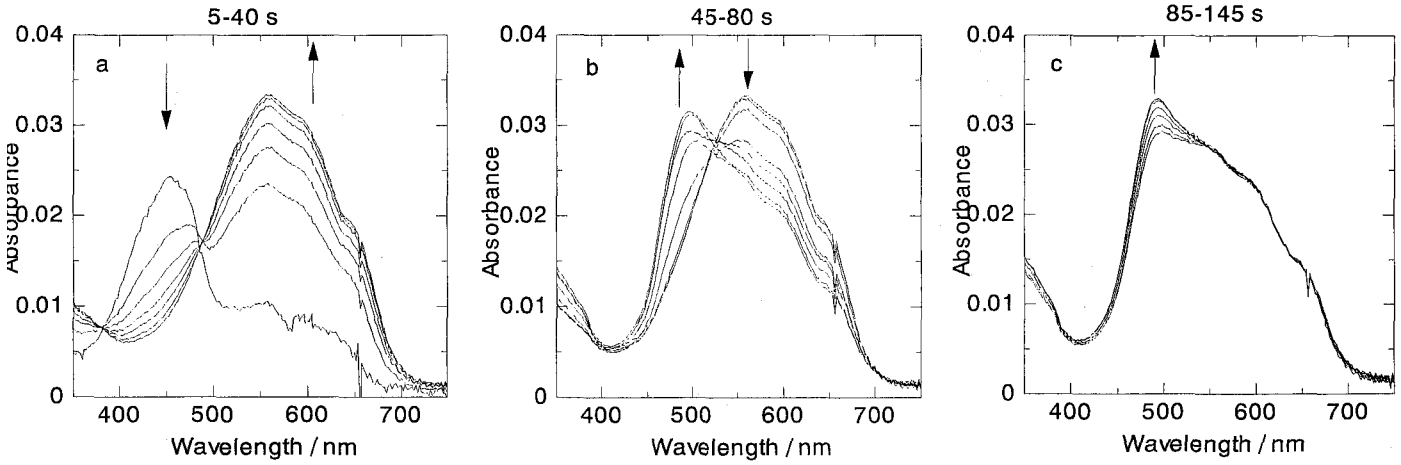

Figure 5.3. The spectral change in the course of time; (a) 5-40 s, (b) 45-80 s (c) 85-145 s: $[Pd(II)]_T = 1.0\times10^{-3}$ M, $[HL]_T = 7.2\times10^{-5}$ M, $[Cl^-] = 0.1$ M, pH 1.0.

preceded by three steps as shown in Figure 5.3; (i) the increase of absorbance around 580 nm indicating the complexation of Pd(II) with HL, (ii) the decrease in the absorbance and the increase of the absorbance at 490 nm which was a maximum absorption wavelength of the aggregate, (iii) further increase of the aggregate. Similar spectra changes were observed under the all conditions that the aggregate could be formed. The molar absorptivity of the aggregate of PdLCl did not decrease. This result implied that the charged quinone structure existed in the aggregate of PdLCl. The maximum wavelength of the aggregate was about 90 nm blue-shifted in comparison with that of PdLCl complex. This blue-shift is attributed to the PdLCl-PdLCl interaction in the high interfacial concentration at the interface. The blue-shift of the maximum absorption wavelength of the aggregate suggested that H-aggregate of PdLCl was formed at the heptane/water interface.[11] The aggregate moved to the rotating-shaft side of the cell in the course of the reaction time due to the centrifugal force or the vibration of the cell by the high-speed rotating. Therefore, it was difficult to know the concentration of the aggregate of PdLCl correctly. This series of the change of the situation at the heptane/water interface was monitored by CLM-RRMS.

Time-resolved measurements of the interfacial reaction by CLM-RRMS

Firstly, it was confirmed that Raman intensity was proportional to the interfacial concentration of PdLCl complex. Raman intensity obtained by CLM-RRMS showed the good linearity against the interfacial concentration of PdLCl complex as shown in Figure 5.4. Enough Raman intensity could be measured even in the low interfacial concentration of PdLCl as 9.2×10^{-12} mol cm^{-2}.

Secondly, to confirm that time-resolved measurements could measure the reaction proceeding at the interface, the complexation rate of PdLCl at the heptane/water interface was measured by CLM-RRMS. Figure 5.5 show the formation profile of PdLCl complex measured by CLM-RRMS (Raman intensity at 1599 cm^{-1}) and by CLM (absorbance at 580 nm). The change of Raman intensity of PdLCl was good agreement with that of absorbance. The relationship between Raman intensity at equilibrium and the interfacial concentration of PdLCl, which was calculated from the initial concentration of HL, was obtained as $I_{eq} = a[PdLCl]_{i,T}$, where I_{eq}, a and $[PdLCl]_{i,T}$ are Raman intensity at equilibrium condition, a proportional constant for Raman intensity against the interfacial concentration (in unit: cm^2 mol^{-1}) and the interfacial concentration of PdLCl at equilibrium condition, respectively. The Raman intensity change was fitted by the exponential curve by least-squares regression, and

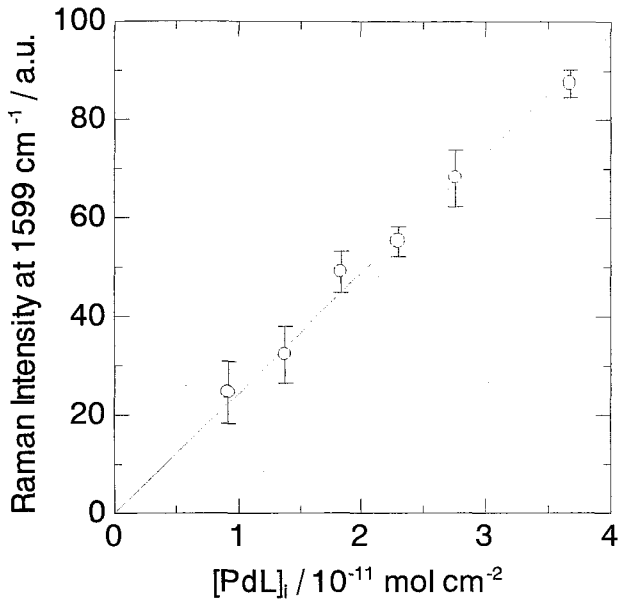

Figure 5.4. Linear correlation between the Raman intensity at 1599 cm^{-1} and the interfacial concentration of PdLCl complex.

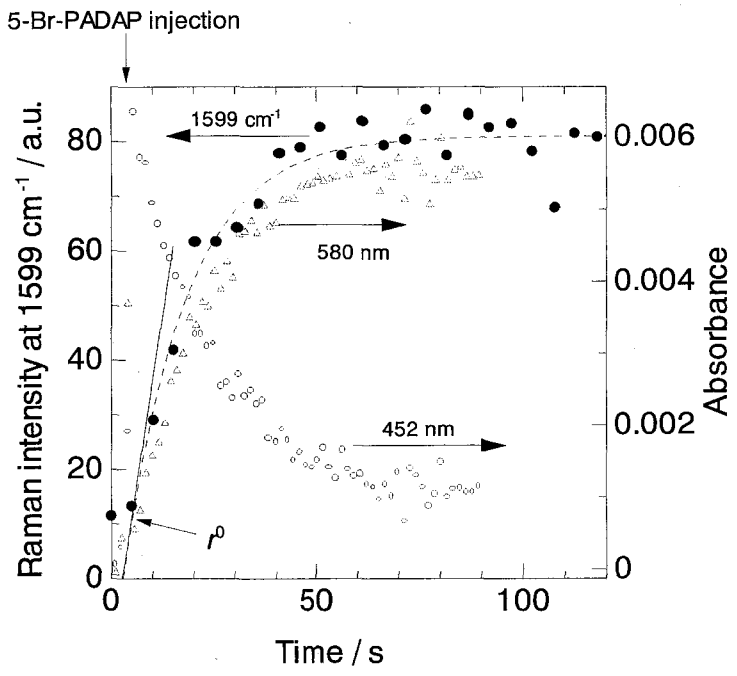

Figure 5.5. Complexation profiles of PdLCl at the interface; (●) Raman intensity at 1599 cm^{-1} measured by CLM-RRMS, (○) absorbance at 452 nm measured by CLM, (△) absorbance at 580 nm measured by CLM: $[Pd(II)]_T = 4.0\times10^{-4}$ M, $[HL]_T = 7.4\times10^{-6}$ M, $[Cl^-] = 0.1$ M, pH 1.0.

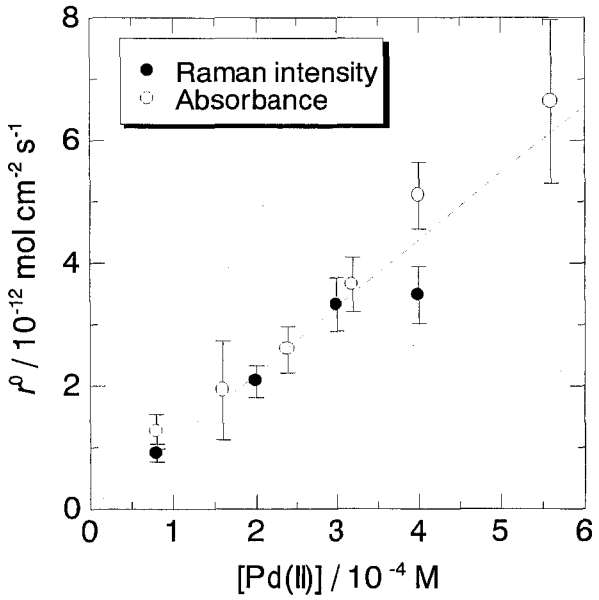

Figure 5.6. Dependency of the initial complexation rate (r^0) on the concentration of Pd(II) measured from the absorbance change by CLM (○) and from the Raman intensity change by CLM-RRMS (●): $[HL]_T$ = 7.4×10^{-6} M, [Cl$^-$] = 0.1 M, pH 1.0. The dish line is the one calculated by using the rate constants estimated in Chapter 2.[10]

the initial complexation rate defined as $r^0 = (dI/adt)_{t=t'} = (d[PdLCl]_i/dt)_{t=t'}$ (t' represents the HL injection time) was calculated by differentiating the exponential curve at the HL injection time. The values of r^0 obtained by CLM-RRMS were good agreement with the values obtained from the absorbance change by CLM in the previous report[10] as shown in Figure 5.6. This agreement shows that CLM-RRMS can be applied to the measurement of the reaction kinetics at the liquid-liquid interface. As far as we know, this is the first report that the reaction kinetics proceeding in a time range of several seconds at the liquid-liquid interface was measured by resonance Raman spectroscopy.

Figure 5.7 shows the formation profiles of PdLCl complex and its aggregate at the HL concentration of 7.2×10^{-5} M which were measured by CLM-RRMS (Raman intensity at 1598, 1591, 1407 and 1401 cm^{-1}) and by CLM (absorbance at 490 and 580 nm). The drastic change in the Raman intensity around 60 s was also observed in that of absorbance change. Figure 5.8 shows the Raman spectra at the time marked in Figure 5.7 in the range of 1700-1100 cm^{-1}. There was an obvious difference between the spectra obtained before and after the drastic change at 60 s in the Raman intensity by the formation of aggregate. In particular, band positions around 1600 and 1400 cm^{-1} of the aggregate were largely shifted to

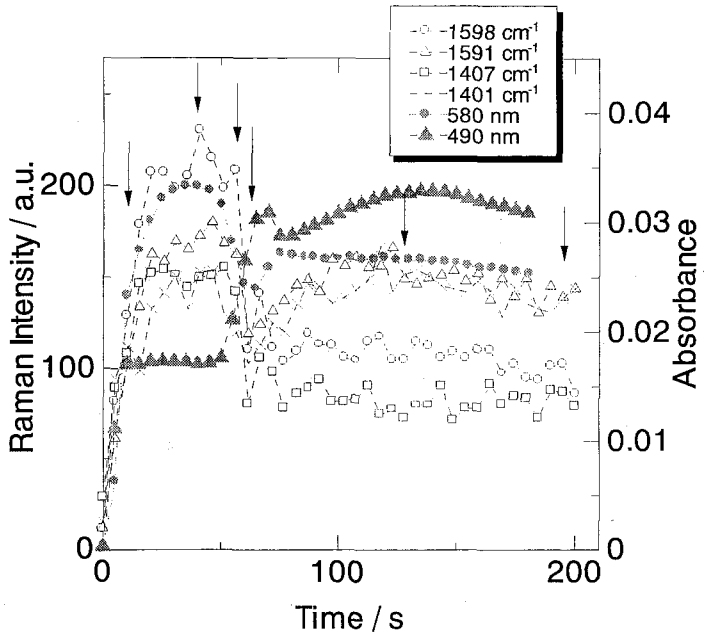

Figure 5.7. Changes in the Raman intensity and absorbance according to the formation of PdLCl and the subsequent aggregation of PdLCl: $[Pd(II)]_T$ = 1.0×10^{-3} M, $[HL]_T$ = 7.2×10^{-5} M, $[Cl^-]$ = 0.1 M, pH 1.0. Arrows indicate the time when Raman spectra are shown in Figure 5.8.

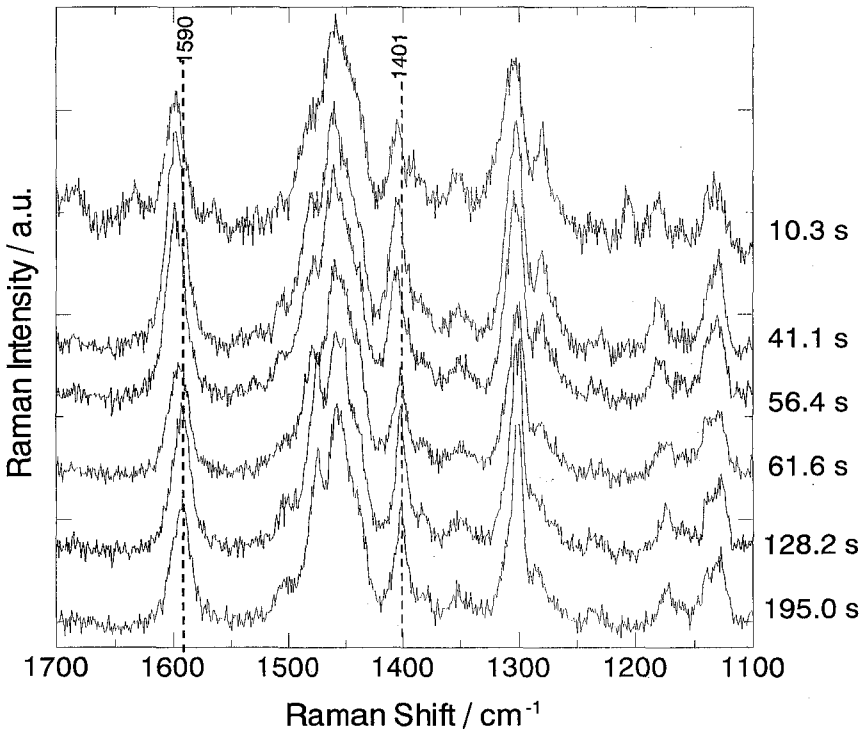

Figure 5.8. Raman spectra observed at the various reaction times in the range of 1700-1100 cm^{-1}. The experimental conditions were same in Figure 5.7.

lower frequencies than ones of PdLCl complex. The bands around 1600 and 1400 cm^{-1} was assigned to the stretching of benzene and pyridine rings and azo stretching, respectively.[12] These shifts in Raman spectra was thought to reflect the formation of the aggregate of PdLCl at the heptane/water interface. Figure 5.9 shows the resonance Raman spectra of PdLCl and its aggregate formed at the heptane/water interface at the equilibrium condition. The Raman spectrum of heptane was already subtracted from the Raman spectra in Figure 5.9. There were several differences between the resonance Raman spectra of the complex and the aggregate, such as lower shifts of almost all peak positions and the changes of the relative intensity of the peaks with the formation of the aggregation, but the spectral pattern was basically the same. It was suggested that the lower shifts of band positions of the resonance Raman spectrum of the aggregate resulted from the molecular interaction of PdLCl-PdLCl. This result implied that there was no large structural change of PdLCl with the formation of the aggregate in spite of large change of the absorption spectrum and supported the suggestion that H-aggregation formed at the heptane/water interface. Moreover, Raman spectrum of the aggregation implied that the aggregation was mainly formed with a complex of azo form,

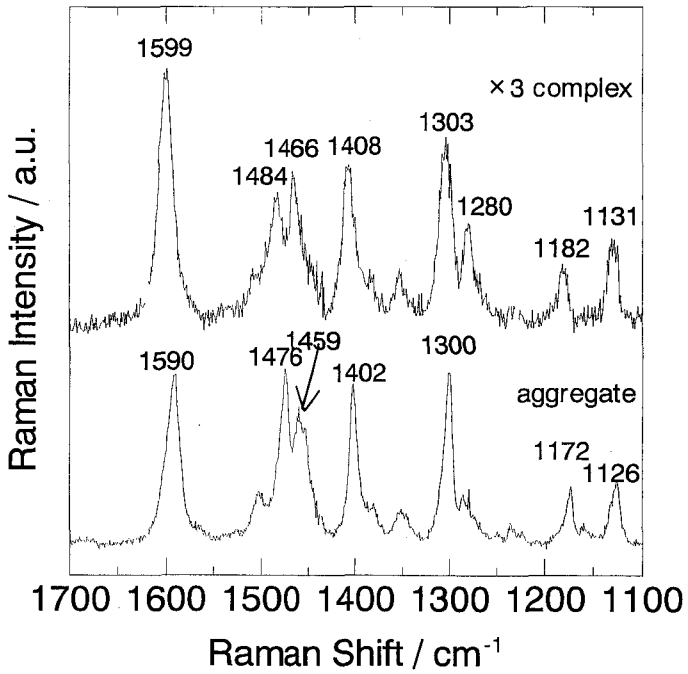

Figure 5.9. Resonance Raman spectra of PdLCl and its aggregate formed at the heptane/water interface: the complex (upper spectrum); $[Pd(II)]_T = 4.0\times10^{-4}$ M, $[HL]_T = 7.4\times10^{-6}$ M , the aggregate (lower spectrum): $[Pd(II)]_T = 1.0\times10^{-3}$ M, $[HL]_T = 7.2\times10^{-5}$ M.

because Raman spectrum of the aggregate was more similar to spectra of PdLCl complex obtained from the solutions of low dielectric constant than ones from the solutions of high dielectric constants.[13]

Conclusion

In the present study, we carried out the time-resolved measurements of the complexation and the aggregation of Pd(II) with 5-Br-PADAP at the heptane/water interface by the resonance Raman spectroscopy for the first time. It was demonstrated that CLM-RRMS was very useful for the measurements of the complexation and aggregation proceeding at the liquid-liquid interface. The absorption and Raman spectra of the aggregate were different from ones of the interfacial complex and suggested the formation of H-aggregate with azo form. It was also found that the molar absorptivity was not reduced by the formation of the self-aggregation of PdLCl. The combination of absorption spectra measurement by CLM and Raman spectra measurement by CLM-RRMS may make possible to study the reaction mechanism in further detail.

References

1. *Liquid-Liquid Interfaces. Theory and Methods*; eds by Volkov, A. G., Deamer, D. W., Eds.; CRC Press: Boca Raton, FL, 1996.
2. Watarai, H. *Tre. Anal. Chem.*, **1993**, *12*, 313.
3. Watarai, H. In *Liquid Interfaces in Chemical, Biological, and Pharmaceutical Applications*; Volkov, A. G., Ed.; Marcel Dekker, New York, 2001.
4. Ohashi, A.; Watarai, H. *Chem. Lett.*, **2001**, 1238.
5. Nagatani, H.; Watarai, H. *Anal. Chem.*, **1998**, *70*, 2860.
6. Takenaka, T.; Nakanaga, T. *J. Phys. Chem.* **1976**, *80*, 475.
7. Takahashi, H.; Umemura, J.; Takenaka, T. *J. Phys. Chem.* **1982**, *86*, 4660.
8. Takahashi, H.; Umemura, J.; Takenaka, T. *J. Phys. Chem.* **1983**, *87*, 739.
9. Johnson, D. A.; Florence, T. M. *Talanta* **1975**, *22*, 253.
10. Ohashi, A.; Watarai, H. *Anal. Sci.* **2001**, *17*, 1313.
11. Kemnitz, K.; Tamai, N.; Yamazaki, I.; Nakashima, N.; Yoshihara, K. *J. Phys. Chem.* **1986**, *90*, 5094.
12. Drozdzewski, P. M. *Spectrochim. Acta* **1985**, *41*, 1035.
13. Ohashi, A.; Watarai, H. *in preparation.*

Chapter 6

Comparison of Crystal and Aggregate Formed at the Heptane/Water Interface of Palladium(II)–Pyridylazo Complex

Introduction

Until now, there have been reported many works about the syntheses of metal-complex crystals that have specific properties such as spin crossover and specific structures such as di- or polynuclear.[1,2] However, most of these syntheses have been carried out in bulk phases. The liquid-liquid interface has received a great deal of attention as a new reaction field for synthesis of organic and inorganic compounds,[3] because the liquid-liquid interface has specific characteristics, such as a nanometer sized thickness and a drastic change in solvent environment in the two-dimensional region. The formation of the aggregate and the precipitate at the liquid-liquid interface in solvent extraction system appeared very often, but there have been few reports about the structures and the characteristics of these interfacial species. Recently, our laboratory found the formation of a specific dinuculear and aggregate at the liquid-liquid interface.[4,5] These results suggested the possibility of the liquid-liquid interface as the specific synthesis field that differs from the bulk phase.

In Chapter 5, it was revealed that the aggregate of the complex of Pd(II) with 2-(5-bromo-2-pyridylazo)-5-diethylaminophenol (5-Br-PADAP or HL) was formed at the heptane/water interface when the interfacial concentration of PdLCl exceeded 3.4×10^{-10} mol cm^{-2}.

In this chapter, the differences in absorption and Raman spectra between the interfacial aggregate and the crystal of PdLCl were revealed, and the structure of the interfacial aggregate of PdLCl was discussed.

Experimental

Reagents

5-Br-PADAP (Dojindo Laboratory) was used as purchased and dissolved in toluene and heptane. Toluene (G.R., Nacalai Tesque) and heptane (G.R., Katayama Chemical) were purified with same means in Chapter 2. Stock solution of palladium(II) was prepared by

dissolving palladium(II) chloride (99.99%, Wako Pure Chemicals) in 0.1 M chloride acid. A PdLCl toluene solution was prepared by the extraction from 1.0×10^{-3} M palladium(II) chloride in the 0.1 M hydrochloric acid with 5.6×10^{-5} M 5-Br-PADAP in toluene. Acetone (E.P., Katayama Chemical) was used as purchased. Water was distilled and deionized with a Milli-Q system (Milli-Q SP.TOC., Millipore).

Synthesis of crystal

The toluene solution (about 10 ml) of 5.6×10^{-5} M PdLCl was added into a crystal dish and the solvent was evaporated at the room temparature. Crystallity of PdLCl was dissolved again in acetone and recrystallized. Dark purple and prismatic crystals were obtained.

X-ray structure analysis

A dark purple crystal of PdLCl having approximate dimensions of 0.20 × 0.20 × 0.20 mm was mounted on a glass needle. The X-ray intensities were measured at 295 K with graphite-monochromated MoKα radiation (λ = 0.71073Å) on a Rigaku AFC-5R four-circle diffractometer using ω-2θ scan technique. Final lattice constants were determined by least-squares refinements of the orientation angles of 25 centered reflections in the range $29.35^{\circ} < 2\theta < 30.03^{\circ}$. Of the 10192 reflections which were collected, 9759 were unique. Over the course of data collection, the standards increased by 0.4%. The structure could be solved reasonably by using direct method (SHELXS-86[6] programs) and refined by a full matrix least squares procedures. The positions of hydrogen atoms were fixed at calculated positions and only their isotropic displacement parameters were refined. All calculations were carried out on an SGI O_2 workstation using TeXsan software.[7]

Absorption spectra measurements

To measure the absorption spectrum for the crystal of PdLCl, the KBr pellet containing PdLCl was prepared in the following ways. The PdLCl acetone solution was introduced into an agate mortar and the solvent was evaporated. KBr of 200 mg was added into the mortar and ground together with the crystals of PdLCl. The powders of the mixture of KBr and PdLCl were pressed and the pellet which diameter and thickness were 10 and 2 mm, respectively, was made.

The absorption spectra of PdLCl complex and aggregate at the heptane/water

interface were measured by the centrifugal liquid membrane (CLM) method as described in Chapter 5. Principals of CLM method was described elsewhere.[8] All measurements were carried out in a thermostated room at 297±2 K.

Resonance Raman spectra measurements

Resonance Raman spectrum for the KBr pellet containing PdLCl was measured by a Raman microscopy, which contained an Ar^+-ion laser (Spectra-Physics, Stabilite 2017), a liquid-nitrogen-cooled/CCD detector (Roper Scientific, LN/CCD-1100-PB/UVAR/1) and a spectrophotometer (Jobin Yvon, HR-320) and was constructed by Photon Design (Japan). The samples were measured on a glass plate. The laser beam of 514.5 nm wavelength was focused into the sample through the objective lens (45×, Mitutoyo) and the scattering light was collected by the same objective lens. The laser power and the exposure time were 40 mW and 10 s, respectively.

The resonance Raman spectra of PdLCl complex and aggregate at the heptane/water interface were measured by the CLM-resonance Raman microprobe spectroscopy (CLM-RRMS) as described in Chapter 5.

Measurements of microscopic images

The shapes of an aggregate of PdLCl formed at the heptane/water interface and the crystal of PdLCl were measured with a microscopy and a CCD camera. A 1.0×10^{-3} M $PdCl_2$ in 0.1 M HCl aqueous solution (10 cm^3) was introduced in a 100 ml beaker, and then 8 cm^3 of 7.2×10^{-5} M HL heptane solution was quietly added on the aqueous phase. After 3 h, the microscopic image of the aggregate of PdLCl formed at the heptane/water interface was obtained by an objective lens (45×) directly above the toluene phase.

Results and Discussion

The X-ray structure of PdLCl

The molecular structure of the X-ray analysis is shown in Figure 6.1 and Crystallographic data and selected bond distance and angles are listed in Table 6.1 and 6.2, respectively. A crystal of PdLCl was constructed by two-type of PdLCl molecules, which were defined as PdLCl**1** and PdLCl**2**, respectively (see Figure 6.1). Both PdLCl molecules were almost the same, except for the positions of carbon atoms in the diethylamino group.

In addition, bond lengths and angles between PdLCl**1** and PdLCl**2** were slightly different as described in Table 6.2. The angle sum around each palldium (α_1(N1–Pd1–N3) + α_2(N3–Pd1–O1) + α_3(O1–Pd1–Cl1) + α_4(Cl1–Pd1–N1), and α_1'(N5–Pd2–N7) + α_2'(N7–Pd2–O2) + α_3'(O2–Pd2–Cl2) + α_4'(Cl2–Pd2–N5)) were 360º. This implied the atoms (N, N, O, Cl) coordinated to palladium lay on the same plane. Two aromatic rings were close to the plane and almost lay on the same plane.

Figure 6.2 shows the packing diagram of PdLCl molecules in the crystal. This diagram indicates that PdLCl**1** forms the dimer in the crystal. It has long been known that the azo dyes are easy to form the dimers in the crystals and in the solutions.[9]

Table 6.1. Crystallographic Data for PdLCl

Chemical formula	$C_{30}H_{32}O_2N_8Pd_2Cl_2Br_2$
Formula weight	980.15
Crystal color, Habit	dark, prismatic
Crystal dimensions (mm)	0.20 × 0.20 × 0.20
Crystal system	triclinic
Lattice type	primitive
a (Å)	11.918(3)
b (Å)	16.920(3)
c (Å)	8.527(1)
α (º)	91.65(1)
β (º)	94.02(2)
γ (º)	77.88(2)
Volume (Å^3)	1676.9(6)
Space Group	$P\bar{1}$ (#2)
Z value	2
D_{calc} (g/cm^3)	1.941
F_{000}	960.00
μ(MoKα) (cm^{-1})	36.65
$R1$[a)]	0.058
$wR2$[b)]	0.184

1. $R1 = \Sigma||F_0| - |F_c||/\Sigma|F_0|$.
2. $wR2 = [(\Sigma w(|F_0| - |F_c|)^2/\Sigma wF_0^2)]^{1/2}$.

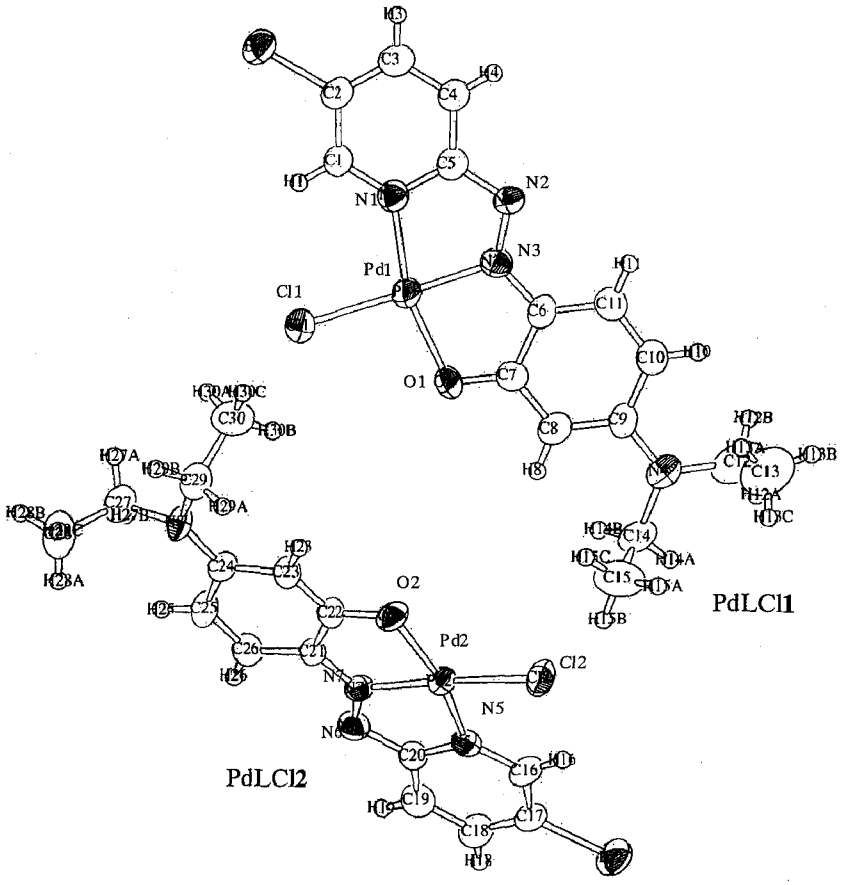

Figure 6.1. The molecular structure of PdLCl

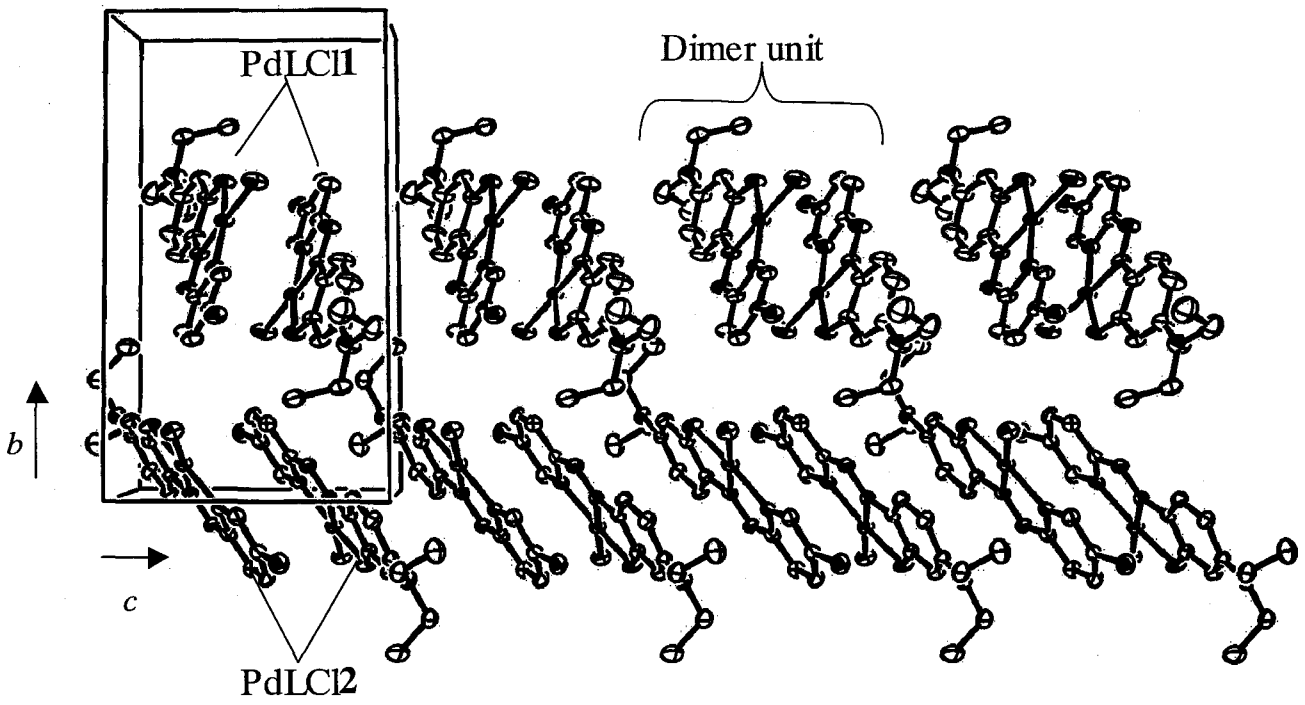

Figure 6.2. The crystal packing in PdLCl viewed along the *a* axis

Table 6.2. Selected bond lengths (Å) and angles (º) of PdLCl

PdLCl1		PdLCl2	
Pd1–Cl1	2.303(3)	Pd2–Cl2	2.308(2)
Pd1–O1	2.018(6)	Pd2–O2	2.032(6)
Pd1–N1	1.994(7)	Pd2–N5	2.009(7)
Pd1–N3	1.921(6)	Pd2–N7	1.929(5)
O1–C7	1.291(10)	O2–C22	1.321(9)
N1–C5	1.37(1)	N5–C20	1.367(9)
N2–N3	1.307(9)	N6–N7	1.315(8)
N2–C5	1.38(1)	N6–C20	1.38(1)
N3–C6	1.36(1)	N7–C21	1.338(10)
C6–C7	1.46(1)	C21–C22	1.447(10)
Cl1– Pd1–O1	98.0(2)	Cl2– Pd2–O2	97.3(2)
Cl1– Pd1–N1	99.2(2)	Cl2– Pd2–N5	99.9(2)
O1– Pd1–N3	83.6(3)	O2– Pd2–N7	83.4(2)
N1– Pd1–N3	79.2(3)	N5– Pd2–N7	79.4(3)
Pd1– O1–C7	109.4(5)	Pd2– O2–C22	108.9(5)
Pd1– N1–C5	110.9(6)	Pd2– N5–C20	109.9(5)
N3– N2–C5	110.7(6)	N7– N6–C20	110.0(6)
Pd1– N3–N2	120.4(6)	Pd2– N7–N6	120.5(5)
Pd1– N3–C6	114.3(5)	Pd2– N7–C21	114.4(4)
N1– C5–N2	118.7(7)	N5– C20–N6	120.2(7)
N3– C6–C7	112.3(7)	N7– C21–C22	114.0(6)
O1– C7–C6	120.2(8)	O2– C22–C21	119.2(7)

Microscopic images

The microscopic picture for the crystal of PdLCl gave the prismatic shape as shown in Figure 6.3a. While, the microscopic image for the aggregate of PdLCl formed at the heptane/water interface showed the shape like crystallites as shown in Figure 6.3b. These images suggested that the structure of the aggregate was similar to that of the crystal.

Absorption spectra

Figure 6.4 shows the absorption spectra for the KBr pellet containing PdLCl, the aggregate and the complex formed at the heptane/water interface. All spectra were

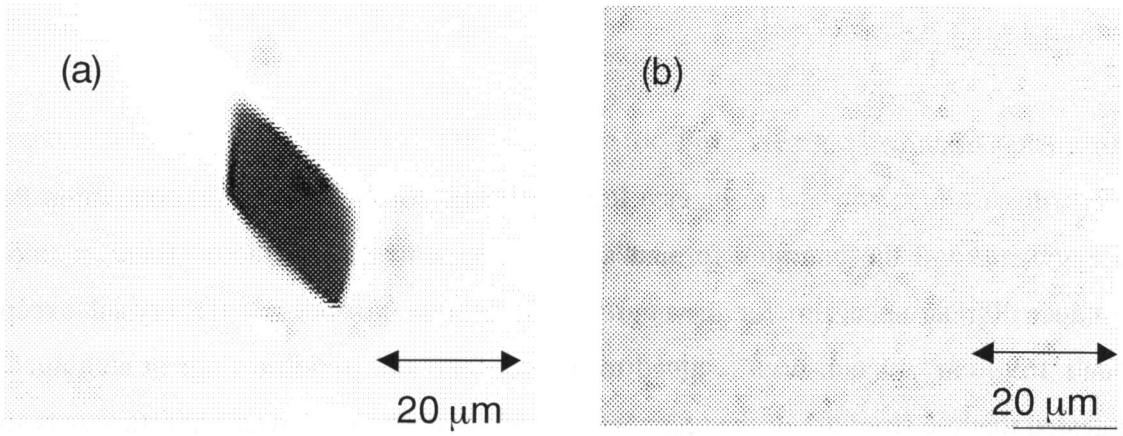

Figure 6.3. Microscopic images for (a) the crystal and (b) the aggregate formed at the heptane/water interface. The images were obtained by 45x objective lens.

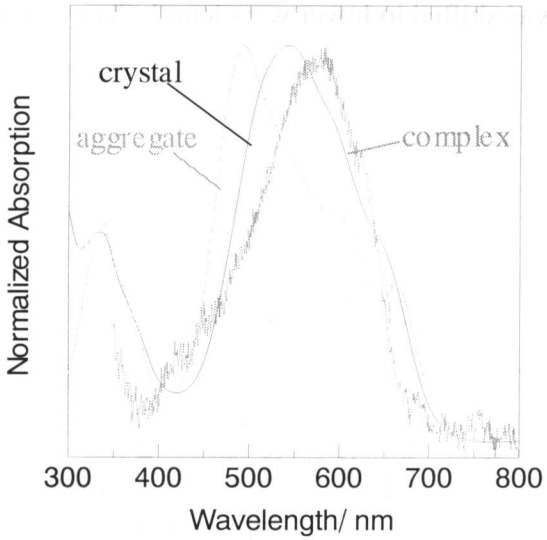

Figure 6.4. Normalized absorption spectra for the crystal and the aggregate and the complex of PdLCl at the heptane/water interface. The absorption spectrum for the crystal was measured by using the KBr pellet. The absorption spectra for the aggregate and the complex were measured by the CLM method. Aggregae: [Pd(II)] = 1.0×10^{-3} M, $[HL]_T = 1.0 \times 10^{-4}$ M, $[Cl^-] = 0.1$ M, pH 1.0; Complex: Pd(II)] = 4.0×10^{-4} M, $[HL]_T = 7.4 \times 10^{-6}$ M, $[Cl^-] = 0.1$ M, pH 1.0.

normalized at the maximum absorbances. Each absorption spectrum had different maximum absorbance wavelength, but absorption spectrum for the aggregate was similar to that for the crystal which showed the maximum at 655 nm. Toluene solution of PdLCl has also an absorption band around 655 nm (see Figure 5.3). This result suggests the similarity of the electronic states of 5-Br-PADAP in the crystal, the aggregate and the complex in toluene

solution.

Resonance Raman spectra

Figure 6.5 show the resonance Raman spectra for the KBr pellet containing PdLCl, the aggregate and the complex formed at the heptane/water interface. Band positions in resonance Raman spectrum for the aggregate was close to ones for the crystal except for around 1590 cm^{-1}, which was assigned to the benzene and pyridine rings stretching. This suggested that the structure of the aggregate formed at the heptane/water interface was similar to that of the crystal. Band position at 1595 cm^{-1} in the crystal was shifted to 1590 cm^{-1} in the aggregate. This was attributable to the extensive π-stacking in the H-aggregate of the aromatic rings of PdLCl molecules in the aggregate was more than that in the crystal where the dimmer formation was principal. This was supported by the result that the absorption spectrum for the aggregate was shifted to lower wavelength than that for the crystal.

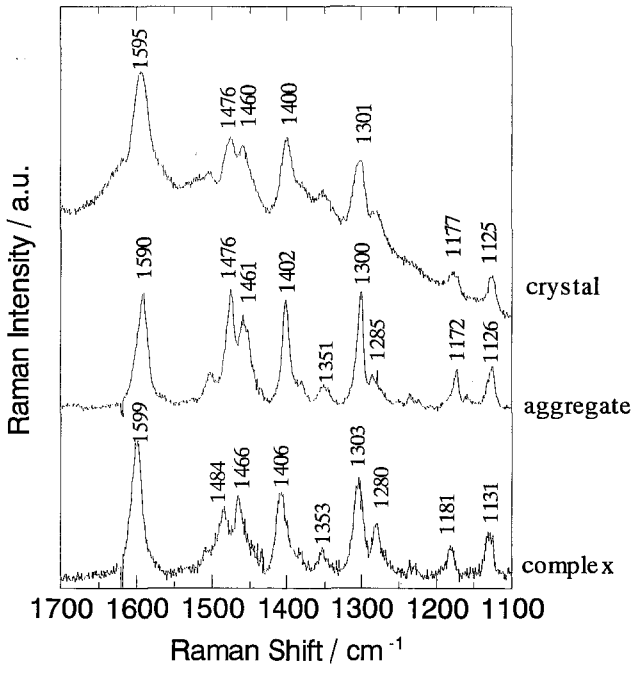

Figure 6.5. Resonance Raman spectra for the crystal and the aggregate and the complex of PdLCl at the heptane/water interface. The resonance Raman spectrum for the crystal was measured by using the KBr pellet. The absorption spectra for the aggregate and the complex were measured by CLM-RRMS. Experimental conditions were same in Figure 5.10.

Conclusion

The comparison of the crystal and the aggregate of PdLCl formed at the heptane/water interface was carried out. Microscopic images and resonance Raman spectra suggested the similarity of the structure between the crystal and the aggregate, but absorption spectra and the difference in the band position around 1590 cm^{-1} in resonance Raman spectra suggested that the degree of the overlap of the aromatic rings of PdLCl molecules in the aggregate was more extensive than that in the crystal. The unit structure in the crystal and the aggregate was the dimmer, but the π-stacking in the aggregate was thought to be more progressed. This study showed the possibility that the liquid-liquid interface could be used as the specific synthetic field of the metal-complexes that differs from those prepared in the bulk solution.

References

1. Ni-iya, K.; Fuyuhiro, A.; Yagi, T.; Nasu, S.; Kuzushita, K.; Morimoto, S.; Kaizaki, S. *Bull. Chem. Soc. Jpn.* **2001**, *74*, 1891.
2. Haynes, J. S.; Rettig, S. J.; Sams, J. R.; Thompson, R. C.; Trotter, J. *Can. J. Chem.* **1987**, *65*, 420.
3. Nur, H.; Ikeda, S.; Ohtani, B. *Chem. Commum.* **2000**, 2235.
4. Fujiwara, M.; Tsukahara, S.; Watarai, H. *Phys. Chem. Chem. Phys.* **1999**, *1*, 2949.
5. N. Fujiwara, S. Tsukahara and H. Watarai, *Langmuir*, **2001**, *17*, 5337.
6. Sfeldrik, G. M. SHELXS-86: Program for Crystal Structure Determination; University of Göttinggen: Germany 1986.
7. TEXSAN: Single-Crystal Structure Analysis Software, Version X.X; Molecular Structure Corporation: The Woodlands, TX, 1995.
8. Nagatani, H.; Watarai, H. *Anal. Chem.* **1998**, *70*, 2860.
9. Hamada, K.; Fujita, M.; Mitsuishi, M. *J. Chem. Soc. Faraday Trans.*, **1990**, 86, 4031.

Part III

Molecular Recognizing Interfacial Aggregation of Palladium(II)–Pyridylazo Complex

Chapter 7

Isomer Recognizing Adsorption of Palladium(II)–2-(5-Bromo-2-pyridylazo)-5-diethylaminophenol with Diazine Derivative at the Toluene/Water Interface

Introduction

The adsorptivity of solutes at two immisible liquid-liquid interface is an attractive subject in various fields, especially in the studies of solvent extraction mechanism of metal ion, and up-take mechanisms of drugs and pesticides by cell membranes. Until now, we have clarified the kinetic mechanisms of complexation and adsorption behavior at the interface in various metal extraction systems by a high-speed stirring method.[1-5] This method is more advantageous for the elucidation of the adsorption mechanism than the classical measurements such as the interfacial tension lowing, because it can offer information about chemical species adsorbed at the interface, even at the extremely diluted concentrations.

Diazine derivatives are utilized as herbicide and antibiotic substances. Pyrazine has recently been used in the coordination chemistry as a framework to synthesize two- and three-dimensional metal complex crystal.[6,7] Diazine includes some structural isomers as shown in Figure 7.1. For the analysis of diazines, the discrimination of the isomers is very important. It would be very useful if some method that can recognize the isomers of pyridazine, pyrimidine and pyrazine is invented.

2-(5-Bromo-2-pyridylazo)-5-diethylaminophenol (5-Br-PADAP or HL) has been known as an analytical reagent of trace amount of metal ions, because it forms intensely colored and stable complexes with various metal ions.[8-11] Since 5-Br-PADAP is a tridentate ligand,[10] it makes a 1:1 complex with palladium(II) of the square-planar conformation leaving one site for the coordination of another ligand. In the present study, we will demonstrate the molecular recognition ability of palladium(II)–5-Br-PADAP chloride complex (PdLCl) for pyridazine derivatives depending on the interfacial complexation ability.

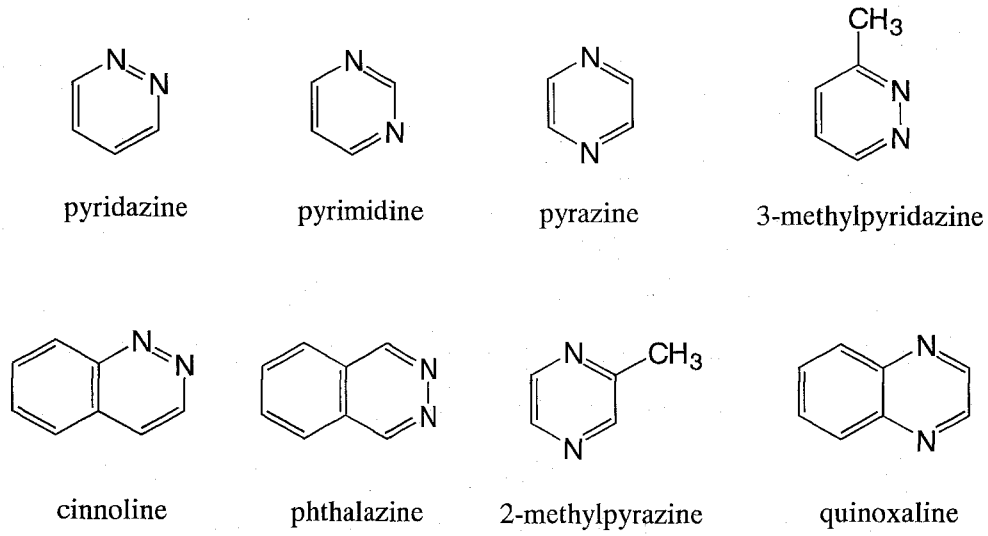

Figure 7.1. Molecular structures of the diazines

Experimental

Reagents

5-Br-PADAP (Dojindo Lab.) was used as purchased. Toluene (G.R., Nacalai Tesque) was purified by stirring three times with concentrated sulfuric acid for one day, washing with distilled water and 5% NaOH aqueous solution, drying by calcium chloride anhydrite overnight, and distilling. A stock solution of palladium(II) was prepared by dissolving $PdCl_2$ (99.99%, Wako Pure Chemicals) in 0.1 M hydrochloric acid. A stock solution of PdLCl in toluene was prepared by the extraction from 1.0×10^{-3} M palladium(II) in the 0.1 M hydrochloric acid media by $(3.8\text{-}4.9)\times10^{-5}$ M 5-Br-PADAP in toluene.[1]

Figure 7.1 shows diazines and their derivatives used in the present study. It includes pyrazine, pyrimidine (G.R., Tokyo Kasei), pyridazine (G.R., Nacalai Tesque) and their derivatives; 2-methylpyrazine (G.R., Nacalai Tesque), quinoxaline, phthalazine (E.P., Tokyo KASEI), 3-methylpyridazine (>97 %, Tokyo KASEI) and cinnoline hydrochlorid hydrate (98 %, Aldrich). 2-Morpholinoethanesulfonic acid monohydrate (MES, Dojindo Lab.) was used as a buffer reagent. Water was distilled and deionized with a Milli-Q system (Milli-Q SP.TOC., Millipore).

Measurement of distribution ratio of diazine derivatives

The distribution ratio, D, of each diazine derivative between toluene and water was measured by a batch method. The toluene phase (5 cm^3) and aqueous phase (5 cm^3) were added to a glass vessel, shaken for 1 h in a thermostatted room at 298±2 K and then the absorbance (190-800 nm) of the phase containing diazine derivative initially was measured. The pH was changed in the range of 1.0-7.1, and the ionic strength was fixed to 0.1 M with (H^+, Na^+)Cl^-. The pH was buffered by 1.0×10^{-3} M MES. The absorption spectra were measured with a spectrophotometer (V-550, Jusco) at 298±2 K.

Measurement of acid-dissociation constants of for diazine derivatives

The acid-dissociation constants, K_a, of the conjugated acid of pyridazine, 3-methylpyridazine, cinnoline and phthalazine were determined from the changes of the absorption spectra (190-800 nm) with pH. Total concentration of each solute was fixed at 3.0×10^{-4} M. The pH was changed in the range of 1.0-7.1 buffered with 1.0×10^{-3} M MES and the ionic strength was kept at 0.1 M with (H^+, Na^+)Cl^-. The absorption spectra were measured with a spectrophotometer (V-550, Jusco) at 298±2 K.

Interfacial adsorption measurements

The interfacial adsorptivities of PdLCl both in the presence and absence of diazines were measured with a high-speed stirring apparatus reported previously.[1] Two-phase solution in the stirring-cell was thermostatted at 298±0.2 K. The organic phase was continuously separated with a PTFE phase separator, passed to a flow-cell with 10 mm optical path length in a detector (SPD-M6A, Shimadzu), returned to the stirring-cell at a flow rate of 15 cm^3 min^{-1}. After agitating toluene and aqueous phases in the stirring-cell at a stirring speed of 5000 rpm, PdLCl toluene solution and diazine aqueous solution were added in this sequence, and the interfacial concentration of PdL^+-complex at each diazine concentration was measured as mentioned in the next section. Total volume of the toluene phase was 50 cm^3 and that of the aqueous phase was within the range of 50.0±1.0 cm^3. The Cl^- concentration, the initial PdLCl concentration and pH were changed in the range of 0.001-0.1 M, $0.3\text{-}1.7\times10^{-5}$ M and 1.0-3.8, respectively. The ionic strength was kept at 0.1 M with (H^+, Na^+)Cl^- or (H^+, Na^+)ClO_4^-.

When the stirring speed is changed from 200 to 5000 rpm, the concentration of an absorbable species, B, in the organic phase decreases due to the interfacial adsorption. The

interfacial concentration, $[B]_i$ (in mol cm^{-2}), was calculated from

$$[B]_i = (A_{200}-A_{5000})V_o/S_i\varepsilon b \qquad (7.1)$$

where A_{200} and A_{5000} are the absorbances in the organic phase under the low-speed stirring (200 rpm) and high-speed stirring (5000 rpm), respectively. V_o (in dm^3) is the volume of the organic phase, S_i (in cm^2) is the interfacial area under the high-speed stirring, ε (in M^{-1} cm^{-1}) is the molar absorptivity of the species in the organic phase, b (in cm) is the optical length of the flow-cell.

Electrospray ionization mass spectrometry

Electrospray ionization mass spectrometry (ESI-MS) measurements were carried out using an API III$^+$ triple quadrupole mass spectrometer (Perkin-Elmer Sciex Instruments) with precoated ESI-MS capillaries of 150 μm o.d. Voltages were applied to the ESI needle (4300 V), the interface plate (650 V) and orifice skimmer potential (35-110 V). The effect of collision activating dissociation was investigated by changing the orifice voltage. The mass range measured in this study was 20-1200 m/z in the step of 0.1 m/z. The sample solution was prepared using a mixed solvent (EtOH : water = 9 : 1 by volume). PdLCl and pyridazine concentrations were 2×10^{-5} M and 2×10^{-4} M, respectively.

Results and discussion

K_a and K_D for diazine derivatives

The distribution ratio, D, was obtained from the following equations:

$$D = \frac{[N]_o}{[N]+[NH^+]} = \frac{A_{w,init}-A_{w,f}}{A_{w,f}}\cdot\frac{V_w}{V_o} \text{ or } \frac{A_{o,f}}{A_{o,init}-A_{o,f}}\cdot\frac{V_w}{V_o} \qquad (7.2)$$

where A is the absorbance, V is the volume, and the subscripts o, w, init and f refer to the organic phase, aqueous phase, initial and final, respectively. N and NH^+ correspond to neutral and protonated diazine derivatives, respectively. The D values of the diazine derivatives were represented as:

$$\log D = \log K_D - \log(\frac{[H^+]}{K_a} + 1) \qquad (7.3)$$

where K_D is the distribution constant of neutral diazine defined as $K_D = [N]_o/[N]$. K_D and K_a values were obtained by analyzing the plots of log$D$ *v.s.* pH with Eq. (7.3). The logK_D and pK_a values of diazine derivatives are listed in Table 7.1. The logK_D values of diazine decreased in the order, pyrazine > pyrimidine > pyridazine, corresponding to the increasing order of the dipole moment[12] of neutral diazine (The value of dipole moment of each diazine is given in Table 7.2.). This tendency is available for the other diazine derivatives; 2-methylpyrazine > 3-methylpyridazine and quinoxaline > cinnoline > phthalazine. These results imply that the hydrophobicity of diazine derivatives increases, as their dipole moments become smaller.

The pK_a values for pyridazine and its derivatives were also determined by the spectrophotometry, since the spectra of the protonated species could be distinguished from the neutral one in the pH range of 1.0-7.1. Absorbance at a wavelength (λ) can be expressed as:

$$A_\lambda = (\frac{\varepsilon_\lambda K_a [N]_T}{[H^+] + K_a} + \frac{\varepsilon'_\lambda [H^+][N]_T}{[H^+] + K_a})b \qquad (7.4)$$

where A_λ, ε_λ and ε_λ' are absorbance and molar absorption coefficients of neutral and protonated diazines at a wavelength (λ), respectively, and $[N]_T$ is the total concentration of the diazine derivatives, i.e., $[N]_T = [N] + [NH^+]$. According to Eq. (7.4), the pK_a values were obtained from the absorbance change. The obtained pK_a values were averaged for twice determination at two wavelengths listed in Table 7.1. The pK_a values determined by the batch extraction and spectrophotometry were in agreement with previously reported ones.[13-15]

It was reported that there was no correlation between the charge density on the nitrogen atoms and the pK_a values of diazines.[16] On the other hand, the pK_a values of the diazines increased with an increase in their neutral dipole moments. This suggests that a diazine with a larger dipole moment has stronger interaction with H^+ and is protonated more stable.[17]

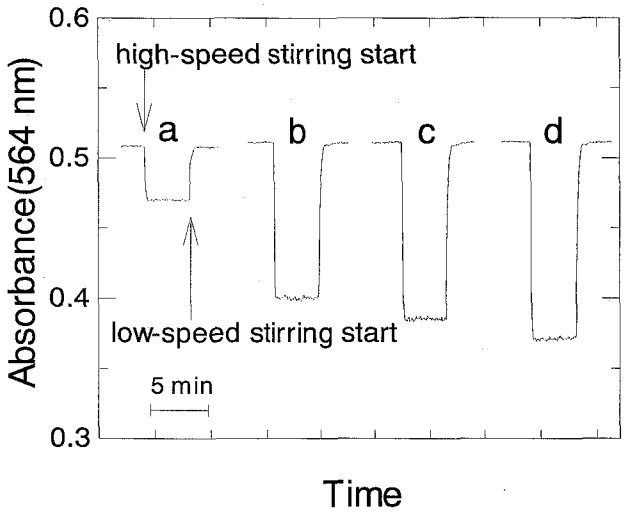

Figure 7.2. A typical absorbance change of Pd(II)-5-Br-PADAP complex in the organic phase caused by the high-speed stirring; $[PdLCl]_T$ = 1.2×10^{-5} M, $[Cl^-]$ = 0.1 M, pH 3.2., (a) [pyridazine] = 0 M, (b) 1.0×10^{-3} M, (C) 1.3×10^{-3} M, (d) 1.6×10^{-3} M,

Interfacial adsorption of Pd(II)–5-Br-PADAP complex

Figure 7.2 shows a typical result of the absorbance change of PdLCl in the organic phase obtained by the high-speed stirring method under the condition that the Cl^- concentration and pH were 0.1 M and 3.2, respectively. The interfacial concentration of PdL^+-complex increased with the addition of pyridazine, but the absorption spectra in the organic phase were not changed. This result suggests that PdL^+-pyridazine complex is formed only at the interface. Since the adsorption and desorption of PdL^+-complexes were fast in response to the change of stirring rate, the complexation between PdLCl and pyridazine occurred at the interface.

An interfacial amount of PdL^+-diazine complex increased with a decrease in the Cl^- concentration. In other words, PdL^+-diazine complex tended to adsorb at the interface more strongly as the ClO_4^- concentration was higher, because of $[Cl^-]+[ClO_4^-]=0.1$ M. The effect of anions on the interfacial adsorption implies that PdL^+-diazine complex adsorbed at the interface has positive charge.

As shown in Figure 7.3, the ratio of the amount of adsorbed PdL^+-complex to the organic phase concentration linearly increased with the diazine concentration at 0.1 M Cl^-. Interfacial adsorption of PdL^+-complex in the absence of diazine refers to the adsorption of

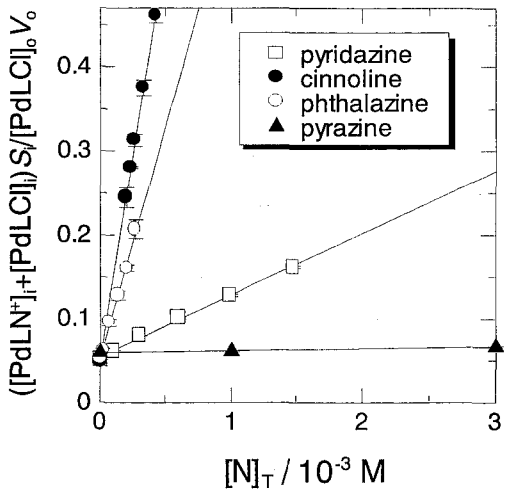

Figure 7.3. Linear dependence of the ratio of the amount of adsorbed Pd(II)-5-Br-PADAP complex to the organic phase concentration on the concentration of diazine; $[PdLCl]_T = 1.2\times10^{-5}$ M, $[Cl^-] = 0.1$ M, pH 2.0.

PdLCl,

$$PdLCl_o \qquad PdLCl_i \tag{7.5}$$

$$K_i = \frac{[PdLCl]_i S_i}{[PdLCl]_o V_o} \tag{7.6}$$

where K_i is the interfacial adsorption constant of PdLCl. Coincidence of the intercepts of the straight lines showed that an increase of the adsorption amount was caused only by the adsorption of PdL^+-diazine complex. The K_i value for PdLCl was obtained as $(6.55\pm1.19)\times10^{-2}$, which was independent of pH. Further, the interfacial concentration of PdL^+-complex was measured at a fixed concentration of pyridazine at 1.0×10^{-4} M. The interfacial concentration was proportional to the PdLCl concentration in the organic phase. These results suggest that PdLCl reacts with pyridazine by the molar ratio of 1:1, and that this complex was adsorbed at the interface. The liner relationship between the ratio of the amount of adsorbed PdL^+-complex to the organic phase concentration and the diazine concentration (Figure 7.3) is represented by the following equation:

$$\frac{[PdLN^+]_i S_i}{[PdLCl]_o V_o} = \alpha[N]_T \tag{7.7}$$

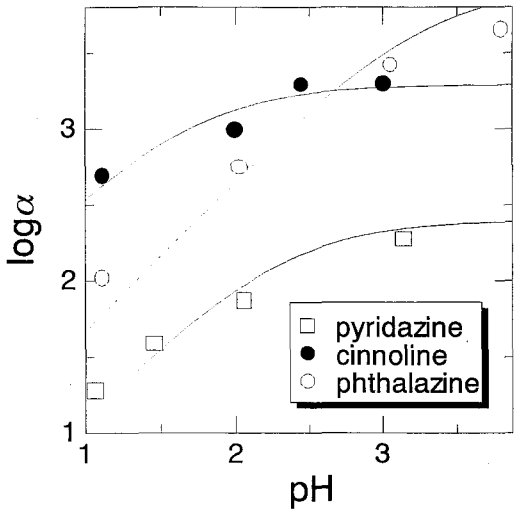

Figure 7.4. Effect of pH on the conditional interfacial formation constant of $PdLN^+$, (the slope, α, of Figure 7.3); $[PdLCl]_T = 1.2\times10^{-5}$ M, $[Cl^-] = 0.1$ M.

where α is the slope and $[N]_T$ is the total concentration of the diazine. The meaning of α is the conditional interfacial formation constant of $PdLN^+$. Table 7.1 shows the obtained α values under the condition that pH and the Cl^- concentration were 2.0 and 0.1 M, respectively.

Figure 7.4 shows the slope, α, as a function of pH for pyridazine, phthalazine and cinnoline. The α values increased with pH for all systems. These results suggest that the protonation of diazine derivatives inhibits the complexation between PdLCl and diazine derivatives. When the ligand substitution occurs between PdLCl at the interface and neutral diazine derivatives in the aqueous phase, the intrinsic interfacial formation constant, β_i, is denoted as:

$$PdLCl_i + N \qquad PdLN^+_i + Cl^- \tag{7.8}$$

$$\beta_i = \frac{[PdLN^+]_i[Cl^-]}{[PdLCl]_i[N]} \tag{7.9}$$

The concentration of the neutral diazine derivatives in the aqueous phase under the high-speed stirring condition is given by the following equations:

$$[N] = [N]_T - [NH^+] - [N]_o$$

$$= \frac{[N]_T}{1 + \frac{[H^+]}{K_a} + K_D} \qquad (7.10)$$

where the interfacial concentration of N is neglected. The combination of Eqs (7.6), (7.7), (7.9) and (7.10) leads to the following equation:

$$\alpha = \frac{K_i \beta_i}{(1 + \frac{[H^+]}{K_a} + K_D)[Cl^-]} \qquad (7.11)$$

The β_i values for pyridazine, cinnoline and phthalazine were obtained as $(3.99\pm0.49)\times10^2$, $(1.48\pm0.15)\times10^4$ and $(2.26\pm0.47)\times10^4$, respectively, by the curve fitting of observed points with Eq. (7.11). As for the other diazine derivatives, the β_i values were obtained from α values at pH 2.0 calculated with Eq. (7.11) and listed in Table 7.1. The solid lines in Figure 7.4 represent the calculated ones with Eq. (7.11), which well reproduce the observed points. This proves the mechanism that the complexation occurs between PdLCl and neutral diazine derivatives.

Detection of $PdLN^+$ by ESI-MS

Figures 7.5a and 7.5b show the mass spectra obtained by ESI-MS at the orifice voltages of 70 V and 100 V, respectively. An intense peak was measured at 535 m/z in any orifice voltage within 35-70 V. This peak corresponds to PdL^+-pyridazine complex. When the orifice voltage was increased to 80 V, the peak of PdL^+ appeared at 455 m/z. When the orifice voltage was changed from 80 to 110 V, 455 m/z peak was increased and 535 m/z peak was decreased. This proves that PdL^+-pyridazine complex with 1:1 molar ratio exists in the sample solution.

Adsorption mechanism at the interface

From the experimental results, the adsorption mechanism of PdL^+-diazine derivative complex at the Cl^- concentration of 0.1 M at the interface is postulated as shown in Figure 7.6. It has been reported that the stability constants, $\log\beta$, of a metal ion with a series of ligands in

homogeneous solvents show a linear relationship with the basicity, pK_a, of the ligands as Eq. (7.12),[18-20]

$$\log\beta = m\mathrm{p}K_a + const. \qquad (7.12)$$

The proportional constant, m, in Eq. (7.12) was reported to be smaller than unity for aromatic ligands due to the contribution of the $\pi_{M\rightarrow L}$ bonding in the interaction of a metal ion with a group of similar ligands.[19,20] In the present process, the diazine has to be removed from the aqueous phase to the interface where it can be combined to PdL^+. This transfer effect of the diazine can be considered by the distribution constant, K_D, because the transfer energy from bulk phase to the interface is found to correlate with the distribution constant for a homologous series of ligands.[21] Thus, the following equation is derived from Eq. (7.12):

$$\log\beta_i = a\log(K_D/K_a) + const. \qquad (7.13)$$

where a is a proportional constant. Figure 7.7 shows the plots of $\log\beta_i$ vs. $\log(K_D/K_a)$. The plots were divided into two groups: pyridazine derivatives and the other compounds. The linear relationships were obtained for the two groups and the following equations were obtained for the pyridazine derivatives and the other systems, respectively:

$$\log\beta_i = 0.765\log(K_D/K_a) + 1.786 \qquad |r| = 0.984 \qquad (7.14)$$

$$\log\beta_i = 0.728\log(K_D/K_a) + 0.341 \qquad |r| = 0.916 \qquad (7.15)$$

Solid and broken lines in Figure 7.7 represent to the results of fittings to Eqs. (7.14) and (7.15), respectively. It seemed that the slopes in Eqs. (7.14) and (7.15) became smaller than unity by the $\pi_{M\rightarrow L}$ bonding. The larger intercept of Eq. (7.14) than that of Eq. (7.15) indicates the selective reactivity of PdL^+ for pyridazine derivatives over the other diazine, i.e. a new type of molecular recognition of pyridazine derivatives by PdLCl at the liquid-liquid interface. The β_i values of pyridazine derivative complexes were about 30 times as large as the ones of pyrimidine and pyrazine derivative complexes. In other words, PdL^+-pyridazine complex is more stable than the pyrimidine and pyrazine complexes at the interface.

Because it was previously reported that the stability constants between Ag^+ and

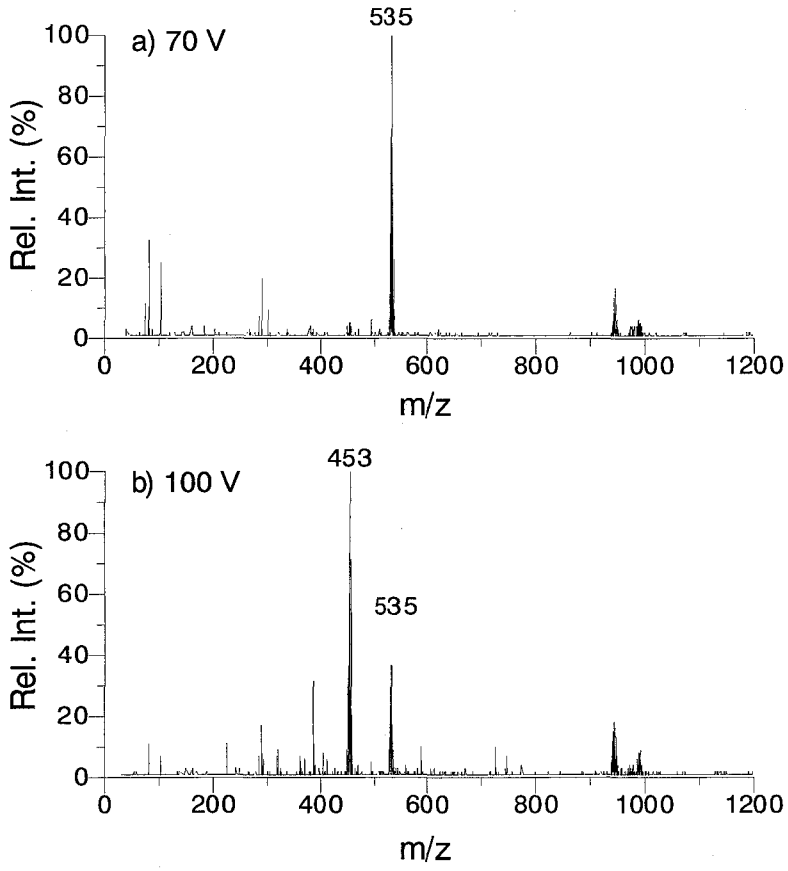

Figure 7.5. ESI-mass spectra of Pd(II)-5-Br-PADAP-pyridazine solution; EtOH : water = 9 : 1, $[PdLCl]_T$ = 2.0×10^{-5} M, [pyridazine] = 2.0×10^{-4} M, a) Orifice voltage = 70 V b) Orifice voltage = 100 V.

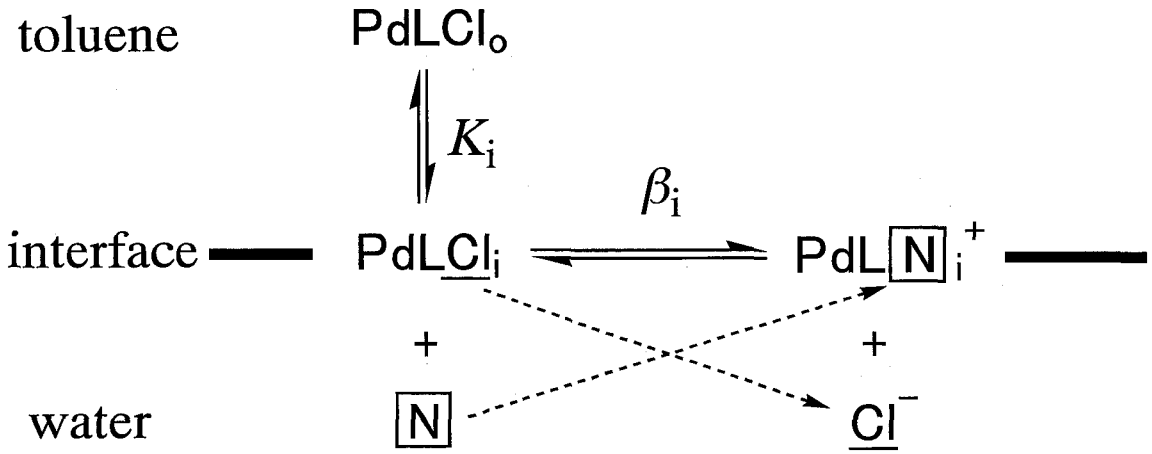

Figure 7.6. Schematic representation of the adsorption mechanism of PdL^+-diazine complex at toluene-water interface.

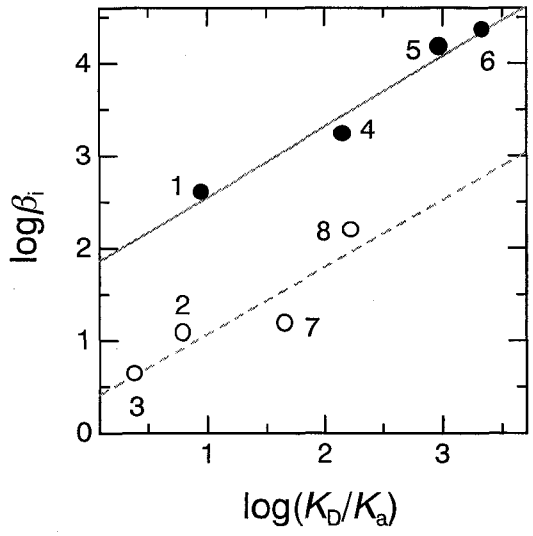

Figure 7.7. Linear correlation between the interfacial formation constant ($\log\beta_i$) for PdL^+-diazine derivative complex and the ratio of the distribution constant to the acid-dissociation constant for diazine derivative ($\log(K_D/K_a)$). Closed and open circles refer to pyridazine derivatives and the other diazine derivatives, respectively. Numbers refer to the diazine in Table 7.1.

pyridazine, pyrimidine and pyrazine showed small difference among them,[15] it could be expected that there was not so large difference among the reactivity between PdL^+ and diazine. Therefore, the large difference of the interfacial formation constants for PdL^+-diazine complex should be caused by the difference in adsorptivity of each complex. This may be caused by the change of hydrophobicity that would be determined by the dipole moments of PdL^+ and N. Table 7.2 shows the calculated values for the dipole moments of neutral and protonated diazines.[15] As for pyridazine derivatives, the dipole moments become smaller by the protonation. While, as for the other diazines, they become larger by the protonation. This result suggests that pyridazine derivative complexes become more liable to adsorb at the interface than pyrimidine and pyrazine derivative complexes, since the bonding of the pyridazine derivative to PdL^+ increases its hydrophobicity by the decrease in the dipole moment.

Table 7.2. Values of dipole moment of neutral and protonated diazine derivatives calculated by CAChe-MOPAC.

diazine derivative	neutral form / D	protonated form / D
pyridazine	3.64	2.22
pyrimidine	1.99	3.83
pyrazine	0	4.63
3-methylpyridazine	3.60	1.25
cinnoline	3.65	0.842
phthalazine	4.47	2.97
2-methylpyrazine	0.405	4.09
quinoxaline	0.422	5.01

Conclusion

The study on the interfacial adsorption mechanism of PdL^+-diazine complex developed a new molecular recognition reaction of diazine isomers by PdLCl at the toluene-water interface.

The interfacial reaction was summarized as (i) PdLCl reacted with a neutral diazine by the molar ratio of 1:1 and the formed PdL^+-diazine complex was adsorbed at the toluene-water interface. (ii) The interfacial formation constant of each $PdLN^+$ complex was determined and was correlated with the distribution constant and acid-dissociation constant of each diazine derivative. (iii) PdL^+-pyridazine complex was thermodynamically more stable than PdL^+-pyrimidine and PdL^+-pyrazine at the interface. This was accounted for an increase in the hydrohobicity of pyridazine by complexation, which was evaluated by the molecular orbital calculation. The interfacial reaction developed in this study could be used as the recognition, separation and detection of pyridazine derivatives or other diazine derivatives.

References

1. Ohashi, A.; Tsukahara, S.; Watarai, H. *Anal. Chim. Acta* **1998**, *364*, 53.
2. Watarai, H.; Sasaki, K.; Takahashi, K.; Murakami, J. *Talanta* **1995**, *42*, 1691.
3. Watarai, H.; Gotoh, M.; Gotoh, N. *Bull. Chem. Soc. Jpn.* **1997**, *70*, 957.
4. Nagatani, H.; Watarai, H. *J. Chem. Soc., Faraday Trans.* **1998**, *94*, 78.
5. Onoe, Y.; Tsukahara, S.; Watarai, H. *Bull. Chem. Soc. Jpn.* **1998**, *71*, 603.
6. Kitagawa, S.; Kondo, M. *Bull. Chem. Soc. Jpn.* **1998**, *71*, 1739.
7. Moreno, J. M.; Suarez-Varela, J.; Colacio, E.; Avila-Róson, J. C.; Hidalgo, M. A.; Martin-Ramos, D.; *Can. J. Chem.* **1995**, *73*, 1591.
8. Miura, J. *Analyst* **1989**, *114*, 1323.
9. S.I. Gusev, G.G. Shalamava, *Zh. Anal. Khim.* **1968**, *23*, 686.
10. Johnson, D. A.; Florence, T. M. *Talanta* **1975**, *22*, 253.
11. Fang, G. Z.; Miao, C. Y. *Analyst* **1985**, *110*, 65.
12. Molecular orbitals were calculated by PM3, MOPAC Version 94.10 in CAChe, Version 3.7, CAChe Scientific, 1994.
13. Albert, A.; Goldacre, R.; Phillips, J. *J. Chem. Soc.* **1948**, 2240.
14. Joris, L.; von Ragué Scheleyer, P. *Tetrahedron* **1968**, *24*, 5991.
15. Kulig, J.; Lenarcik, B.; Rzepka, M. *Pol. J. Chem.* **1986**, *60*, 715.
16. Spencer, J. N.; Holmboe, E. S.; Kirshenbaum, M. R.; Barton, S. W.; Smith, K. A.; Wolbach, W. S.; Powell, J. F.; Chorazy, C. *Can. J. Chem.* **1982**, *60*, 1183.
17. Rao, C. V. R.; Jacob, C.; Chandra, A. K. *J. Chem. Soc., Faraday Trans. 1* **1982**, *78*, 3025.
18. Jabalpurwala, K. E.; Mildurn, R. M.; *J. Am. Chem. Soc.* **1966**, *88*, 3224.
19. Sun, M. S.; Brewer, D. G. *Can. J. Chem.* **1967**, *45*, 2729.
20. Barszcz, B.; Gabryszewski, M.; Kulig, J.; Lenarcik, B. *J. Chem. Soc. Dalton Trans.* **1986**, 2025.
21. Vilallonga, F. A.; Koftan, R. J.; O'connell, J. P. *J. Colloid Interface Sci.* **1982**, *90*, 539.

Chapter 8

Molecular Recognizing Aggregation of Palladium(II)–Pyridylazo Complex with Diazine Isomers at the Toluene/Water Interface

Introduction

Specific chemical reactions at the liquid-liquid interface have received a great attention in various fields, such as, electrochemistry, biochemistry, and photochemistry.[1-3] In particular, the formation of aggregate or assembly is one of the most specific reactions at the interface, because the interfacial concentration of adsorbate becomes much higher than those in bulk phases. Recently, various spectroscopic methods have been developed to measure the liquid-liquid interface directly, for example, attenuated total internal reflection (ATR) spectroscopy,[4,5] total internal reflection fluorometry (TIRF),[6-9] total internal reflected resonance light scattering (TIR-RLS),[10] external reflection (ER) spectroscopy,[11,12] and second harmonic generation (SHG) spectroscopy.[13,14] Among these methods, the centrifugal liquid membrane (CLM) method is the most useful technique to measure the interfacial reaction, because this method utilized an ultra-thin two-phase liquid membrane in a rotating cell by a centrifugal force and it can directly measure the interfacial species by transmission spectrometry[15-17] or other spectrometries.[18,19]

2-(5-Bromo-2-pyridylazo)-5-diethylaminophenol (5-Br-PADAP) have been utilized as an analytical reagent for trace amounts of metal ions by the formation of intensely colored and stable complexes with various metal ions.[20,21] Since 5-Br-PADAP is a tridentate ligand, it forms a 1:1 square-planar complex with palladium(II) leaving one site of palladium(II) for the coordination of another ligand.[21,22] Palladium(II)–5-Br-PADAP (PdL) complex has some characteristics, such as extremely high molar light absorptivity, interfacial adsorptivity and soft Lewis acid. We clarified previously its molecular recognition ability for diazine (Dz) isomers at the toluene-water interface; the interfacial formation constants of 1:1 complex between PdL and Dz isomer became larger in the order of basicity of Dz: pyridazine (1,2-Dz, pK_a 2.33) >> pyrimidine (1,3-Dz, pK_a 1.34) > pyrazine (1,4-Dz, pK_a 0.59).[23]

In this study, we investigated the aggregation of each ternary PdL-Dz complex by the CLM method, and demonstrated the molecular recognition ability for Dz isomers. Moreover, it was shown that the interfacial aggregation could be applied to the molecular recognition of

bases.

Experimental

Reagents

5-Br-PADAP (Dojindo Lab.) was used as purchased and dissolved in toluene. Toluene (G.R., Nacalai Tesque) was purified with the same means as the literature.[22] A PdLCl toluene solution was prepared by the solvent extraction in the following way; aqueous solution (20 ml) of 1.0×10^{-3} M palladium(II) chloride (99.99%, Wako Pure Chemicals) in 0.1 M hydrochloric acid and toluene solution (60 ml) of 5.6×10^{-5} M 5-Br-PADAP were introduced into the Erlenmeyer flask with stopper and stirred for one night. Pyridazine (G.R., Nacalai Tesque), pyrimidine and pyrazine (G.R., Tokyo Kasei) were used as purchased and dissolved in water. Structures of Dzs are shown in Figure 7.1. Adenine, guanine, cytosine, thymine, and adenosine were purchased from Nacalai Tesque. These compounds except for guanine were dissolved in water and guanine was dissolved in 0.01 M $HClO_4$ and 0.09 M $NaClO_4$ aqueous solution due to low solubility. These stock solutions were stored at 4 ºC in a refrigerator.Water was distilled and deionized with a Milli-Q system (Milli-Q SP.TOC., Millipore).

Batch examinations

Preliminary experiments for the formation of the aggregates of PdL-Dz and PdL-base complexes were carried out by the batch method. Equal volumes (5 cm^3) of 1.2×10^{-5} M PdLCl toluene solution and Dz or base aqueous solution were shaken in a glass tube for 2 h. The concentrations of 1,2-Dz, 1,3-Dz and 1,4-Dz were 4.0×10^{-4} M, 1.0×10^{-2} M and 4.0×10^{-4} M, respectively, and the concentrations of adenine, guanine, cytosine and thymine were 9.7×10^{-4} M, 1.1×10^{-4} M, 1.2×10^{-3} M and 9.0×10^{-4} M, respectively. After the phase separation, the absorption spectra of both phases were measured with a UV/VIS spectrophotometer (V-570, Jasco). All measurements in this study were carried out under the conditions that the ionic strength and pH were fixed at 0.1 M and 2.0 with $(H^+, Na^+)ClO_4^-$, respectively, in a thermostated room at 298±2 K.

UV-vis absorption spectra measurements of interfacial aggregates

Principals of CLM method was described elsewhere.[15] The apparatus of CLM

method was essentially the same as the one reported previously.[24] An aqueous solution (0.250 cm^3) of Dz or base and a toluene solution (0.150 cm^3) of 5.6×10^{-5} M PdLCl were introduced into a cylindrical cell, whose height and outer diameter were 3.3 and 2.1 cm, respectively. The cell was rotated at 10000 rpm. The sum of absorption spectra of bulk phase and interface was measured with a UV/VIS spectrophotometer (V-570, Jasco) in the wavelength range of 350-800 nm. The concentration of chloride ion was chosen at 0 and 2.0×10^{-3} M. The concentrations of Dz isomers and bases were varied in the ranges of 0-0.08 M and 0-2.9×10^{-3} M, respectively.

Raman spectra of interfacial aggregates

Direct measurements of Raman spectra for aggregates of ternary PdL-Dz complexes formed at toluene/water interface were carried out by a CLM-resonance Raman microprobe spectroscopy, whose apparatus was the same as the one reported previously.[19] An aqueous solution (0.300 cm^3) of 1.3×10^{-3} M Dz and a toluene solution (0.300 cm^3) of 5.1×10^{-5} M PdLCl were introduced into the cylindrical cell and then the cell was rotated at 10000 rpm. The Raman spectra were measured in the range of 1700-800 cm^{-1} by the use of 514.5 nm line of an Ar^+-ion laser with the power of 40 mW. To improve the S/N ratio, the exposure time was set to 50 s. The focal point was moved along the *Z*-axis, which was perpendicular to the interface, at four points of 600, 660, 740 and 810 μm by controlling the height of XYZ-stage. The *Z* values of 600, 660, 740 and 810 μm of focal point corresponded to the inner surface of the cell, the bulk aqueous phase, the toluene/water interface and the bulk toluene phase, respectively.[19] The position of $Z = 0$ was defined at an outer surface of the cylindrical cell. The observed frequencies were calibrated with respect to the Raman peaks of toluene and were accurate to within ±2 cm^{-1}.

Microscopic measurement

The aggregates of PdL-Dz complexes formed at the toluene-water interface were observed with a microscopy with a CCD camera. A 6.0×10^{-4} M Dz aqueous solution (15 cm^3) was introduced in a laboratory dish, and then 8 cm^3 of 5.1×10^{-5} M PdLCl toluene solution was quietly added on the aqueous phase. After one night, the microscopic images of the aggregates of PdL-Dz complexes formed at the toluene/water interface were obtained by an objective lens (45×) directly above the toluene phase. Clear microscopic image for the interfacial aggregate of PdL-1,4-Dz was not obtained due to the formation of membrane-like

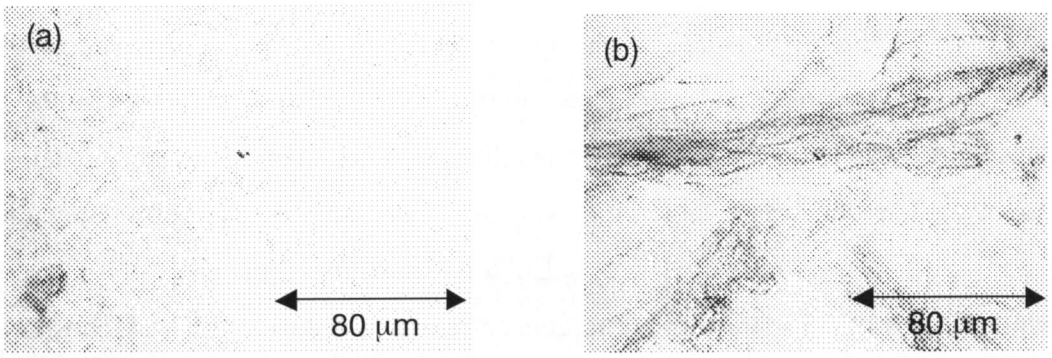

Figure 8.1. Microscopic images of the assembly of PdL-1,2-Dz complex at the toluene/water interface (a) and the assembly of PdL-1,4-Dz complex transferred on the glass substrate (b). Each interfacial aggregate was formed under the condition of $[PdLCl]_T$ = 5.1×10^{-5} M, [1,2-Dz] = [1,4-Dz] = 6.0×10^{-4} M, $[ClO_4^-]$ = 0.1 M, $[Cl^-]$ = 0 M and pH 2.0.

species with homogeneous surface, and thus it was carefully transferred on a glass substrate and then observed.

Results and Discussion

Microscopic images of the interfacial aggregates

From the result of batch experiments, we confirmed that PdLCl scarcely existed in both phases after shaking in glass tubes with Dz, but PdLCl remained in the toluene phase, unless it contained Dz. Colored species were formed at the toluene/water interface for all Dzs (1,2-Dz and 1,3-Dz: blue, 1,4-Dz: pink). These interfacial species disappeared by the addition of 1.0×10^{-2} M NaCl, because PdLCL returned into the toluene phase. This result suggested that the aggregates of complexes of Pd(II)–5-Br-PADAP with Dz isomers were formed by the exchange of chloride ion with Dz isomer at the interface.

Microscopic images of the aggregates of PdL-Dz isomers complexes formed at the interface were observed in the laboratory dish as shown Figure 8.1. The microscopic observations revealed that the shape of the aggregates of PdL-1,2-Dz and PdL-1,3-Dz was somewhat crystal-like. The microscopic observation of the aggregate of PdL-1,4-Dz on the glass substrate revealed that the aggregate of PdL-1,4-Dz was membrane-like. These microscopic images found that the shapes of the interfacial aggregates of PdL-Dz complexes were greatly different among Dz isomers.

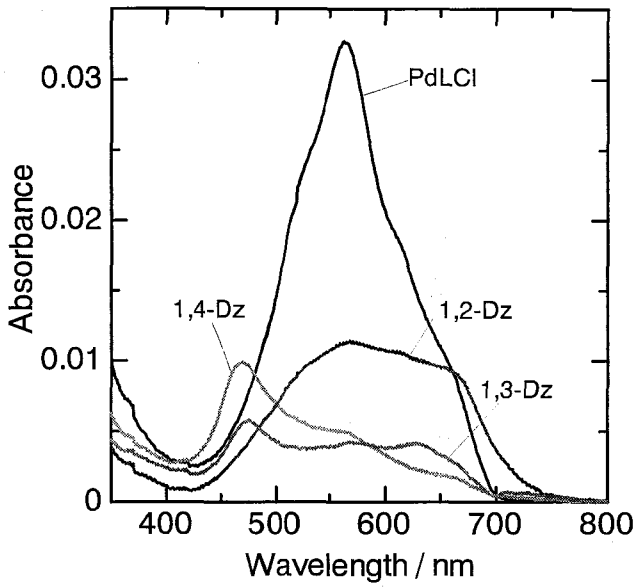

Figure 8.2. The absorption spectra of PdLCl and the interfacial aggregates of ternary PdL-Dz complexes measured by CLM method. $[PdLCl]_T = 5.6\times10^{-5}$ M, $[1,2\text{-Dz}] = 2.0\times10^{-4}$ M, $[1,3\text{-Dz}] = 8.0\times10^{-3}$ M, $[1,4\text{-Dz}] = 8.0\times10^{-5}$ M, $[ClO_4^-] = 0.1$ M, $[Cl^-] = 0$ M, pH 2.0.

Absorption spectra of the interfacial aggregates of PdL-Dz isomer complexes

The absorption spectra of aggregates of PdL-Dz complexes were directly measured by CLM method. Figure 8.2 shows the absorption spectra of PdLCl and the aggregates of PdL-Dz complexes. The spectrum of PdLCl in the absence of Dzs was the sum of absorption spectrum of PdLCl in the toluene phase and that adsorbed at the interface, because PdLCl also existed in the toluene phase. When the Dz isomers were added into the aqueous phase, the absorption maximum (564 nm) of PdLCl in the toluene phase was significantly decreased and a new maximum rose for each Dz isomer. In the case of 1,2-Dz, a broad peak appeared around 600-700 nm. Addition of 1,4-Dz produced a peak at 469 nm. The spectrum observed by CLM method in the case of 1,4-Dz coincided with that of the aggregate of PdL-1,4-Dz transferred on the glass substrate, indicating that the interfacial aggregate was stable. The interfacial concentrations of PdL ($>3.0\times10^{-10}$ mol cm^{-2}) calculated from the decrease in the absorbance of PdLCl in toluene were four times higher than the saturated concentration of NiL_2 (6.5×10^{-11} mol cm^{-2}).[25] From these results, it was confirmed that these new spectra were not those of the PdL-Dz complex monomer, but those of the aggregates of PdL-Dz complexes formed at the interface.

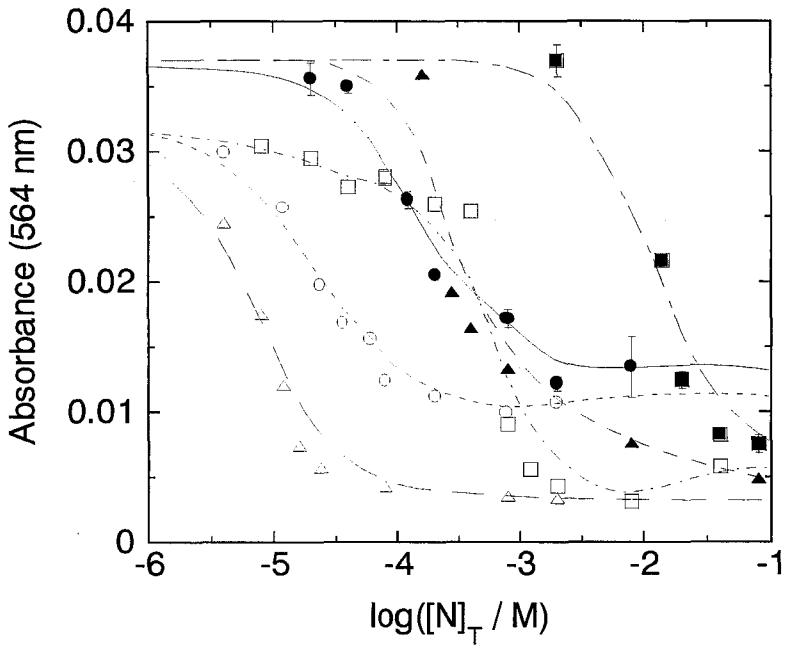

Figure 8.3. The Dependencies of the absorbance at 564 nm on the additional concentration of Dz. $[PdLCl]_T$ = 5.6×10^{-5} M, $[ClO_4^-]$ = 0.1 M, pH 2.0, circle: 1,2-Dz, square: 1,3-Dz, triangle: 1,4-Dz, opened: $[Cl^-]$ = 0 M, closed: $[Cl^-]$ = 2.0×10^{-3} M. Each line in Figure serves as a guide for the eyes.

Influence of chloride ion on the aggregation

Figure 8.3 shows the dependencies of equilibrium absorbance at 564 nm measured by the CLM method on the concentration of Dz isomers at $[Cl^-]$ = 0 M and 2.0×10^{-3} M. As the concentration of Dz isomers was higher, the absorbances at 564 nm decreased due to the formation of the interfacial aggregates of PdL-Dz isomers. $[N]_{1/2}$ was defined as the Dz concentration at which the absorbance at 564 nm reached the half value ($A_{1/2}$) by the sum of the absorbances in the initial (A_0) and the equilibrium (A_e) conditions, $A_{1/2} = (A_0 + A_e)/2$, and its value in each system was estimated from Figure 8.3 and listed in Table 8.1. A higher concentration of Dz isomers was needed to form the interfacial aggregates at $[Cl^-]$ = 2.0×10^{-3} M than those at $[Cl^-]$ = 0 M in all cases. This interference effect of the chloride ion could be accounted for by the decreases of the interfacial concentrations of PdL-Dz isomers complexes, which were formed by the exchange

Table 8.1. Value of $\log[N]_{1/2}$ in each system estimated from Figure 8.3.

diazine	$\log([N]_{1/2}$ / M)	
	$[Cl^-]$ = 0 M	$[Cl^-]$ = 2.0×10^{-3} M
1,2-Dz	-4.7	-3.8
1,3-Dz	-3.3	-1.9
1,4-Dz	-5.1	-3.6

of the coordination between Cl^- and Dz isomers. This result implied that chloride ion of PdLCl was exchanged to Dz isomers in the aggregates. In spite of the much lower concentrations (4.0×10^{-6} M) of 1,2-Dz and 1,4-Dz, the aggregates of PdL-Dz were formed at the interface. This phenomenon was caused by the specific concentration effect of the liquid-liquid interface. Absorbance slightly decreased in a lower 1,3-Dz concentration range, and then drastically decreased above about 8.0×10^{-4} M. Slight decrease in absorbance resulted from the formation of PdL-1,3-Dz complex whose composition was 1:1 at the interface.[23] The drastic decrease in absorbance above 8.0×10^{-4} M was attributable to the formation of aggregate between PdL and 1,3-Dz polymer, because 1,3-Dz formed a polymer of itself in a high concentration range that contained neutral and protonated 1,3-Dz together.[26] Interestingly the ability to form the interfacial aggregate of PdL-1,4-Dz complex was highest among all Dzs, although the ability to form the interfacial complex of 1:1 PdL-1,4-Dz at $[Cl^-]$ = 0.1 M was lowest.[23] This result implied that the formation of the interfacial aggregate of PdL-Dz isomer was greatly influenced by the structure of Dz, not the basicity of Dz.

Stoichiometry of the interfacial aggregates

Figure 8.4 shows the results of the mole ratio method to determine the composition of the interfacial aggregates of PdL-1,2-Dz and PdL-1,4-Dz. The mole ratio was defined by the use of the initial concentration added in the system as:

$$\text{Mole-Ratio} = \frac{[\text{Dz}]_{\text{ini}} V_{\text{a}}}{[\text{PdLCl}]_{\text{ini}} V_{\text{o}}} \qquad (8.1)$$

where the subscript ini refers to the initial, and V_a and V_o were the volumes of the aqueous and the organic phases, respectively (V_a = 0.250 cm^3 and V_o = 0.150 cm^3). The initial concentration of PdLCl was kept at 5.6×10^{-5} M. Equilibrium absorbances at 564 nm were plotted against the concentration of Dz isomers added. The composition ratios of 1,2-Dz/PdL and 1,4-Dz/PdL were found to be 1:1 and 1:2, respectively, from the cross points. Two chloride ions should be released, when one 1,4-Dz was consumed to form the aggregate of PdL-1,4-Dz complex. Therefore, the hindrance effect of chloride ion for the formation of the interfacial aggregate was largest in the case of 1,4-Dz. A large number of papers that 1,4-Dz was used as a framework to synthesize one- and two-dimensional metal complex crystals have been reported.[27-29] Therefore, we assumed that the unit structure of the

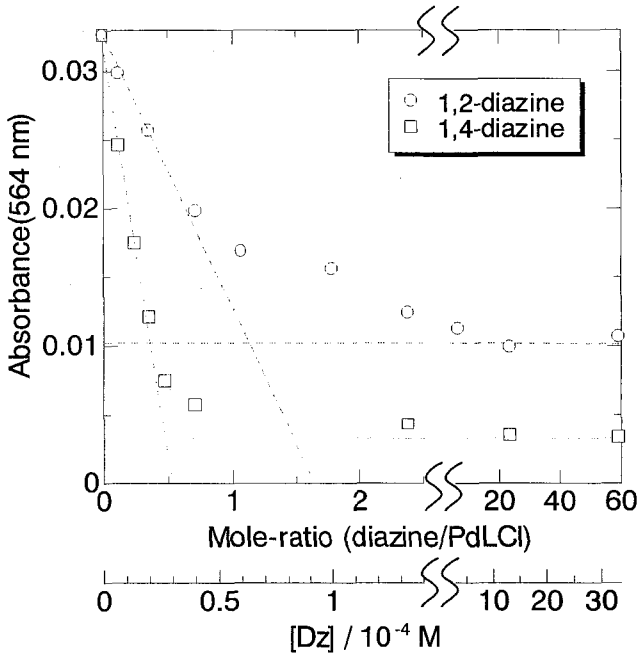

Figure 8.4. Determination of the composition ratio of Dz/PdL in the interfacial aggregate by the mole ratio method. $[PdLCl]_T = 5.6\times10^{-5}$ M, $[ClO_4^-] = 0.1$ M, $[Cl^-] = 0$ M, pH 2.0

aggregate of PdL-1,4-Dz contained that two palladium(II) atoms bound to each nitrogen atom of 1,4-Dz. This 1:2 complex aggregated and the membrane-like aggregate was formed.

Resonance Raman spectra of the interfacial aggregates

To discuss the structures of the aggregates in detail, direct Raman spectral measurements of the aggregates of ternary PdL-Dz complexes formed at the toluene/water interface were carried out with a CLM-resonance Raman microprobe spectroscopy. The Raman spectra measured at the inner surface of the cell (Z = 600 μm) and the bulk aqueous phase (Z = 660 μm) did not show any peaks attributable to PdLCl, because PdLCl scarcely existed in these regions. Because Raman spectrum measured at Z = 740 μm contained both information of the liquid-liquid interface and both bulk phases, the interfacial Raman spectrum was obtained by subtracting the spectrum measured at Z = 810 μm (the bulk toluene phase) from that at Z = 740 μm (the interface) after the normalization by using the Raman intensity at 1210.5 cm^{-1} of toluene. Resonance Raman spectrum of PdLCl in the toluene phase (Z = 810 μm) was also obtained by the subtracting the spectrum for toluene after the normalization of Raman intensity at 1210.5 cm^{-1} of toluene. Figures 8.5a-d show the

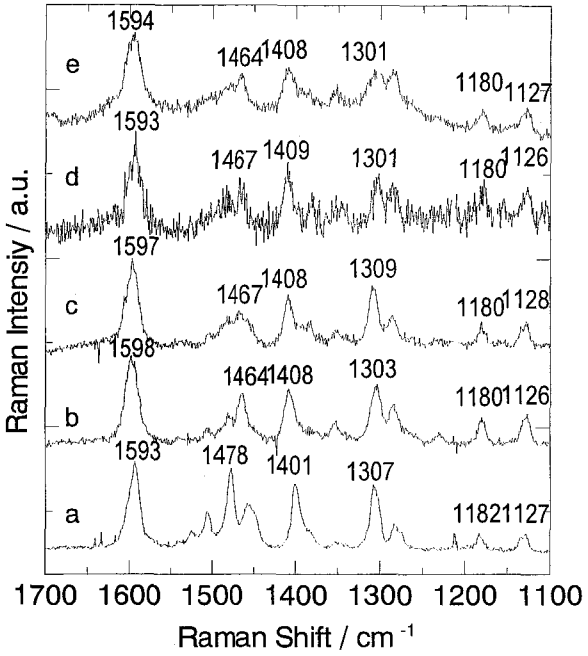

Figure 8.5. Resonance Raman spectra of PdLCl (a) in the toluene phase and (b) at the interface, (c) the assemblies of PdL-1,2-Dz complex at the interface and the aggregates of PdL-1,4-Dz complex (d) at the interface and (e) on a glass substrate. $[PdLCl]_T$ = 5.1×10^{-5} M, $[ClO_4^-]$ = 0.1 M, $[Cl^-]$ = 0 M, pH 2.0, [1,2-Dz] = [1,4-Dz] = 1.3×10^{-3} M.

resonance Raman spectra of PdLCl in the toluene phase, PdLCl at the interface, the aggregate of PdL-1,2-Dz at the interface and that of PdL-1,4-Dz at the interface, respectively, measured by CLM-resonance Raman microprobe spectroscopy. Fine resonance Raman spectrum for the aggregate of PdL-1,3-Dz was not obtained due to low absorbance at 514.5 nm. In the same manner, the S/N ratio of the Raman spectrum of the aggregate of PdL-1,4-Dz was lower, since its absorbance at 514.5 nm was small for resonance Raman spectroscopy (see Figure 8.2). Figure 8.5e shows the resonance Raman spectrum for the aggregate of PdL-1,4-Dz on the glass substrate. This spectrum was close to the one measured by CLM-resonance Raman microprobe spectroscopy. The bands at 1594, 1478, 1401 and 1307 cm^{-1} in Figure 8.5a were assigned mainly to ν(C=C) of benzene and pyridine rings, ν(C=C) of pyridine ring, ν(N=N) and ν(CNNC), respectively, by comparison with those reported for pyridylazo complexes[30-32]. Compared with the Raman spectrum of PdLCl in the toluene phase, that of PdLCl at the interface was different at around 1470 cm^{-1}, and the bands at 1593 and 1401 cm^{-1} in the toluene phase shifted to higher frequencies of 1598 and 1408 cm^{-1}, respectively. When the dielectric constant of solvent increased, similar spectral change of PdLCl was observed.[33]

Therefore, we thought that spectral change of the interfacial PdLCl resulted from the influence of the polar aqueous phase. In Raman spectra for the interfacial aggregates of PdL-1,2-Dz and PdL-1,4-Dz complexes, the band at 1408 cm^{-1} hardly changed. This result revealed that the formation of the interfacial aggregates of PdL-Dz complexes did not accompany a large structural change of 5-Br-PADAP such as twisting or *cis*-isomerization. From this result, it was confirmed that the large structural change did not result in the course of the formation of the interfacial aggregates of PdL-Dz complexes.

The complex of metal ion with 5-Br-PADAP exists as a mixture of three resonance forms: two imine and one azo tautomers, and it is postulated that the charged quinone resonance structure in the imine tautomer results in the high molar absorptivity, which is twice as sensitive as that of 4-(pyridylazo)resorcinol (PAR).[20,34] In the charged quinone resonance structure, diethylamino-group play an important role as an electron-donor. The significant decrease in the absorptivity of the aggregates of PdL-Dz complexes seemed to result from the decrease in the ratio of the charged quinone structure in these aggregates. This could not be explained by π-stacking between PdL-PdL in the aggregates, because the hypochromic phenomenon was not observed in the aggregation of PdLCl itself at the heptane/water interface (see Chapter 5). Therefore, we assumed that the interaction of ClO_4^- as a counter ion with PdL-Dz complexes prevented the electric donation from the diethylamino-group and lowered the possibility of a π-π* transition. Because Raman shift peaks attributed to the imine structure was still observed in the spectrum of the aggregates of PdL-Dz complexes in Figure 8.5, the resonance in the PdL did not completely disappeared.

Table 8.2 lists the observed Raman shifts and the value of Raman intensities at the peak positions around 1307 and 1284 cm^{-1} of PdL in the various situations; the bands at 1307 and 1284 cm^{-1} were assigned to ν(CNNC) in azo form and imine form, respectively (see Chapter 4). The value of the ratio of Raman intensities at the peak positions around 1307 and 1284 cm^{-1} (I_{1307}/I_{1280}) of the aggregate of PdL-1,2-Dz complex was larger than that of the aggregate of PdL-1,4-Dz complex. In other words, the ratio of the azo form in the aggregate of PdL-1,2-Dz complex was larger than that of the aggregate of PdL-1,4-Dz complex. This result suggested that the microenvironment around the interfacial aggregate of PdL-1,2-Dz complex has lower polarity than that around the interfacial aggregate of PdL-1,4-Dz complex from the dependency of the value of I_{1307}/I_{1280} on the dielectric constant of the solvent in Chapter 4. The shape of the aggregate of PdL-1,4-Dz was membrane-like from the microscopic image, though that of PdL-1,2-Dz was crystal-like. The structure of the

Table 8.2. Shapes, Raman shifts and the values of the ratio of Raman intensities around 1307 and 1284 cm^{-1} of a crystal, aggregates and complex of PdLCl. The absorption spectra measured by CLM method in various base systems.

	shape	Raman Shift / cm^{-1}			
		νN=N	$\nu CNNC_{azo}$	$\nu CNNC_{imi}$	I_{1307}/I_{1284}
$PdLCl_{crystal}$	crystal	1400	1301	1279	2.19
$PdLCl_{aggregate}$	crystal-like	1402	1300	1285	3.52
$(PdL\text{-}1,2\text{-}Dz)_n$	crystal-like	1408	1309	1286	2.11
$(PdL\text{-}1,4\text{-}Dz)_n$	membrane-like	1409	1301	1286	1.16
$PdLCl_{toluene/water\ interface}$	———	1408	1303	1280	1.47
$PdLCl_{hepate/water\ interface}$	———	1408	1303	1284	1.85
$PdLCl_{toluene\ bulk}$	———	1401	1307	1283	2.87

aggregate of PdL-1,2-Dz complex seemed to be similar to that of the PdLCl crystal as described in Chapter 6, because the composition ratio of PdL/1,2-Dz in the aggregate was 1:1. It was suggested that the values of I_{1307}/I_{1280} of Raman spectra of a crystal and aggregate of PdLCl and the aggregate of PdL-1,2-Dz complex relatively became larger, because the crystal-like structures of these species made the microenvironment around PdL-complex hydrophobic. On the other hand, the value of I_{1307}/I_{1280} of Raman spectrum of the aggregate of PdL-1,4-Dz complex relatively became smaller. Figure 8.6 shows (a) a possible structure of the aggregate unit of PdL-1,4-Dz complex and (b) a schematic illustration of this aggregate at the toluene/water interface. It was expected that two PdL complexes bonded to each nitrogen atom of 1,4-Dz and the one-dimensional aggregate was formed with the PdL-1,4-Dz complexes in the mole ratio of 2:1 as a fundamental structure by a π-stacking interaction between the PdL molecules. Assembling some one-dimensional aggregates might form the membrane-like aggregate. Since this fundamental structure in the mole ratio of 2:1 prevented to form the compact structure as crystal, the shape of the interfacial aggregate of PdL-1,4-Dz complex became membrane-like. We thought that the microenvironment around PdL in the aggregate of PdL-1,4-Dz complex became hydrophilic, because the membrane-like structure was easy to contain water molecules in the aggregate than the

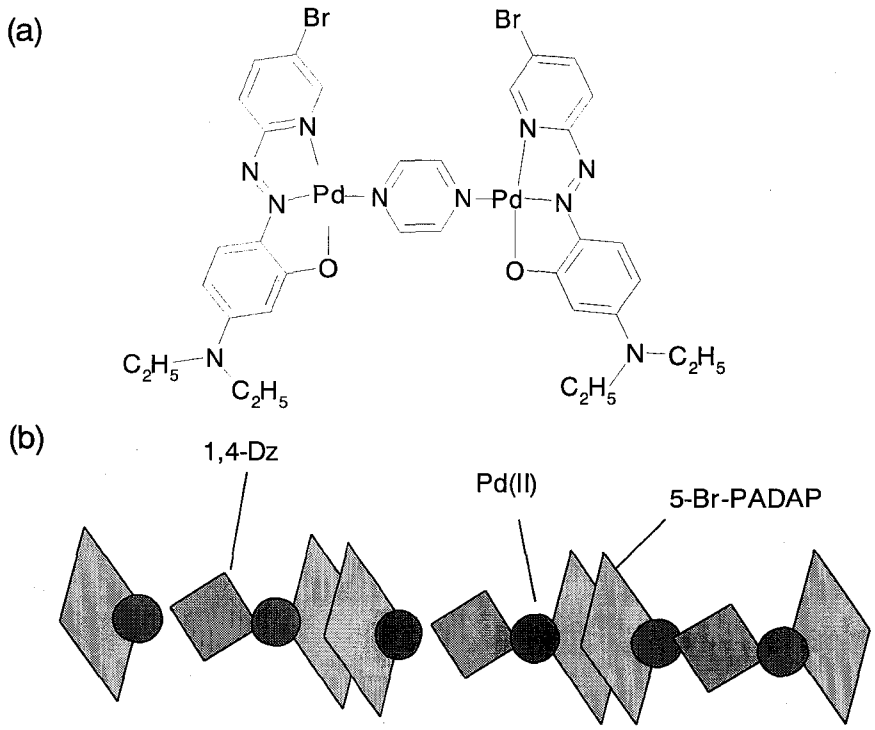

Figure 8.10. Possible structure of (a) the assembly unit of PdL-1,4-Dz complex and (b) a schematic illustration of the assembly of PdL-1,4-Dz complex at the interface.

crystal-like structure. The structure of the interfacial aggregate of PdL-1,3-Dz could not be discussed in detail, because it was difficult to measure in various conditions due to a lower ability for the aggregation. Further studies are needed to confirm these structural assumptions.

Application of molecular recognition aggregation to base systems

After shaking the glass tubes, PdLCl scarcely existed in both phases, when adenine or guanine was contained in the aqueous phase. Blue species were formed at the toluene/water interface and somewhat on the glass wall. On the other hand, PdLCl decreased from the toluene phase in the addition of cytosine or thymine, too. However PdLCl somewhat remained in the toluene phase (about 58% of all). The formation of the aggregate at the toluene/water interface was not confirmed in appearance in each system. Therefore, the decrease in the absorbance of PdLCl seemed to result from the adsorption of PdL-cytosine or PdL-thymine complexes at the toluene/water interface and on the glass wall. This result implied that the abilities for the formation of the interfacial aggregates of PdL-base

complexes were greatly different between purine bases and pyrimidine bases.

Figure 8.7 shows the absorption spectra of the two-phase liquid membranes in the systems contained bases in the aqueous phase. The absorbance at 564 nm of PdLCl in toluene decreased due to the formation of the interfacial aggregates of PdL-base complexes in purine base systems. While, the absorbance at 564 nm also decreased in pyrimidine base systems, however, these changes of absorbance were obviously smaller than those in purine base systems. From the results of the batch experiments, we thought that it was not the formation of the interfacial aggregates of PdL-pyrimidine base complexes but the adsorption of PdL-pyrimidine base complexes that decreased in the absorbance at 564 nm. Therefore, the absorption spectra measured in pyrimidine base systems were the sum of the absorption spectrum of PdLCl in the toluene phase and PdL-base complexes at the interface. Figure 8.8 shows the dependencies of equilibrium absorbance at 564 nm measured by the CLM method on the concentration of bases. As the concentration of bases was higher, the absorbance at 564 nm decreased due to the formation of the interfacial aggregates of PdL-purine base complexes in the purine base systems. The decreases in absorbance proceeded steeply and finished at about 1.2×10^{-5} M of the purine base concentrations. The compositions of the interfacial aggregates of PdL-adenine and PdL-guanine were determined by the mole ratio method as PdL : adenine = 6 : 1 and PdL : guanine = 7 : 1, respectively. This result suggested that the interfacial aggregation was used as the sensitive detection method of the vital materials. The structure of these interfacial aggregates cannot be discussed in detail at this stage.

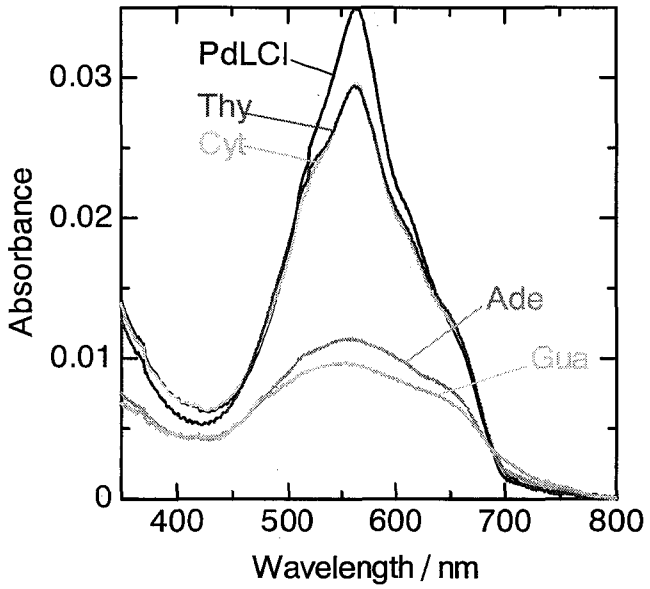

Figure 8.7. The absorption spectra measured by CLM method in various base systems. $[PdLCl]_T = 5.6\times10^{-5}$ M, [adenine] = 7.7×10^{-5} M, [guanine] = 4.4×10^{-5} M, [cytosine] = 8.8×10^{-4} M, [thymine] = 8.8×10^{-4} M, $[ClO_4^-] = 0.1$ M, $[Cl^-] = 0$ M, pH 2.0.

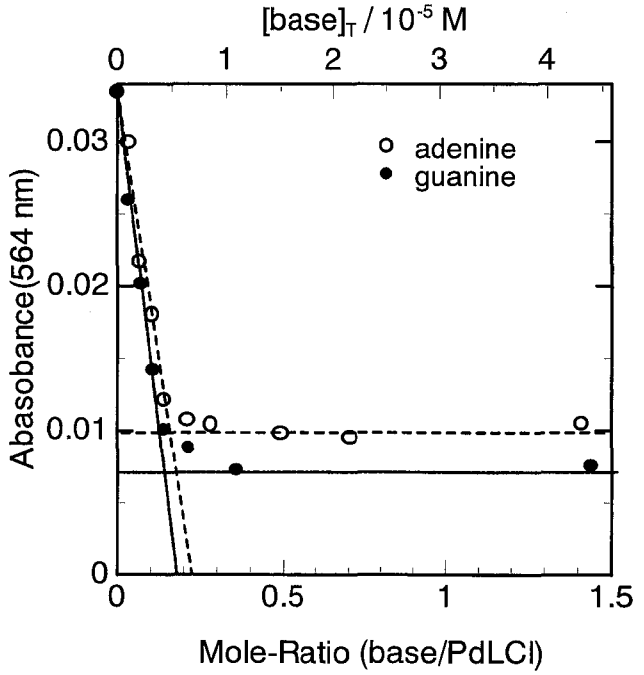

Figure 8.8. Determination of the composition ratio of base/PdL in the interfacial aggregate by the mole ratio method. $[PdLCl]_T = 5.6\times10^{-5}$ M, $[ClO_4^-] = 0.1$ M, $[Cl^-] = 0$ M, pH 2.0

Conclusion

We found the isomer recognizing reaction using the aggregation between Pd(II)–5-Br-PADAP and Dz isomers at the toluene-water interface by CLM method. The formation of each interfacial aggregate of PdL-Dz was accompanied with drastic absorbance decrease at 564 nm of PdLCl and the appearance of new spectrum. The differences of the structure and the composition ratio of the interfacial aggregate of PdL-Dz were observed between Dz isomers; that of 1,2-Dz was as a blue domain and the composition ratio 1,2-Dz/PdL 1:1, whereas that of 1,4-Dz was as a membrane and 1,4-Dz/PdL 1:2. In spite of the lowest ability for 1:1 complexation between PdL and 1,4-Dz at the toluene-water interface, the ability for the formation of the interfacial aggregate became the highest among the Dz isomers. This result revealed that the formation of the interfacial aggregate of PdL-Dz isomer was greatly influenced by the structure of Dz, not the basicity of Dz.

The resonance Raman spectra of the interfacial aggregates were measured by CLM-resonance Raman microprobe spectroscopy and showed that any large structural changes of 5-Br-PADAP such as twisting or *cis*-isomerization were not induced by the formation of the aggregate. From the hypochromic effect in the UV-visible spectra and no large change of the Raman band of the N=N stretching, it was suggested that the formation of the charged quinone structure in the aggregates of PdL-Dz complexes was prevented by the interaction with ClO_4^-.

The interfacial isomer recognizing aggregation was demonstrated for the first time. The aggregates of PdL-1,2-Dz and PdL-1,4-Dz were formed by the low concentration of Dzs. This phenomenon of the molecular recognizing aggregation at the interface will be applied to the high sensitive and selective detection of various species in the aqueous phase.

References

1. *Liquid-Liquid Interfaces. Theory and Methods*; eds by Volkov, A. G.; Deamer, D. W., Eds.; CRC Press: Boca Raton, FL, 1996.
2. *Liquid Interfaces in Chemical, Biological, and Pharmaceutical Applications*; Volkov, A. G., Ed.; Marcel Dekker, New York, 2001.
3. *Liquid Interfaces in Chemistry and Biology*; Volkov, A. G.; Deamer, D. W.; Tanelian D. L.; Markin, V. S., Eds.; John Wiley & Sons CRC Press, Chicester, 1998.
4. Perera, J. M.; Stevens, G. W.; Grieser, F. *Colloids Surf. A* **1995**, *95*, 185.
5. Tsukahara S.; Watarai, H. *Chem. Lett.* **1999**, 89.
6. Fujiwara, M.; Tsukahara, S.; Watarai, H. *Phys. Chem. Chem. Phys.* **1999**, *1*, 2949.
7. Fujiwara, N.; Tsukahara S.; Watarai, H. *Langmuir* **2001**, *17*, 5337.
8. Tsukahara, S.; Yamada, Y.; Watarai, H. *Langmuir* **2000**, *16*, 6787.
9. Bessho, K.; Uchida, T.; Yamauchi, A.; Shioya, T.; Teramae, N. *Chem. Phys. Lett.* **1997**, *264*, 381.
10. Feng, P.; Shu, W. Q.; Huang, C. Z.; Li, Y. F. *Anal. Chem.* **2001**, *73*, 4307.
11. Moriya, Y.; Amano, R.; Sato, T.; Nakata S.; Ogawa, N. *Chem. Lett.* **2000**, 556.
12. Fujiwara, K.; Watarai, H. *Bull. Chem. Soc. Jpn.* **2001**, *74*, 1885.
13. Corn, R. M.; Higgins, D. A. *Chem. Rev.* **1994**, *94*, 107.
14. Conboy, J. C.; Daschbach J. L.; Richmond, G. L. *J. Phys. Chem.* **1994**, *98*, 9688.
15. Nagatani, H.; Watarai, H. *Anal. Chem.* **1998**, *70*, 2860.
16. Yulizar, Y.; Ohashi, A.; Watarai, H. *Anal. Chim. Acta* **2001**, *447*, 247.
17. Ohashi, A.; Watarai, H. *Anal. Sci.* **2001**, *17*, 1313.
18. Nagatani, H.; Watarai, H. *Chem. Lett.* **1999**, 701.
19. Ohashi, A.; Watarai, H. *Chem. Lett.* **2001**, 1238.
20. Johnson, D. A.; Florence, T. M. *Talanta* **1975**, *22*, 253.
21. Busev, S. I.; Vin'kova, V. A. *Zh. Anal. Khim.* **1967**, *22*, 552.
22. Ohashi, A.; Tsukahara S.; Watarai, H. *Anal. Chim. Acta* **1998**, *364*, 53.
23. Ohashi, A.; Tsukahara S.; Watarai, H. *Anal. Chim. Acta* **1999**, *394*, 23.
24. Yulizar, Y.; Ohashi, A.; Nagatani; H., Watarai, H. *Anal. Chim. Acta* **2000**, *419*, 107.
25. Watarai, H.; Gotoh, M.; Gotoh, N. *Bull. Chem. Soc. Jpn.* **1997**, *70*, 957.
26. Peral F.; Gallego, E. *J. Mol. Struct.* **1995**, *372*, 101.
27. Belford, R. C. E.; Fenton D. E.; Truter, M. R. *J. Chem. Soc. Dalton Trans.* **1974**, 17.
28. Haynes, J. S.; Rettig, S. J.; Sams, J. R.; Thompson R. C.; Trotter, J. *Can. J. Chem.* **1987**,

65, 420.

29. Moreno, J. M.; Suarez-Varela, J.; Colacio, E.; Avila-Róson, J. C.; Hidalgo, M. A.; Martin-Ramos, D.; *Can. J. Chem.* **1995**, *73*, 1591.
30. Drozdzewski, P. M. *Spectrochim. Acta* **1985**, *41*, 1035.
31. Dines, T. J.; Wu, H. *J. Chem. Soc. Faraday Trans.* **1995**, *91*, 463.
32. Drozdzewski, P. M. *J. Raman Spectrosc.* **1988**, *19*, 111.
33. A. Ohashi and H. Watarai, in preparation.
34. Ueno, K.; Imamura T.; Cheng, K. L. *Handbook of Organic Analytical Reagents* 2nd ed.; CRC Press: Boca Raton, 1992, pp237-243.

Chapter 9

Concluding Remarks

The complexation and aggregation reactions of pyridylazo compounds at the liquid-liquid interface were investigated by means of conventional and new methods and the new-type isomer recognizing reactions by the complexation and aggregation at the liquid-liquid interface were proposed in this thesis. Their isomer recognizing reactions are not observed in the homogeneous system and the specificity of the liquid-liquid interface as a reaction field has been revealed. The author considers that these results give the significant information to understand the property of the liquid-liquid interface and develop the new function of the liquid-liquid interface as the analytical and synthetic field.

A new microscopic method, named as a centrifugal liquid membrane-resonance Raman microprobe spectroscopy (CLM-RRMS), was proposed, and its advantage for the measurement of the interfacial species was revealed. This method permitted selective observation of Raman spectra for the interface and the bulk phases in the CLM system and time-resolved measurements of the interfacial reaction by resonance Raman scattering at the first time. The combination of new method and the conventional method such as the CLM method and the high-speed stirring method allows us to obtain the much information to understand the property and the roles of the liquid-liquid interface in analytical chemistry and biochemistry.

Acknowledgement

The author would like to express his greatest gratitude to Professor Hitoshi Watarai for his helpful guidance, discussion and support in coordinating this work.

The author also would like to express his sincere thanks to Dr. Satoshi Tsukahara for his helpful discussion, accurate instruction, and encouragement in this work.

The author also would like to express his sincere thanks to Dr. Iwao Watanabe, Dr. Hideaki Monjushiro and Dr. Takao Fukumoto for his helpful suggestion, kind instruction and encouragement in this work.

The author thanks Dr. Hirohisa Nagatani for helpful advice and assistance on the high-speed stirring method and the CLM method measurements.

The author also thanks Dr. Toshiaki Tsukuda of Kaizaki Laboratory for his help and suggestion on the X-ray structure analysis.

The author is grateful to all members of Watarai Laboratory, in both present and past, for their helpful advice, assistance, and encouragement.

Finally, the author thanks all his friends and family for their help and encouragement.

Papers Relevant to the Present Study

1. "Isomer Recognizing Adsorption of Palladium(II)–2-(5-Bromo-2-pyridylazo)-5-diethylaminophenol with Diazine Derivatives at the Interface"
   Akira OHASHI, Satoshi TSUKAHARA, Hitoshi WATARAI
   Analytica Chimica Acta, **1999**, *394*, 23-31.

2. "Direct Spectrophotometric Measurement of Acid-catalyzed Complexation of Palladium(II) with 2-(5-Bromo-2-pyridylazo)-5-diethylaminophenol at the Heptane/Water Interface by a Centrifugal Liquid Membrane Method"
   Akira OHASHI, Hitoshi WATARAI
   Analytical Sciences, **2001**, *17*, 1313-1319.

3. "Resonance Raman Spectroscopic Detection of Pyridylazo Complex Formed at Liquid-Liquid Interface in Centrifugal Liquid Membrane System"
   Akira OHASHI, Hitoshi WATARAI
   Chemistry Letters, **2001**, 1238-1239.

Paper Relate to the Present Study

1. "Acid-catalyzed Interfacial Complexation in the Extraction Kinetics of Palladium(II) with 2-(5-Bromo-2-pyridylazo)-5-diethylaminophenol"
   Akira OHASHI, Satoshi TSUKAHARA, Hitoshi WATARAI
   Analytica Chimica Acta, **1998**, *364*, 53-62.

2. "Kinetic Study of Ni(II) and Zn(II) Complexation with a Pyridylazo Extractant by a Centrifugal Liquid Membrane Method"
   Yoki YULIZAR, Akira OHASHI, Hirohisa NAGATANI, Hitoshi WATARAI
   Analytica Chimica Acta, **2000**, *419*, 107-114.

3. "Kinetic Complexation Mechanisms of Ni(II) and Zn(II) with a Pyridylazo-ligand at Liquid/Liquid Interfaces"

Yoki YULIZAR, Akira OHASHI, Hitoshi WATARAI

Analytica Chimica Acta, **2001**, *447*, 247-254.